REPORT DOCUMENTATION PAGE

Form Approved OMB No. 0704-0188

1. AGENCY USE ONLY (Leave blank)	2. REPORT DATE	3. REPORT TYPE AND DATES COVERED
	1996	Final Report

4. TITLE AND SUBTITLE

Development of PPT Laboratory Model Which Is As Close To The Flight One As Possible

5. FUNDING NUMBERS

F6170895W0336

6. AUTHOR(S)

Dr. Nikolay Antropov

7. PERFORMING ORGANIZATION NAME(S) AND ADDRESS(ES)

Research Institute of Applied Mechanics and Electrodynamics
4, Volokolamskoye shosse
Volokolamskoe Shosse,4
Moscow 125671
Russia

8. PERFORMING ORGANIZATION REPORT NUMBER

N/A

9. SPONSORING/MONITORING AGENCY NAME(S) AND ADDRESS(ES)

EOARD
PSC 802 BOX 14
FPO 09499-0200

10. SPONSORING/MONITORING AGENCY REPORT NUMBER

SPC 95-4033

11. SUPPLEMENTARY NOTES

12a. DISTRIBUTION/AVAILABILITY STATEMENT

Approved for public release; distribution is unlimited.

12b. DISTRIBUTION CODE

A

13. ABSTRACT (Maximum 200 words)

This report results from a contract tasking Research Institute of Applied Mechanics and Electrodynamics as follows: Develop a PPT laboratory model which is as close to the flight one as possible.

14. SUBJECT TERMS

EOARD

15. NUMBER OF PAGES

16. PRICE CODE
N/A

17. SECURITY CLASSIFICATION OF REPORT	18. SECURITY CLASSIFICATION OF THIS PAGE	19. SECURITY CLASSIFICATION OF ABSTRACT	20. LIMITATION OF ABSTRACT
UNCLASSIFIED	UNCLASSIFIED	UNCLASSIFIED	UL

RESEARCH INSTITUTE OF APPLIED MECHANICS AND
ELECTRODYNAMICS OF MOSCOW AVIATION INSTITUTE

"Development of PPT laboratory model which is as close to the flight one as possible"

Final report

Supervisor of work

_____ G.A.Popov

Authorized scientific official

_____ N.N.Antropov

Moscow

1996

CONTENTS

INTRODUCTION

Having a number of advantages, one of which is a surprising design and functional simplicity, the pulsed plasma thruster (PPT) of erosion type has one considerable disadvantage. It is rather low efficiency of its operational process. In fact, speaking about it one should bear in mind that with typical expected energy consumption (tens, hundreds of J) for prospective small satellites none of the existing EP excluding maybe the ion thruster (IT) (which, thus, has its own problems) promises reaching high values of the thrust efficiency, and many of them will be simply inoperative. Nevertheless, the problem of raising thrust efficiency of the erosion PPT is still very urgent[1)], because its solution allows to widen the range of the thruster application and thus to raise its competitiveness. Comparative assessments of mass characteristics of various types of EP (PPT, SPT, IT) show that increase of thrust efficiency of erosion pulsed thruster with energy consumption of about 100 J from 10 to 15% allows it to compete successfully with SPT and IT while solving problems requiring total impulse up to $50 \cdot 10^3$ Ns per one thruster. If to speak about small satellites and groups of small satellites, the named value of total impulse allows to solve practically the whole spectrum of tasks of controlling their position in the orbit.

Speaking about raising the PPT thrust efficiency we have to state that this problem is not a trivial one, because all evident possibilities of its solution are exhausted. Besides, existing mathematical models describing the processes in PPT, are rough and, offering general approaches to the problem of raising its efficiency do not give the definite answer to the question how to do it[2)]. The most effective approach to the problem is helding complex experimental studies, which take place

in the discharge channel of one particular PPT, that gives chance to affect purposefully its operation process.

Anticipating, one can say that, for example, the results of magnet probes measurements made in RIAME allow to show some real possibilities of raising the PPT thrust efficiency.

Together with such rather laborious studies which do not give quick effect, the direct experiment on studies of influence of various factors of outer circuit, and the discharge channel on the PPT operation process efficiency can be of great use. In experiments of this kind one should rely upon the experimenter's intuition. These both approaches are being realized in RIAME MAI at present.

1. DEVELOPMENT AND STUDY OF PULSED PLASMA THRUSTER MODULE (MPPT-1)

The studies of operational processes of pulsed plasma thrusters (PPT) of various design have been on since the beginning of 1960s in Moscow Aviation Institute (and RIAME has become its successor in this field). The problems connected with the outer discharge circuit, discharge channel geometry, type of the working body, characteristic properties of its supply into the channel and their influence on the PPT operation were studied, as well as other questions. Some measures on raising the thrusters productivity were planned and some experiments were carried out. Thus, in the 60s—70s a considerable scientific and technical reserve was created, which provided the possibility to develop the flying models of the PPT. But in the end of the 70s financing of the studies on electric propulsion (EP) was cut down, which also influenced the PPT as well. The works in this field were practically stopped, and MAI specialists worked mostly on the development and design of pulsed plasma injectors (PPI) designed for the Earth ionospheric studies. During 20 years starting from 1975, fourteen PPIs with the pulse energy from 100 to 2000 J have been developed and ground and flying tests have been carried out successfully[3]. In despite of serious differences in design between PPI and PPT and the tasks which are being solved with their help, the works on PPI helped considerably in development and testing flying samples of the technique and allowed to start at once the PPT flying prototype.

Though some of the PPT diagrams developed and tested in laboratories showed high thrust efficiency (up to 30%)[4], in the beginning of the new cycle of works on PPT in 1993 the so called rail thruster design was chosen. This design

possesses important operating advantages, and first of all, the possibility to preserve the stable geometry of the discharge channel at working out a considerable amount of the propellant[5].

1.1. Basic parameters and diagram of MPPT-1

The works on PPT were renewed in RIAME MAI in 1993, when the task on creating the propulsion set (PS) on supporting the Earth artificial satellite (EAS) in the geostationary orbit[6]. The following parameters of the thruster were specified:

– relative share of the PS mass in the EAS mass;

– total PS impulse in the existence time of the EAS;

– individual thrust impulse determining the precision of the control of the EAS position in the orbit.

The last two parameters define unambiguously the necessary number of PS startings:

$$N = P_N/P \tag{1.1}$$

The propulsion set comprises several thruster modules which create the thrust along different axes. Let us study PPT thruster module mass. It can be presented as a sum of masses of working body, capacitor battery, voltage transformer and constructive elements with the electrode system[7]

$$M_p = M_m+M_c+M_w+M_k \tag{1.2}$$

The equations for the PPT mass components can be written in the following way:

$$M_m = mN,\ M_c = \gamma_c W,\ M_w = \gamma_w Wf/\eta_w,\ M_k = M_{k0}+\gamma_k W$$

where m – working body output per impulse, W – capacitor battery energy, f – thruster operation frequency, η_w – voltage transformer efficiency, $\dot{\gamma}$ – specific

mass, M_{k0} – is the minimal mass of the PPT constructive elements, which does not depend on energy. In our calculations we assume this mass equal to 0.1 kg.

After processing a large number of the experimental data the empirical relationship for the thrust efficiency was obtained:

$$\eta = (K_A/m_w)^{1/2}\varepsilon,$$

where coefficient $\varepsilon = 1\text{-}1/(W/20+1)$.

Using the known relationships for the pulse "price" and the thrust efficiency – $C_p = W/P$, $\eta = P^2/2mW$; after little algebraic manipulations equation (1.2) can be rewritten in the following way:

$$(M_p\text{-}M_{k0})/P_N = (m_w+\gamma/N)C_p \qquad (1.3)$$

Here:
$$C_p = 1/(4K_A m_w \varepsilon^2)^{1/4}, \qquad (1.4)$$

and
$$\gamma = \gamma_k+\gamma_c+\gamma_w f/\eta_w \qquad (1.5)$$

is the generalized specific mass of the PPT module which is $(M_p\text{-}M_{k0}\text{-}M_m)/W$. Total thrust impulse adds to the velocity increment ΔV for EAS with the mass M, that is $P_N = M\Delta V$. Taking into consideration the previous relationship, and the equation (1.4), the equation (1.3) can be transformed in the following way

$$(M_p\text{-}M_{k0})/M = \Delta V(m_w+\gamma/N)/(4K_A m_w \varepsilon^2)^{1/4} \qquad (1.6)$$

Minimum for the left part (1.6) can be achieved at

$$m_w = \gamma/3N \qquad (1.7)$$

The value of the specific consumption of m speaks of the existence of the proportion between electromagnetic and gas-kinetic mechanisms of plasma acceleration in the discharge channel. The first one depends on magnetic pressure value or on the current value to second power. The second one is determined

through gas-dynamic pressure[8]. For the Teflon at $m_w < 3 \cdot 10^{-9}$ kg/J, electromagnetic mechanism of the plasmoid acceleration prevails, which realizes itself most of all in the PPT end diagram, where $m \approx 10^{-9}$ kg/J.

At $m_w > 7 \cdot 10^{-9}$ kg/J gas-dynamic forces influence most of all plasma acceleration. These forces realize themselves in axisymmetric discharge chambers and slot channels with ablating dielectric.

Thus calculation of the specific consumption on the (1.7) equation allowes to evaluate the PPT discharge chamber type, with which minimal mass share of the thruster module in the EAS is achieved.

Minimal PPT mass share in the EAS is determined through the equation:

$$(M_p - M_{k0})/M = 4\Delta V C_p m_w \qquad (1.8)$$

It allows to determine the change of the performance velocity of the SV, for which the propulsion set with PPT can be used.

Let us try to evaluate the change of the performance velocity of the EAS, when the propulsion set mass does not exceed 25% from the EAS mass. When plasma acceleration in PPT has electromagnetic character, which has the highest value of the thrust efficiency, specific consumption is $m_w \approx 10^{-9}$ kg/J, and $C_p \approx 5 \cdot 10^4$ W/N , then $\Delta V \approx 10^3$ m/s.

One of the most power-consuming tasks of EAS control is the support of the station keeping along the North-South line in the geo-stationary orbit, where the increment of the performance velocity is 50 m/s per year. Assuming that EAS existence is 10 years, total change of the performance velocity is 500 m/s. According to (1.8) equation mass share of the electromagnetic PPT is about 12%. At double redundance we obtain 24% from EAS mass. Thus, PPT can in particular be used as EAS control bodies in the geostationary orbit.

As it stems from (1.8), in order to increase the increment of the performance velocity when the PS mass share is fixed in the EAS mass, it is necessary to decrease the specific mass flow rate per impulse. The impulse is directly proportional to the generalized specific mass γ and inversely proportional to N resource. Thruster module resource in its turn is determined through the comprising blocks: capacitor battery, discharge channel with the propellant storage and supply systems, PPU and DIU. At present pulsed capacitors resource is about $(1...2) \cdot 10^7$ startings[8], and that limits PPT resource if there is no redundance.

Generalized specific mass, according to (1.5) is a sum of specific masses of the constructive elements (electrodes, body, insulators and so on), capacitors, PPU. Using up-to-date radio-elements base, new materials and good arrangement, the said parameters can reach the following values: $\gamma_c = 1.5 \cdot 10^{-2}$ kg/J, $\gamma_k = 1.5 \cdot 10^{-2}$ kg/J, $\gamma_w = 2 \cdot 10^{-2}$ kg/W. For transformer efficiency – $\eta_w = 0.8$ and mean PPT frequency operation – f = 0.5 Hz. Generalized specific mass is $3.25 \cdot 10^{-2}$ kg/J, and specific mass flow is $m_w \approx 1.1 \cdot 10^{-9}$ kg/J. The said value of the specific mass flow corresponds to the plasma acceleration electromagnetic mechanism in the PPT. For the Teflon $K_A = 4 \cdot 10^{-11}$ kg/J, and calculation on (1.4) equation gives the value of $C_p = 5 \cdot 10^4$ W/N, where $\varepsilon \approx 1$ to simplify the calculations. Close to these values of m_w and C_p were used to evaluate the maximal increment of the performance velocity of the SV with PPT which is about 10^3 m/s. At such performance velocity value the thruster application can be reasonable.

In table 1 the results of calculations of the PPT mass-energetic parameters for creating total impulse of $2 \cdot 10^4$ Ns with the resource of 10^7 impulses and mean impulses frequency mode of 0.5 Hz are presented as an example. The specific

masses of the capacitor, PPU and of the construction were assumed 0.02 kg/J, 0.02 kg/W, 0.015 kg/J. At Fig.1.1 the PPT parameters change depending on the propellant specific mass in the impulse. As it was shown analytically above, dependence of the PPT module mass from plasmoid specific mass has minimum which defines optimal parameters of the thruster designed for a certain problem. When shifting from the minimum to the right impulse energy and thrust efficiency decrease, and gas-kinetic mechanism role in plasma acceleration increases. So plasmoid mass and working body reserve increase. To the left from the minimum there are thrusters with higher thrust efficiency and impulse energy. At that the higher the thrust efficiency is, the heavier is the thruster. While increasing the thrust efficiency with the stable impulse energy the individual thrust impulse decreases, as well as propellant mass flow per impulse. In order to preserve the total thrust impulse at the specified resource it is necessary to increase the impulse energy at the expense of the capacitor battery capacitance (it is assumed that the initial voltage in the battery is stable). Battery mass increases, whereas stored propellant mass decrease does not compensate the increase of the capacitor battery mass. As a result thruster module mass increases. Special attention should be drawn to the gently sloping curve in the minimum area. It means that the specified total impulse at chosen total operation period is being provided by the series of the thruster modules with practically identical masses. So there are some doubts about the necessity of the struggle for the highest values of the thrust efficiency at the expense of lowering an individual thrust impulse. In the same way the task of choosing the thruster module parameters taking into consideration the characteristic features of the power installation in the space vehicle is being solved. RIAME MAI has a special calculation program which shows that there is always a

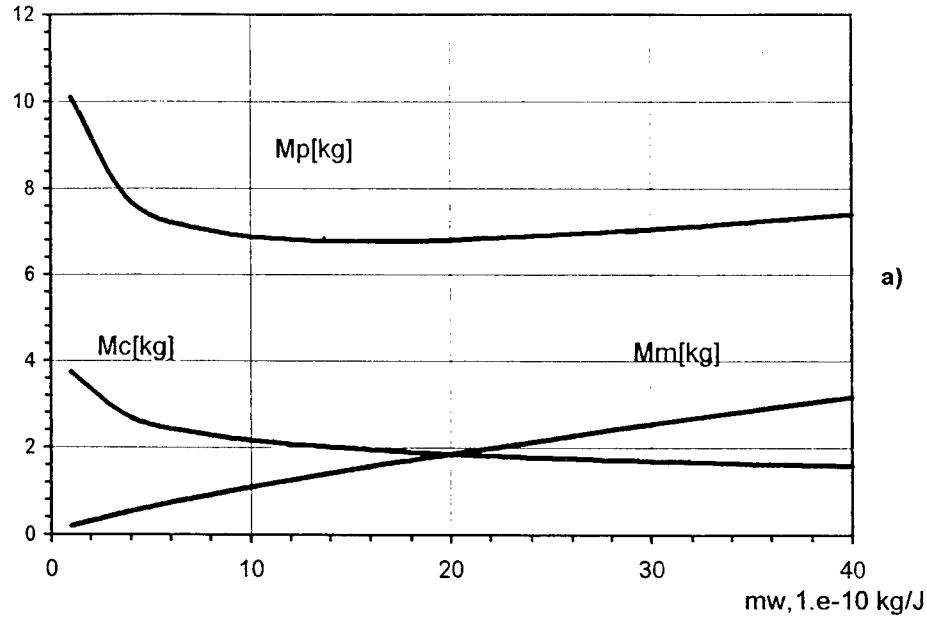

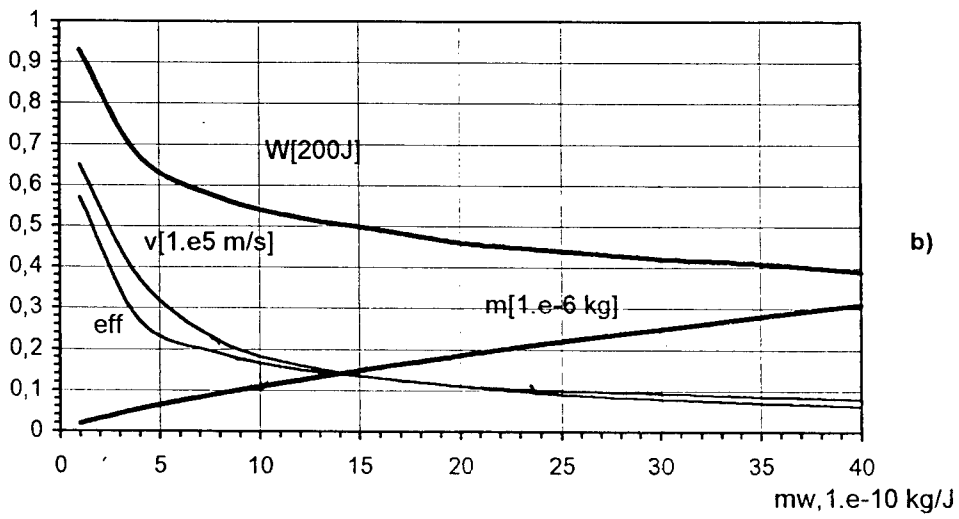

Fig.1.1. PPT parameters

series of the thrusters with minimal mass, that help to solve the task of the position control of the space vehicle in the orbit.

The analysis of various PPT designs made in a number of works[7,9] showed that the most prospective design from the point of view of the arrangement and providing the specified parameters is the thruster of the rail type with the side feed of the working stuff. It is shown on Fig.1.2. In the said design the geometry of the discharge gap practically does not change – after 10^5 impulses there appears slight curve in the form of a barrel, whereas the working surface of the dielectric gets the parabolic profile. The discharge channel is formed by the working ends of the bars in the form of semi-rings, main discharge electrodes and end ceramic insulators with the concave working surface near which the igniter is placed. Fig.1.2 shows two variants of the supply system, which provides moving of the Teflon semi-rings around the common axis till the stop in the fixer (shoulder) on the cathode. Longitudinal position of the working surfaces of the bars with respect to plasma jet direction allows to increase the localization area of the current cord on the electrodes thus permitting to decrease the density of heat flow and electrodes erosion. Ring form of the bars makes the supply system as compact as possible. For example at cross section of the bars 30x35 mm and propellant supply of 1.8 kg, supply system diameter of the outer ring is about 30 cm. By changing the width, height and aperture of the channel specific mass flow value in the vast range can be varied.

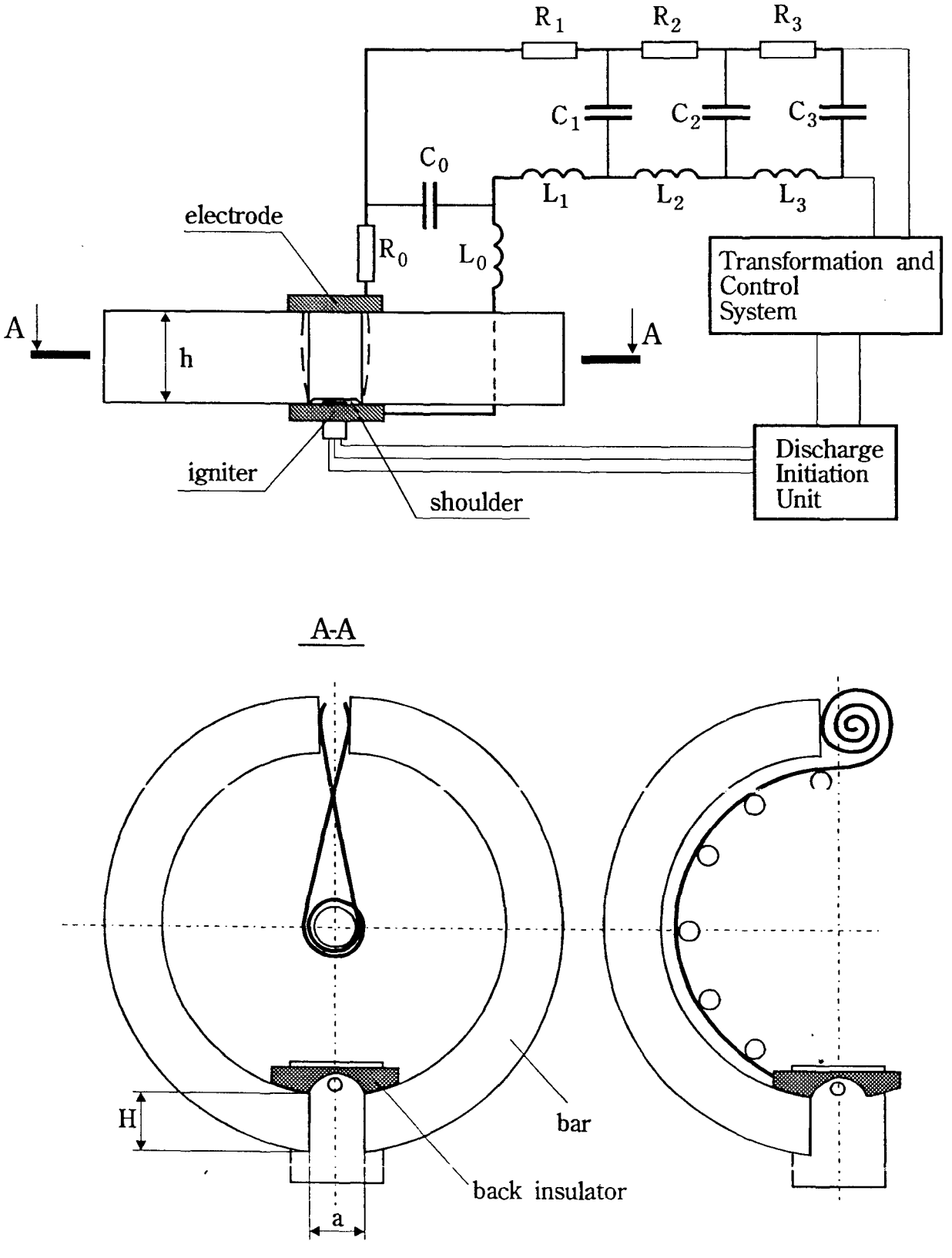

Fig.1.2. Side feed thruster discharge chamber and PPT electric scheme.

1.2. MPPT-1 module description

At designing the laboratory type of PPT-100 with energy storage up to 100 J, its arrangement was made as compact as possible, but it provided easy replacement of blocks and units. Fig.1.3 shows the appearance of the first variant of PPT-100 (MPPT-1). One can see that the supply and storage system (SSS) of the working body, combined in the design with the discharge chamber, is connected with the body in the form of the rectangular parallelepiped where the power unit is. The power unit in this arrangement variant includes capacitor battery and discharge initiating unit (DIU).

DIU reservation can be done through the diagram of full reservation of the object, as well as through the diagram of unit reservation and sectioning. The diagram is chosen issuing from the possibility of the reliable operation of the PPT elements and units. We think that minimal values of possibility of reliable operation are characteristic for the pulsed capacitors which are the part of the capacitor bank and discharge initiator unit.

That is why MPPT-1 provides the possibility of the double reservation of the DIU and capacitor bank sectioning (five capacitors switched in a parallel way with the capacitance of 5 mcF each). The most possible reasons for capacitor malfunction is the break of the current supplies to the current outputs. In that case the storage system capacitance consisting of several capacitors decreases. Thus impulse energy and PPT thrust impulse decrease. PPT mean thrust is preserved on the same level by increasing DIU frequency operation mode. MPPT-1 discharge channel is workable in the energy range 50...100 J.

Preliminary results of the experimental studies of the discharge channel with the cross supply of propellant allowed to choose the dimensions of the PPT-1

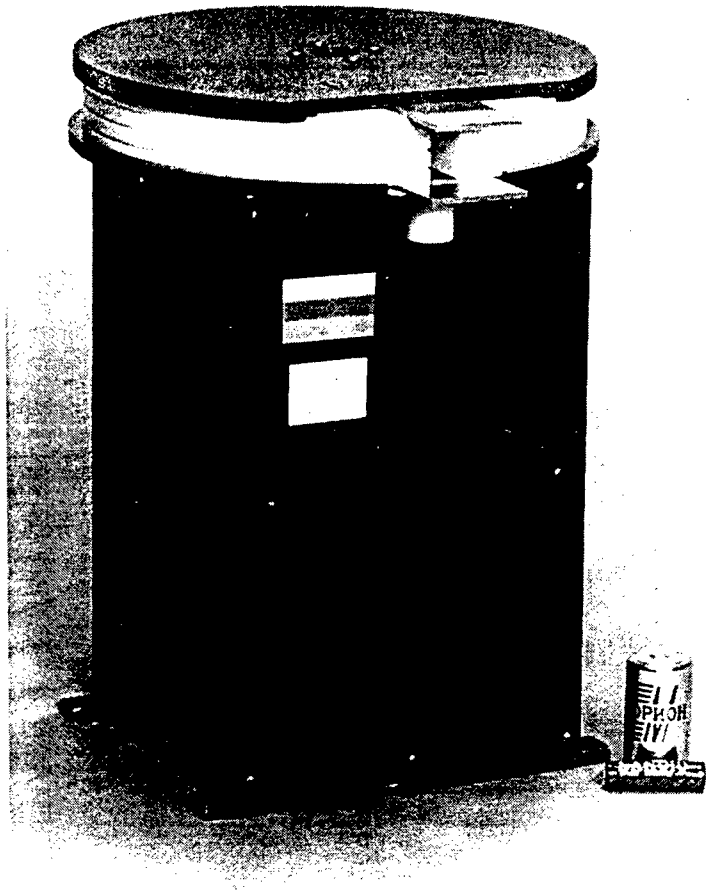

Fig.1.3. MPPT-1 arrangement

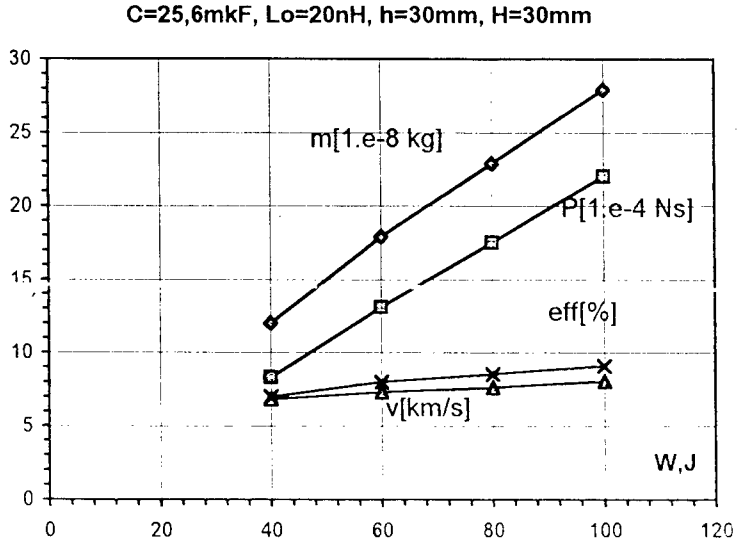

Fig1.4. MPPT-1 integral parameters

reasonably. In the thruster laboratory model presented on Fig.1.3 initial width of the discharge channel - a (the distance between working ends of the Teflon bars) is 15 mm, and its height – h (the distance between the electrodes) is 30 mm. The channel length formed by the bars working surfaces – H is 33 mm. The working surface of the back ceramic insulator made of boron nitride (ABN) turned into the channel, has the concave cylindrical form, forming thus the precombustion chamber with the maximal depth of 7 mm.

Electrodes of the main discharge are made of copper and are 40 mm wide and 3 mm thick. The cathode opposite the bars ends has a fixer (shoulder), trapezoidal in its cross-section, with the large base of 15 mm and height of 1.5 mm (see Fig.1.2).

Propellant bars are made in the form of two semi-rings with the outer radius of 128 mm and radial cross-section of 30x33 mm. The outer cylindrical surface of the bars has three circular grooves 1.5 mm wide and 3 mm deep (see Fig.1.3). Propellant bars are fixed between two disks and can move along the circular guidelines in the azimuthal direction till the stop into the fixer on the cathode. The disks are made of aluminium-magnesium alloy. While the Teflon is evaporated from the bars ends in the heavy-current impulse discharge, the bars move till they stop into the fixer with the help of the rotation spring (see Fig.1.2). Discharge channel elements are fixed rigidly on the SSS low disk through the dielectric adapters of the fiber glass laminate and Teflon.

The igniter through the hole in the cathode is introduced into the discharge channel very close to the precombustion chamber. The igniter is a ceramic tube made of aluminium oxide with 4.5 mm in the diameter with two longitudinal holes 1 mm in diameter in which copper electrodes are fixed.

SSS with the discharge chamber is fixed rigidly on the body in the form of the rectangular parallelepiped where the power unit is placed (capacitor battery and discharge initiating unit (DIU)).

Power unit body is made of aluminium-magnezium alloy. The body framework consists of the walls and the bottom. In order to decrease the framework mass and to provide access to the capacitors and DIU the windows are made in the walls which after the compilation of the power unit are closed by the panels 1 mm thick. The bottom does not have windows and is supporting and heat-removing element of the whole thruster module.

The capacitor battery comprises five capacitors connected in a parallel way. Each capacitor has capacitance about 5 mcF, designed for maximal voltage of 2.8 kV. Measured capacitance of the capacitor battery is 25.6 mcF. Thus maximal stored energy in the capacitor battery is 100 J. With the help of copper busbars capacitors are connected in a parallel way to the electrodes of the main discharge. Measured inductivity of the top-feed (initial inductivity of the thruster is $- L_o$) is $2.0 \cdot 10^{-8}$ H. In order to eliminate electrical self-breakdowns in the capacitor battery the capacitor outlets and busbars are divided by the Teflon film 0.25 mm thick.

DIU is designed for forming short (about 1 mcs) impulses with the voltage about 30 kV. High-voltage impulses are supplied to the igniter electrodes to initiate the main discharge. Plasmoid igniting the main discharge is formed as a result of high-voltage breakdown in the carbon film which is deposited from the main discharge on the igniter working surface.

1.3. Experimental tests of MPPT-1

In the process of experimental tests of MPPT-1 the following tasks were solved:

– the thruster tests with total number of startings of $3 \cdot 10^5$ were held,

– the possibility of continuous operation period of $5 \cdot 10^3$ startings at pulses frequency mode of 1 Hz was shown,

– the studies of discharge channel running in dynamics were held, and the profile of the bars working surfaces stabilized by the discharge was determined.

Experimental tests of the PPT-100 were held in the vacuum chamber with the volume of 2 cubic meters, and remaining gas pressure not more than 0.01 Pa. High-vacuum evaporation of the chamber was held with the help of the oil-diffusion pump.

The thruster operated both in the regime of individual impulses and continuously with the impulses frequency mode of 0.5...2 Hz. At PPT frequency operation the number of impulses in the series was $(1...5) \cdot 10^3$. Minimal period of time between the series of $5 \cdot 10^3$ impulses did not exceed one hour.

In the process of experimental tests initial voltage on the capacitor battery as well as oscillograms of the thruster discharge current were registered, its mean thrust at frequency operation was defined.

Discharge current was registered with the help of digital oscillograph. On its input the signal from Rogovsky belt was sent. Rogovsky belt was placed between the commutation busbars of the capacitor battery near the discharge chamber.

The mean thrust of the PPT was determined with the help of the direct thrustmeter.

In order to estimate consumption of the propellant mass per impulse the bars

were weighted on the analytical balance before and after the series of $10^3...10^4$ impulses.

According to the measurements data of thrust impulse and mass consumption per impulse effective rate of plasmoid outflow and the thruster efficiency were calculated. On Fig.1.4 integral parameters of MPPT-1 in energy range of 60...100 J at the expense of changing the discharge voltage are presented.

As it was shown in studies[10], when PPT operates on solid dielectric the initial flat working surface of each bar obtains complicated profile, the form of which depends on distribution of energy plane in the discharge channel. It was supposed that in order to stabilize the working surface profile the thruster must work not less than $2 \cdot 10^5$ startings. After that the profile should not change, and mean speed of bars supply into the discharge area must be stable. That is why one of the main tasks of the tests is direct experimental support of the duration of the so-called "run-in cycle", during which stabilizing of working surface profile of each bar occurs. MPPT-1 tests were held at initial voltage of 2.5 kV for the capacitor battery (stored energy – 80 J). Criteria for efficiency of the thruster were: absence of uncontrollable electrical breakdowns in the discharge chamber, stability of discharge ignition, discharge current oscillogram, stability of the thrust impulse. The thruster operation in the individual impulses mode and continuous operation with frequency of 0.5...2 Hz were tested. The thruster mostly operated with frequency of 1 Hz in series of $5 \cdot 10^3$ impulses. When thrust measures were taken impulses frequency increased up to 2 Hz.

To study dynamics of change of the profiles of the bars working surfaces the distance between the bars in six points was measured. The points are marked on Fig.1.5 by the figures 1...6. The measures showed that the bars move into the

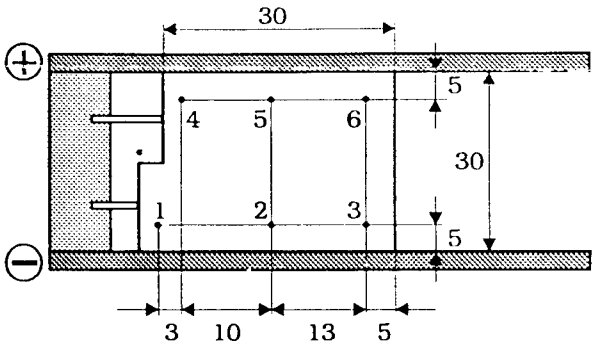

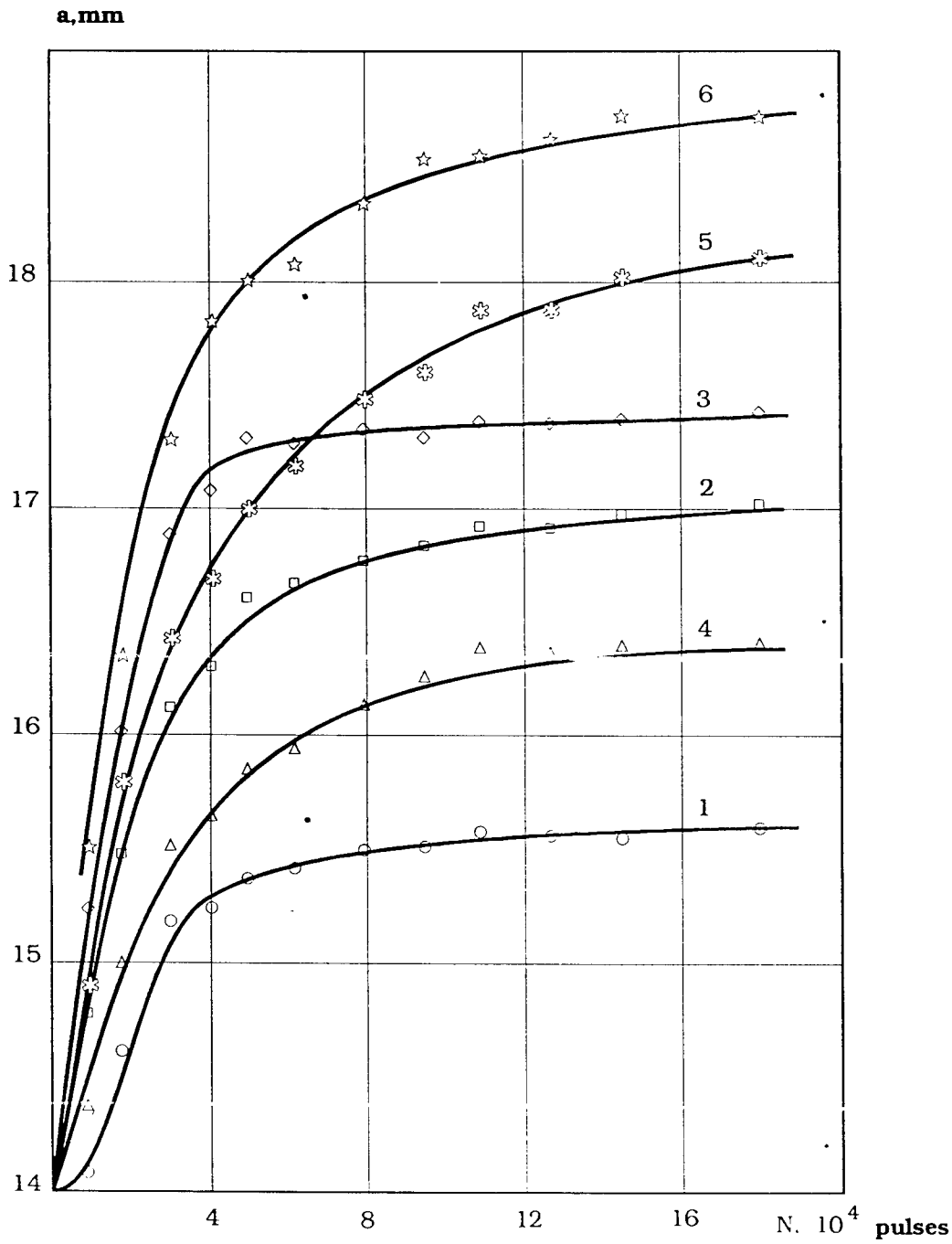

Fig.1.5. Discharge channel width variation.

discharge zone irregularly. It is connected with the dynamics of the bars exhaustion in the stop zone on the cathode. It also happens because the step on the surface which connects with the stop, is crushed. We think that each act of the bar shift passes 3 stages: thinning of the step on the bar, its crush because of. the spring pressure and the evaporation of the step which contacts the cathode stop. In fact these three processes occur simultaneously but one of them dominates. So bars shift is of stage character.

Fig.1.5 shows the dynamics of stabilization of the bar working surface profile in points 1...6. Points 1...3 are in the near-cathode area of the discharge channel, and points 4...6 are in the near-anode area. In general, stabilization of bars in the near-cathode area is faster than in the near-anode one, and finishes after $1.5 \cdot 10^5$ operations. In the near-anode area especially at the outlet of the channel stabilization finishes after $2 \cdot 10^5$ impulses. The bars working surfaces stabilized by the discharge have a complex concave form, and the channel extends at the outlet. At average the channel widens by 3 mm and becomes 17 mm wide.

Thus the duration of the run-in cycle of the discharge channel with cross-sectional supply of propellant bars was determined and the channel profile stabilized by the discharge was obtained for the first time.

Experimental tests of MPPT-1 showed reliable operation of all units and individual elements of the thruster. Carbon traces on the working surfaces of the propellant bars are absent. That proves the correct choice of geometry of the discharge channel for the specified impulse energy – 80 J.

1.4. Study of discharge current distribution in the PPT discharge channel

Magnet probe measurements in the coaxial discharge channel of the high-

current plasma accelerator with its own magnetic field allow to define the picture of the current distribution in the channel and to follow its evolution in the process of discharge. But in the channel which has railgun geometry these measurements and their interpretation face serious difficulties. All three components of the discharge current j_x, j_y, j_z and magnetic induction B_x, B_y, B_z changing with time, must be taken into consideration. That is why the problem is principally three-dimensional and non-stationary, in contrast to the case for coaxial channel. The main difficulty of magnet probe measurements in three-dimensional channel is connected with the interpretation of the results. The task of restoring current distribution according to the picture of measured magnet-fields relates to inverse mathematically incorrect tasks, excluding some particular cases such as azimuthal current symmetry, because generally speaking an infinite set of the current distribution may correspond to one picture of fields distribution.

Taking into consideration these difficulties we assumed the following succession of magnet probe studies, which consisted of the three stages increasing in complexity:

1. Determining of the shift of the current "gravity center" in the process of discharge and the current outflow beyond the discharge channel with the help of the B_z-probe which moves along the longitudinal axis of the accelerator. Measurements by B_z-probe in the vertical plane of the channel symmetry in order to study the current lines bending due to Hall effect.

2. Processing of measurements data in accordance with any elementary mathematical model and obtaining calculation picture of currents distribution which corresponds in the first approximation to the measured magnet fields.

3. Measurements of all three components of magnetic field along the whole

volume of the channel and behind its cut, as well as restoring distribution fields of the discharge current according to the obtained picture.

At present first two steps of studies were obtained, which in fact are the solution to the one-dimensional task.

Measurements were held on the pulsed plasma thruster (railgun) MPPT-1 which had larger dimensions of the acceleration channel than the MPPT-3. The channel diagram is shown on Fig.1.6.

Fig.1.7 gives the diagram of magnet-probe measurements in the PPT channel. Inductive-type magnet probes with RC-integrator and coordination device with two degrees of freedom were used. In order to register the discharge channel.and signals from the probe two-beam storage oscillograph was used. Magnetic fields measurements were carried with two probes with different sensitivity. In order to tune the probes pulsed discharge in solenoid was used.

Outer diameter of the magnet probes was 5 mm. It was evident, that introduction of such a probe into the relatively small discharge channel can influence considerably on the discharge current distribution and gas-dynamics of the current. That is why on this stage of the studies the obtained picture of distribution and dynamics of the discharge current in the PPT in the PPT channel can be regarded only as qualitative. Further on, while methods of mathematical processing of the experimental results are being developed, the measurements with the help of probes outside the channel will be held. This will not bring distortions into the picture of current distribution.

Measurements of the cross-sectional component B_z were held along three straight lines in the vertical plane of the acceleration channel symmetry: along the top electrode, along the bottom electrode and between them at equal distance. The

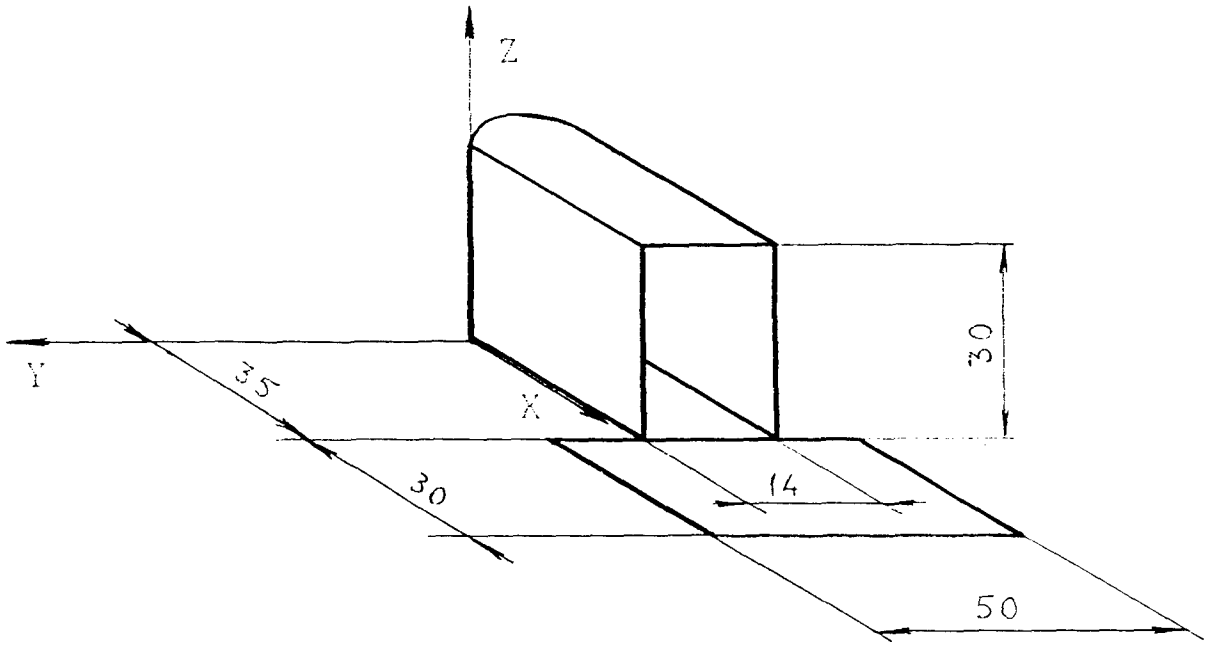
Z
Y
X
35
30
14
50
30

Fig.1.6

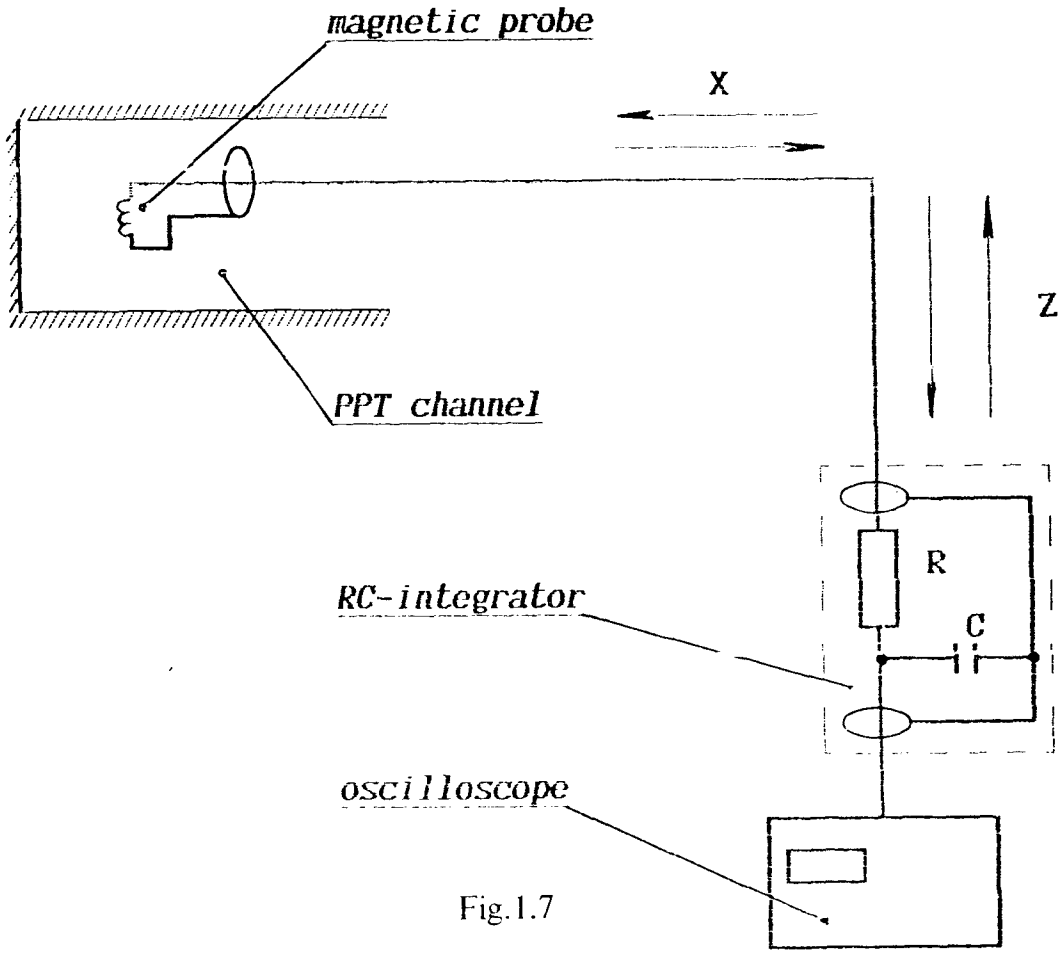
magnetic probe
X
Z
PPT channel
R
C
RC-integrator
oscilloscope

Fig.1.7

probe moved with the step of 0.5 cm from the back insulator till the point which was 16 cm far from it. Fig.1.8 shows oscillograms of the discharge current J and signals from magnet probes which were on the channel symmetry axis at the distance of x = 1, 3, 5 and 7 cm from the back insulator. Thruster capacitor battery was charged up to 2.5 kV which corresponds to the discharge energy of 80 J. Discharge current amplitude was 54 kA, discharge half-period was 2.9 mcs. Reversing of the polarity of the signal from the probe in the discharge channel can be observed. It is possible to define through the time of this reversing the moment of discharge current "gravity center" passing through the probe. Having the data from probes moving along the top and bottom electrodes it is possible to evaluate the current lines slopes.

Fig.1.9 shows the oscillogram of the signal from the most remote probe (x=16.5 cm). In its first half-period it repeats the curve of the discharge current in its form. On Fig.1.10 the amplitude values of the signals from remote probes (x>10 cm) are given. It is clear that the discharge magnetic field at large distance practically coincides with the field of the point magnet dipole:

$$B_z = 2JS/x^3 \sim 0.1x^{-3}, \qquad (1.4.1)$$

where JS – magnetic moment of the discharge current. This fact easies the process of measurements results and allows to increase the accuracy of the current distribution in the first half-period, as it is shown later.

Fig.1.11 shows the qualitative picture of discharge current distribution in the acceleration channel, which was obtained on the basis of the analysis of the time of reversing of the polarity of the signals from magnetic probes (places of the probes are marked by crosses). Two areas of the discharge current localisation can be observed: area I in which current flows from the discharge beginning to

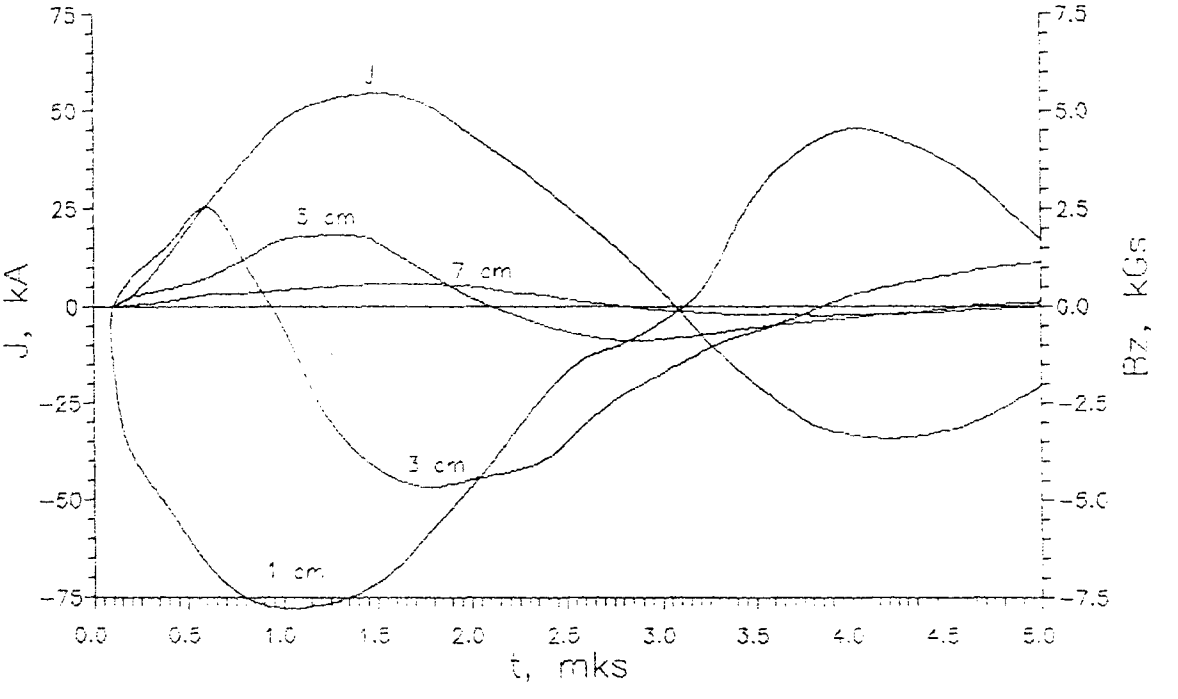

Fig.1.8

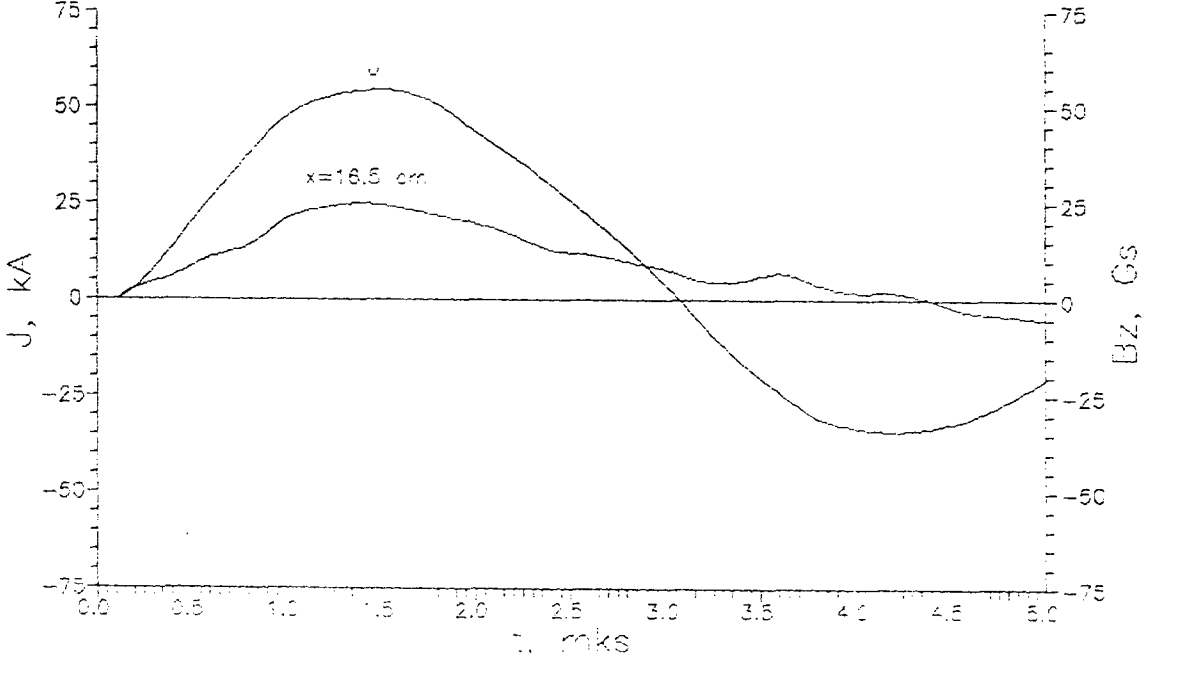

Fig.1.9

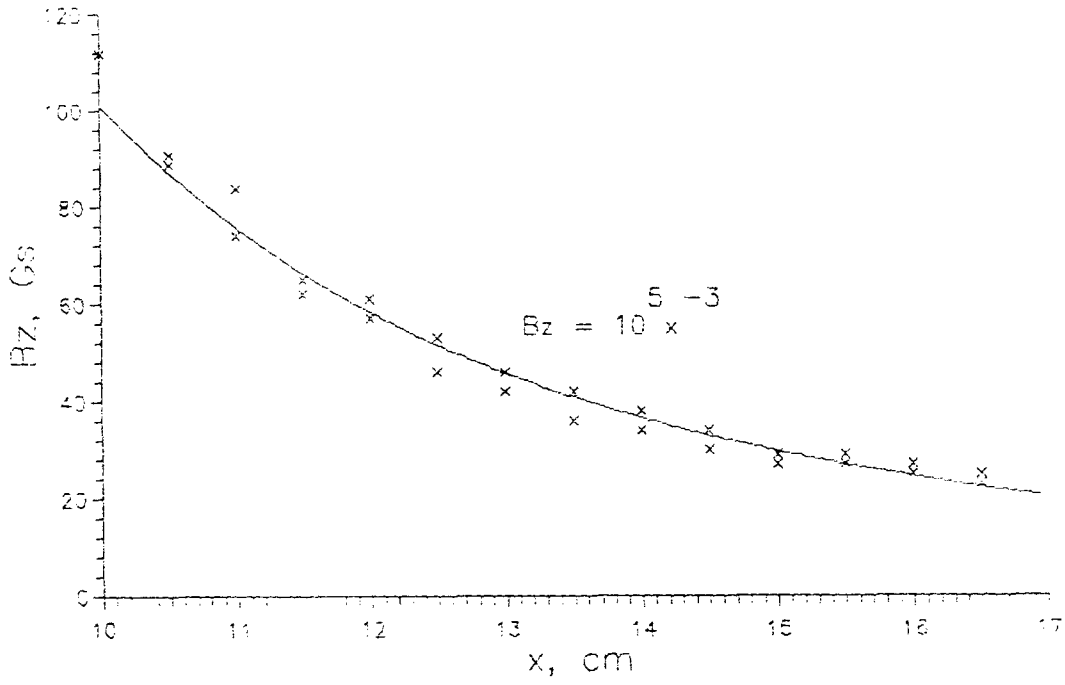

Fig.1.10

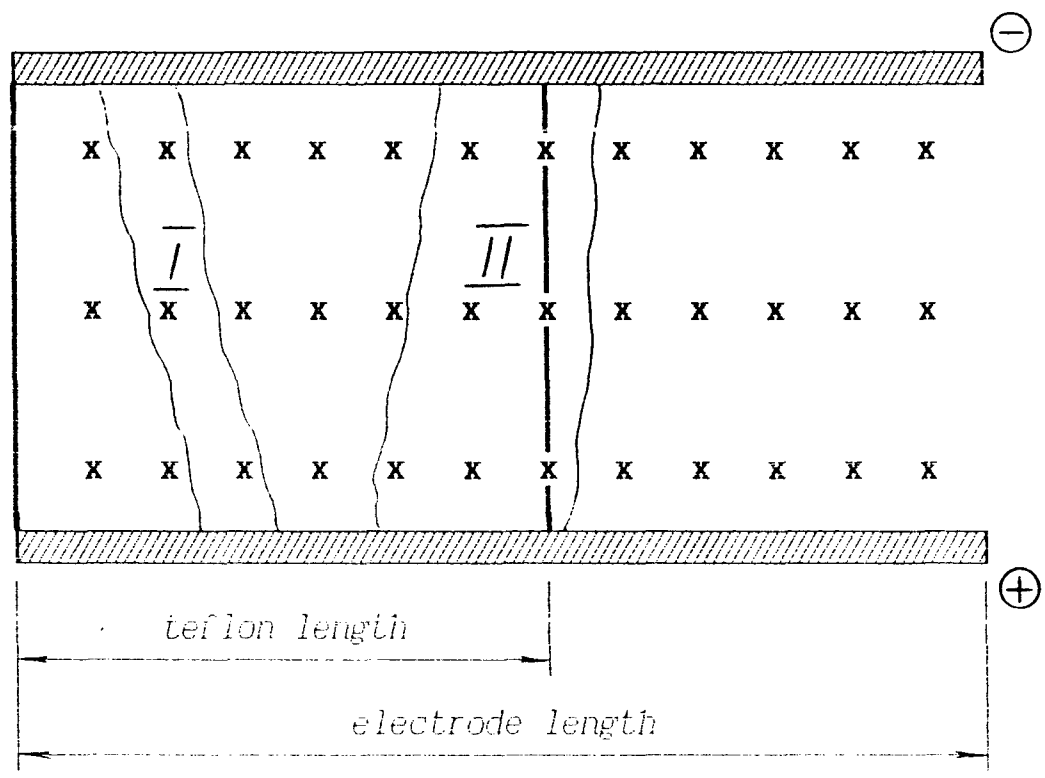

Fig.1.11

t ~ 0.5 mcs, and area II in which it burns from t ~ 1.7 mcs till the end of the first half-period. Current lines warp does not exceed the probes step, which corresponds to the current slope of not more than 10°.

Gentle slope of the current lines allows to use simple one-dimensional calculation model of currents distribution for the interpretation of the experimental measurements. The diagram of these currents distribution is given on Fig.1.12. The task is to find at any moment of time $j_{yi}(x)$ current distribution, which corresponds to the measured distribution of magnetic field $B_{zj}(x)$ and complete J(t) discharge current.

According to Bio-Savare-Laplace equation, magnetic field induction B_{zij}, created in point x_j by the i-th element of the calculation system of the currents is

$$B_{zij} = \frac{\mu_0 \cdot j_{yi}}{4\pi}\left[\frac{d}{(x_j - x_i)\sqrt{(x_j - x_i)^2 - (d/2)^2}} + \frac{4x_j}{d\sqrt{x_j^2 - (d/2)^2}} - \frac{4(x_j - x_i)}{d\sqrt{(x_j - x_i)^2 - (d/2)^2}}\right] \quad (1.4.2)$$

Total magnetic field in x_j point is:

$$B_{zj} = \sum_{i=1}^{n} B_{zij} \quad (1.4.3)$$

Calculated distribution of currents $j_{yi}(x)$ must create magnetic field $B_{zj}(x)$ which corresponds to experimentally measured field $B_{zj\ exp}(x)$ with a certain specified error. Besides, the desired currents distribution must correspond to the condition of:

$$J = \sum_{i=1}^{n} j_{yi} \quad (1.4.4)$$

Distribution currents function $j_{yi}(x)$ was found numerically by the method of local variations[14]. The method is of iteration character, where each iteration is transition from a certain function $j_{yi}(x)$ to the one close to it, better in the value of minimizing functional. Relative root-mean-square deviation S of the calculated

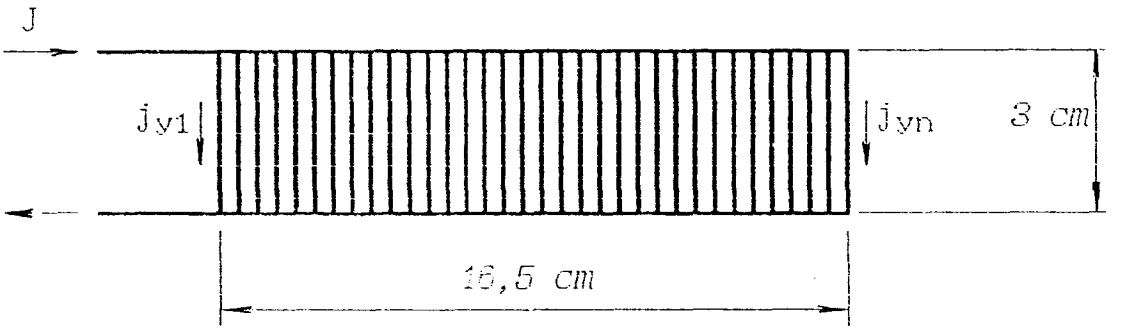

Fig.1.12

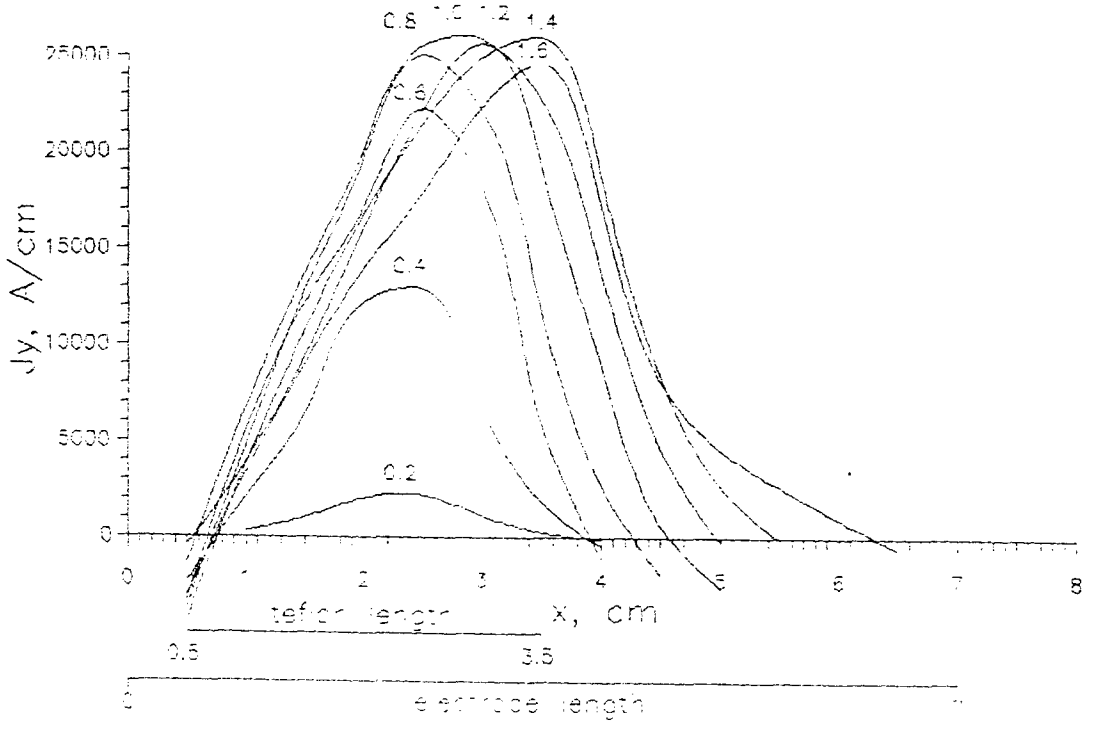

Fig.1.13

values of magnetic field B_{zj} from experimentally measured $B_{zj\ exp}$ was used as minimizing functional. It was calculated by the equation:

$$S = \sqrt{\frac{1}{n} \cdot \sum_{j=1}^{n} \left(\frac{2 \cdot \left(B_{zj} - B_{zj,\exp} \right)}{B_{zj} + B_{zj,\exp}} \right)^2} \qquad (1.4.5)$$

Method of local variations is one of the most universal and vastly used numerical methods of solving variational tasks of mathematical physics. Its drawback is a rather slow convergence, which can be usually improved using changing step of variation. Another drawback of the method is that it studies rather narrow set of functions neighbouring with the given one if it is optimal. The best one may fail to appear in this set, but it does not speak of this function as the best, and can be the result of the fact that algorithm does not study all its possible variations. Thus, if to speak strictly from the mathematical point of view, convergence of this method as well as all other numerical methods of solving variational tasks can not be proved[15]. That is why the correct choice of initial approximation is of great importance. In our case of calculation of current distribution $j_{yi}(x)$ using measured values of magnetic field $B_{zj\ exp}(x)$, current distribution in the previous period of time is a natural initial approximation. At that algorithm convergence improves considerably when the step in time Δt decreases. In our calculations $\Delta t = 0.2$ mcs is assumed.

There are two simultaneous conditions in our task which is a certain obstacle for the algorithm. The desired function $j_{yi}(x)$ must meet two following requirements:

1. Condition of the minimum of root-mean-square deviation, calculated on the equation (1.4.5);

2. Condition of preserving integrated current J (1.4.4).

Experimentally measured values J and $B_{zj\ exp}$ are involved in the (1.4.4) and

(1.4.5) equations. They are measured independently from each other by Rogovsky belt and by magnetic probe, which are calibrated with a certain error. The error usually does not exceed 10%. These errors usually make it difficult numerical agreement of conditions 1 and 2. Calculations can be simplified considerably if we use the fact that in the first half-period magnetic field practically coincides with the field of point magnetic dipole (1.4.1.) at large distance from the discharge (x>10 cm). Then the readings of all probes are normalized according to the readings of 5 the most distant ones. At that errors of calibrating of Rogovsky belt and magnetic probes are insignificant, because calculations are held in relative values. Unfortunately, in the second half-period this procedure is impossible, that is why the accuracy of calculations decreases considerably (see Appendix to the Report).

As it was mentioned above the inverse task of calculation the current distribution according to the obtained values of magnetic fields is mathematically incorrect. At present there exist approximate methods of solution of incorrect problems of mathematical physics[15]. All of them are reduced roughly speaking to adding one qualitative information about the solution to the task, for example, that the solution is a rather smooth function. Standard approach is adding small regulating additives to minimized functional $S[j_{yi}(x)]$. In our case the task of minimizing the sum is being solved:

$$S\left[j_{yi}(x)\right] + \alpha_1 \int_0^x \left(\frac{dj_{yi}}{dx}\right)^2 dx + \alpha_2 \int_0^x \left(\frac{d^2 j_{yi}}{dx^2}\right)^2 dx, \qquad (1.4.6)$$

where α_1 and α_2 are certain small positive figures, chosen so that regulating additives should not exceed in their total $0.1 \cdot S$. Such operation leads to the fact that among a set of functions of current distribution $j_{yi}(x)$ which practically do not

differ from each other as to the root-mean-square deviation of the calculated magnetic field from experimentally measured one, the preference is given to a more smooth one. Of course there is a certain subjective element, but it is inevitable at solving mathematically incorrect problems.

The described algorithm of one-dimensional calculations of current distribution on measured values of magnetic field is realized by our specialists in the form of a number of programs in FORTRAN-77 for the IBM PC–386. The results of the calculations in the form of the curves are presented in Appendix to the Report. By these curves the calculated values of the magnetic fields can be compared with the experimentally measured ones. Let us pass to the analysis of calculated curves of discharge current distribution along the acceleration channel.

Fig.1.13 presents the curves of current distribution from 0.2 to 1.6 mcs. The figure also shows the length of the working body Teflon bars and electrode length. In the initial moments of time (at $0.2<t<0.6$) the discharge burns approximately in the middle of the bars. At $t>0.6$ mcs it starts to shift and when the current is maximal ($t \sim 1.4$ mcs) it approaches the end of the bar. Current front rate is about 20–25 km/s. Such a rate agrees with the existing concept about freezing magnetic field, and consequentially, current lines into the plasma. At $t>1.4$ mcs the discharge current goes to the outer part of electrodes.

Curves which correspond to the attenuation of the current in the second half of the first half-period (at $1.6<t<3.0$), are presented on Fig.1.14. When current attenuates its considerable part goes to the outer part of electrodes and further. At that characteristic non-homogeneity of the current ("waves") also moves with the rate of about 20–25 km/s, which proves the freezing of the magnetic field into the plasma before the end of the first half-period. At the end of this period a certain

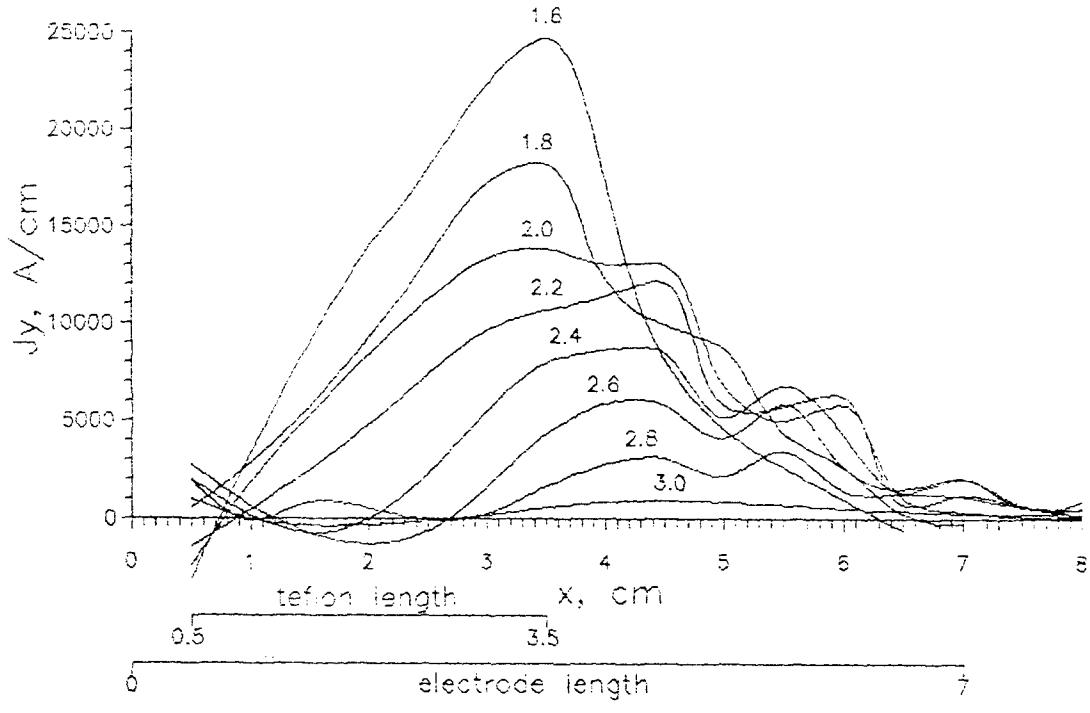

Fig.1.14

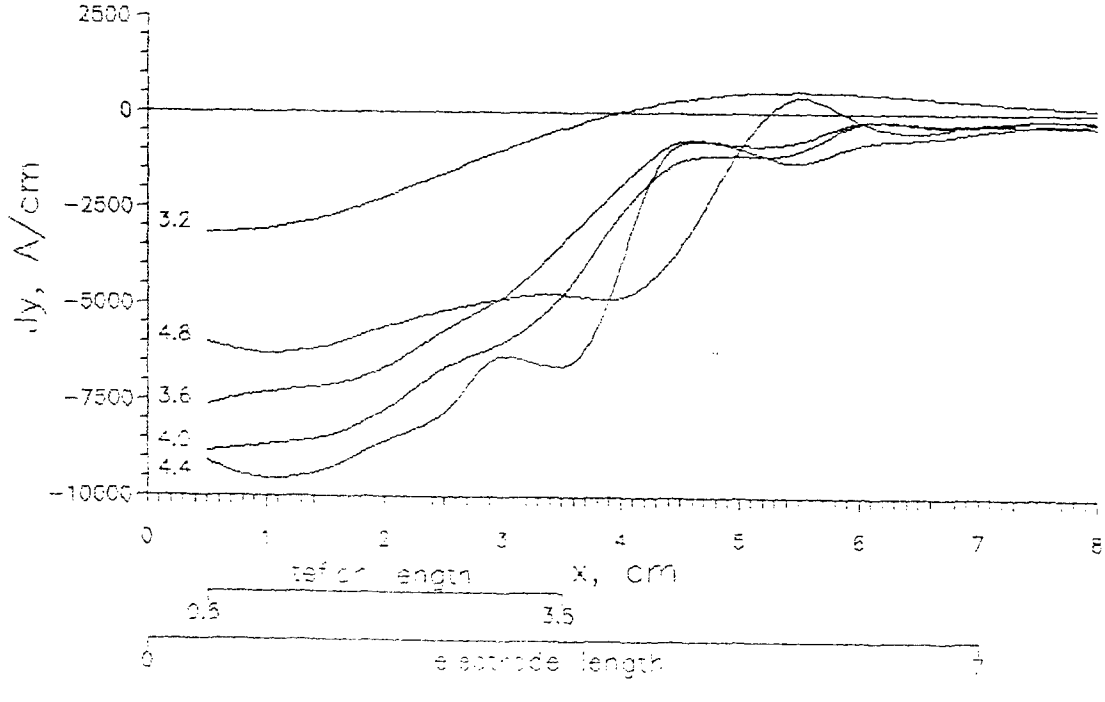

Fig.1.15

current vortex is formed in the discharge channel. It is preserved even at transformation of integral current into zero.

Distribution of currents in the second, negative half-period (at $3.2<t<4.8$) is shown on Fig.1.15. It is clear that during the whole second half-period current maximum is at the back insulator, and shift of current front towards the outlet from the acceleration channel is practically absent. It speaks of the absence of freezing magnetic field into plasma, and, consequently, about domination of thermal acceleration mechanism and not electrodynamic one.

Information about changes of inductivity in the process of discharge plays a great role in understanding the working processes in pulsed plasma accelerators of electrodynamic type. It is known[16] that effectivity of electrodynamic acceleration is proportional to the relationship $\Delta L/(L_c+\Delta L)$, where L_c and ΔL are constant and variable components of discharge circuit inductivity, respectively. That is why a unit calculating inductivity of the discharge channel at each moment of time was introduced in the program of calculations. Discharge channel inductivity L was found in the following way:

$$L = \sum_{i=1}^{n} \Phi_i \Big/ \sum_{i=1}^{n} j_{yi} \qquad (1.4.7)$$

where $\sum_{i=1}^{n} \Phi_i$ – is full current flow passing through the calculated area,

$\sum_{i=1}^{n} j_{yi} = J$ – is full discharge current.

The calculation results are presented on Fig.1.16 where two curves show the changes in discharge channel inductivity in the first and second half-periods. During each half-period inductivity grows monotonically, as it should be steming

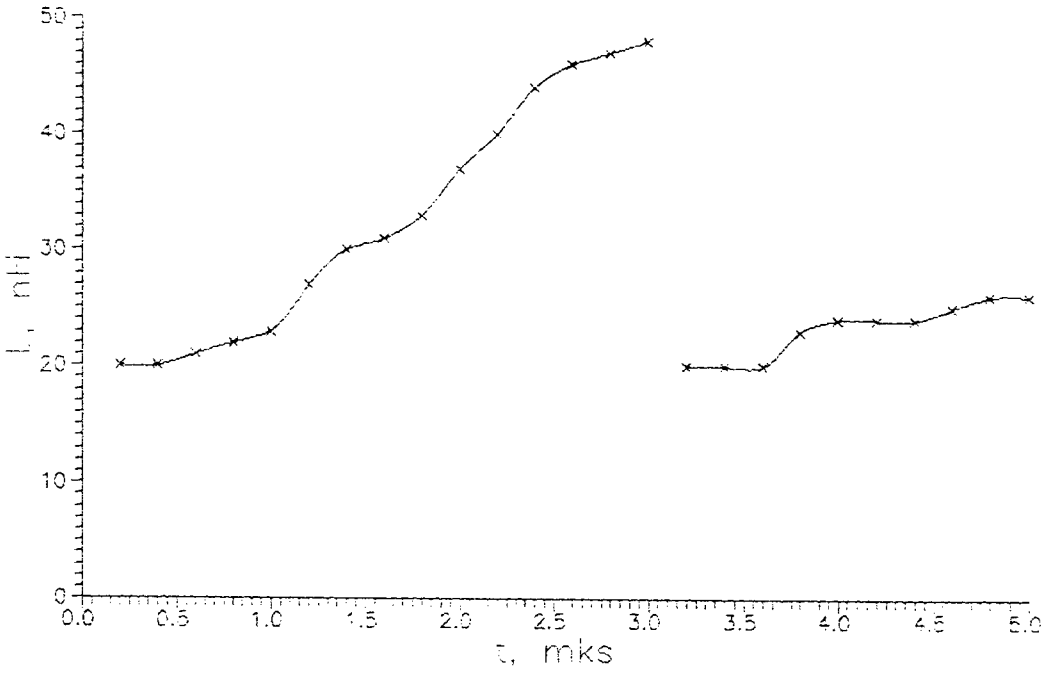

Fig.1.16

from the preservation energy law. As in the discharge circuit MPPT-1 $L_c \sim 30$ nH, in the first half-period $\Delta L/L_c \sim 0.5$, and in the second – $\Delta L/L_c \sim 0.14$. It speaks once again that the main contribution in plasma acceleration is made by the discharge first half-period.

At analysing the results of the calculation of the discharge current one should remember that we speak about the discharge channel diagnostics with magnetic probe introduced into it. Further on it seems reasonable to make such measurements with the probe placed outside the discharge channel based on our method of processing the results of magnetic-probe measurements.

2. CALCULATED STUDIES OF ELECTROTECHNICAL PARAMETERS INFLUENCE OF THE DISCHARGE CIRCUIT AND DISCHARGE CHANNEL GEOMETRY ON THE PPT CHARACTERISTICS

2.1. Possibilities of increasing PPT efficiency

One of the main tasks of improvement of PPT is raising its thrust efficiency which can be presented in the following way:

$$\eta_t = \eta_z \eta_k \eta_w \eta_p \qquad (2.1)$$

where η_z – outer efficiency which characterises energy losses in the outer circuit (matching of outer circuit parameters with load parameters), η_k – heat efficiency connected with energy consumption in the thruster design, η_w – kinetic efficiency which characterizes energy consumption for plasma formation, η_p – reactive efficiency, which characterizes energy consumption connected with spatial-temporal distribution of plasma formation rate.

According to [11] in real samples of the pulsed plasma accelerators these efficiencies have approximately the following values: η_z = 0.5...0.9, η_k = 0.8...0.9, η_w = 0.8...0.9, η_p = 0.4...0.7, η_t = 0.1...0.5.

It is clear that in order to raise PPT efficiency it is necessary first of all to obtain higher values of "outer" and "reactive" efficiencies.

To raise "outer" efficiency first of all energy losses in the outer circuit must be minimal, that is to decrease in any possible way resistance of the current-carrying busbars from the storage system (for the capacitor bank) to main discharge electrodes. And, second, to match outer circuit parameters with the discharge gap parameters.

Analysis of the PPT operation process without the forming line in the outer

circuit in electrodynamic approximation showed that thrust efficiency value is defined by two non-dimensional parameters[8].

$$\lambda_1 = C(dL/dz)^2/m_w L_o, \tag{2.2}$$

$$\lambda_2 = (dL/dz)^2/2m_w(R+R_o)^2, \tag{2.3}$$

where C – capacitor battery capacitance, m_w – specific mass outflow (plasmoid mass relationship to the value of supplied energy into the discharge), L_o – initial inductivity (current supply inductivity), (dL/dz) – linear inductivity of the discharge channel, R, R_o – plasma and current supply resistance).

First electrodynamic parameter can be written in the following way:

$$\lambda_1 = L/L_o, \tag{2.4}$$

where L = l(dL/dz) – effective inductivity of the discharge channel and l – characteristic acceleration length, which in practice can be defined by the size of visible zone of contact of discharge with electrodes.

The value of the specific consumption m_w speaks of the proportion between electromagnetic and gas-kinetic mechanisms of plasma acceleration in the discharge channel. The former depends on the value of magnetic pressure or of the current value to second power. The latter is defined through gas-dynamic pressure[8]. For Teflon at $m_w << 3 \cdot 10^{-9}$ kg/J electromagnetic mechanism of plasmoid acceleration prevails, which is fully realised in the end diagram of the PPT, where $m_w \approx 10^{-9}$ kg/J. Relationships (2.2), (2.3) are true for PPT with domination of electromagnetic mechanism of plasma acceleration.

PPT thrust efficiency increases with the increase of both parameters[8]. The first electrodynamic parameter defines the degree of agreement between outer circuit and accelerator parameters and grows when initial inductivity of the discharge circuit decreases whereas accelerator channel inductivity grows. In order

to provide effective acceleration mode acceleration channel inductivity must be much higher than the initial (spurious) inductivity of the discharge circuit. The second electrodynamic parameter confirms the said above concerning the necessity of reducing ohmic resistance of the current supplies to raise thrust efficiency. Linear inductivity of the discharge channel must be raised, but it must not lead to the proportional growth of plasma resistance.

Analysis of "reactive" efficiency in magnet-dynamic approximation for coaxial PPT showed that its theoretical value for aperiodic and quazi-stationary modes of the discharge can reach 0.7...0.8 when plasma jet aperture is up to 30 degrees[11]. Thrust efficiency at quazi-stationary discharge is about 15...20% higher than at aperiodic one. In the oscillation mode of discharge irregularity of velocities increases, and "reactive" efficiency will be lower. It happens because mass outlet slows down when discharge slides along dielectric surface (PPT with solid dielectric as a propellant is meant). Experiments show that characteristic period of time of this delay is about several microseconds. That is why transition to PPT operation in quazi-stationary mode is of interest, when discharge duration exceeds all other characteristic periods of forming the flow in the acceleration channel. The only characteristic period of time which can exceed discharge duration is the period of establishing of stationary heat mode of the electrodes. Transition to discharge quazi-stationary mode or mode close to it must lead to the increase of the thruster reactive efficiency as well as its thrust efficiency. Such transition can be performed through creation of a forming line, which provides aperiodic discharge (range of microseconds) or discharge close to quazi-stationary form (range of milliseconds). Approximation of the discharge form to quazi-stationary must lead to decrease of velocities spread and plasma jet aperture, to the increase of mean outflow velocity.

Besides these advantages quazi-stationary character of the discharge must provide regularity of heat flows in time, and as a result, regularity of erosion mass of the propellant in time, as well as raising the coefficient of propellant use.

It should be reminded that this theoretical conclusion was obtained for the coaxial PPT. As for the rail PPT, its quantity effect of thrust efficiency growth at transition to quazi-stationary form of discharge may be not so vivid. But obtaining aperiodic form of the discharge is vital even at stable value of the thrust efficiency, because this operation mode is preferable for the pulsed capacitors as far as the increase of their resource is concerned. At PPT long operation on board of the space vehicle its resource is as important as thrust efficiency.

The purpose for this calculation study is examination of the influence of the discharge contour electrotechnical parameters and geometrical dimensions of the PPT discharge channel on its integral parameters, as well as forming line parameters influence on the discharge current oscillogram form.

2.2. Calculated model of the PPT

Calculated study of the PPT was held in the frames of the so called balanced mathematical model where homogeneous and equilibrium plasma occupying a certain effective plasma volume substitutes spatially non-homogeneous plasma formation in the discharge channel. The size of this volume depends on geometrical dimensions of the discharge channel and its localization area. The size of the localization area depends on the proportion between magnetic and gas-dynamic pressures; the value of this proportion can be considered as the main factor of spatial non-homogeneity of plasma in the discharge channel. Spatial non-homogeneity affect on plasma resistance in the channel and its other parameters is

taken into account through introduction of supplementary factors of non-homogeneity. Mathematical description of the operation process was held in the frames of the following physical model. The main mechanism of propellant supply into the discharge channel is connected with emission absorption in the front layer of the dielectric and molecules destruction[12]. Emission flow density to the wall follows Stephan-Boltzman law. In the discharge neutral particles are ionized by electron shock. Plasma is three-particle (atoms, ions and electrons), isothermal and equilibrium and has Maxwell distribution function. Atomic weight of "heavy particles" (atoms, ions) is equal to mean atomic weight of dielectric erosion products. The term "mean energy of chemical boundaries splitting" in the working body, as well as mean energy of heavy particles ionization. Plasma conductivity is attributed by electron-ion collisions. Evaporated stuff is considered to go into the discharge channel without delay in time. It is also assumed that kinetic energy of plasma jet is an additive function of electromagnetic and gas-dynamic mechanisms of acceleration[13].

The examined mathematical model is described by the closed equation system without attracting empirical dependencies and coefficients for certain modes of PPT operation. As for the introduced non-homogeneity factors, they are specified by analytical equations for each PPT type. Equation system was solved by numerical method on IBM PC. In the process of check calculations expressions for all non-homogeneity factors were defined while energy supplied into the discharge changed from dozens to hundreds of Joules.

On the basis of mathematical model the method for calculation and optimization of integral parameters of the rail PPT with cross-sectional or longitudinal supply of propellant bars. The calculations of plasma mean parameters

in the PPT discharge channel with different plasmoid acceleration mechanisms were held. Comparison of calculation results with experimental data showed their satisfactory agreement.

Disadvantage of the offered model is the use of the supposition about "immediate" outflow of mass from the propellant bar surface after absorption of radiant energy from plasma. It does not permit to draw conclusions on the quantitative level about discharge duration affect on the PPT integral parameters, while experimental data are absent for the specific thruster. That is why for different proportions of inductivity and capacitance in forming line sections only oscillograms of the discharge current were calculated in order to show the possibility of obtaining aperiodic form of the discharge at chosen thruster energetics.

2.3. Calculating analysis of the influence of discharge circuit and discharge channel geometry on PPT characteristics

In the present study the object for calculating analysis is the rail PPT with the cross-sectional supply of propellant. Its diagram is given on Fig.1.2. Discharge channel is formed by electrodes of the main discharge, side bars of solid dielectric (Teflon), end ceramic insulator. Igniter is introduced into the discharge channel through the hole in the cathode. While Teflon is evaporated from the bars ends in heavy-current pulsed discharge, the bars are shifted till they stop into the step with the help of the spring pushers. Electrodes of the main discharge are connected to the capacitors by the forming line.

The behaviour of integral characteristics of the thruster with the concentrated parameters (without the forming line) were studied with the help of the said above

mathematical model of the PPT, depending on current supplies inductivity – L_o, linear inductivity of the acceleration channel, geometry of the discharge channel, capacitor battery capacitance and stored energy. Linear inductivity of the discharge chamber was changed by varying the distance between the electrodes in the range of 30...60 mm with the channel 17 mm wide and rail 40 mm wide. For capacitor bank energy of 60, 80 and 100 J current supplies inductivity was changed in the range of 5...35 nH, whereas capacitance was in the range of 25...160 mcF.

Fig.2.1,4,6 present calculated dependencies of the PPT integral parameters on initial inductivity (inductivity of leading busbars) for capacitor battery capacitance which is 25 mcF, and initial energy of 60, 80, 100 J respectively. Fig.2.5,7 show the influence of initial inductivity on the discharge channel oscillogram. The results back the conclusion obtained on electrodynamic model[8] about improvement of thrust characteristics at lowering initial inductivity. As it stems from the presented curves, when initial inductivity decreases from 35 nH to 5 nH, thrust efficiency grows from (7...8)% to (11...12)%, whereas thrust impulse is constant. The thrust efficiency grows at the expense of decrease of mass outflow per impulse. It is interesting to note that with the growth of energy at the expense of raising initial voltage, relatively rapid growth of the efficiency starts at lower value of the initial inductivity. Fig.2.2,8,10 show calculated dependencies of the PPT integral parameters on linear inductivity (the distance between electrodes) for initial inductivity of 15 nH and capacitance of 25 mcF. In contrast to initial inductivity, linear inductivity influences both thrust impulse value and mass outflow per impulse. Thrust efficiency and effective outflow rate increase practically linearly with the increase of the distance between electrodes. At capacitor bank energy of 100 J the maximal calculated value of efficiency is 12%, and effective outflow rate

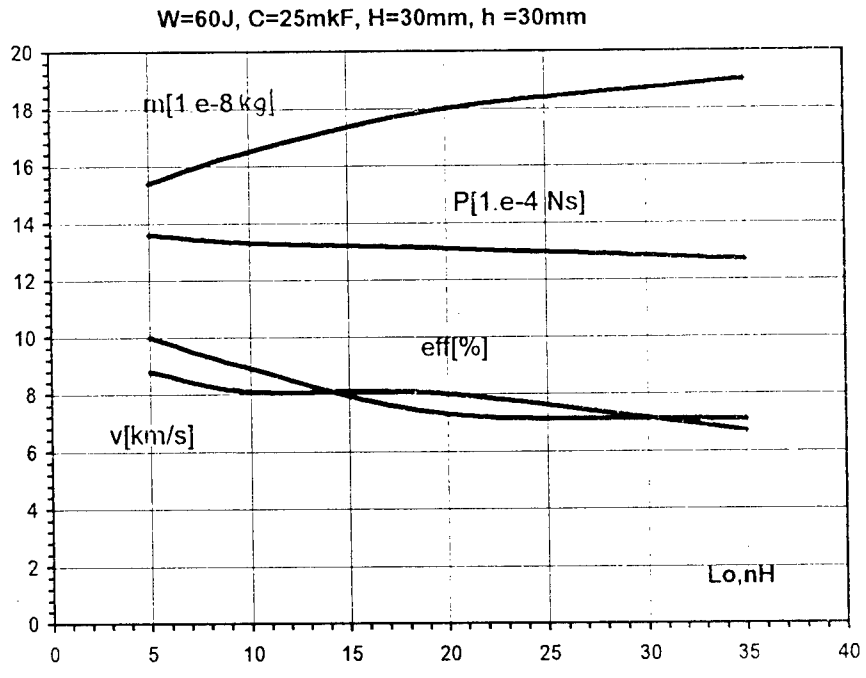

Fig.2.1. PPT integral parameters

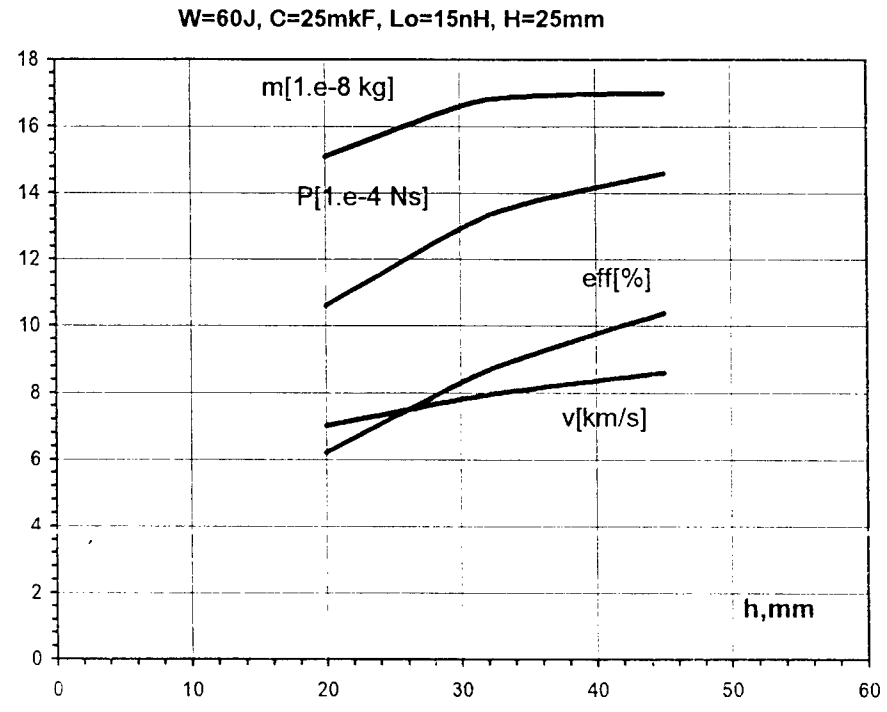

Fig.2.2. PPT integral parameters

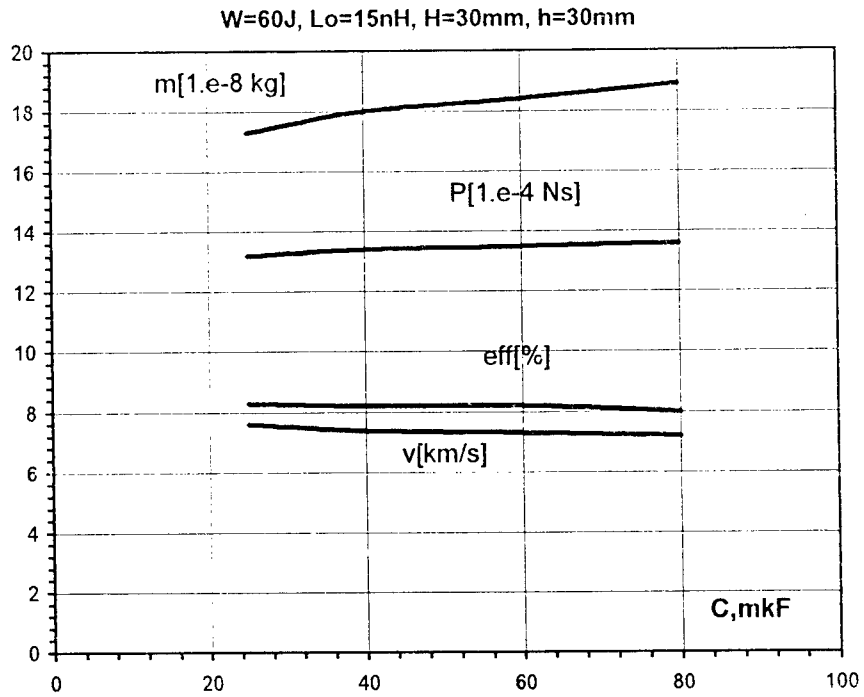

Fig.2.3. PPT integral parameters

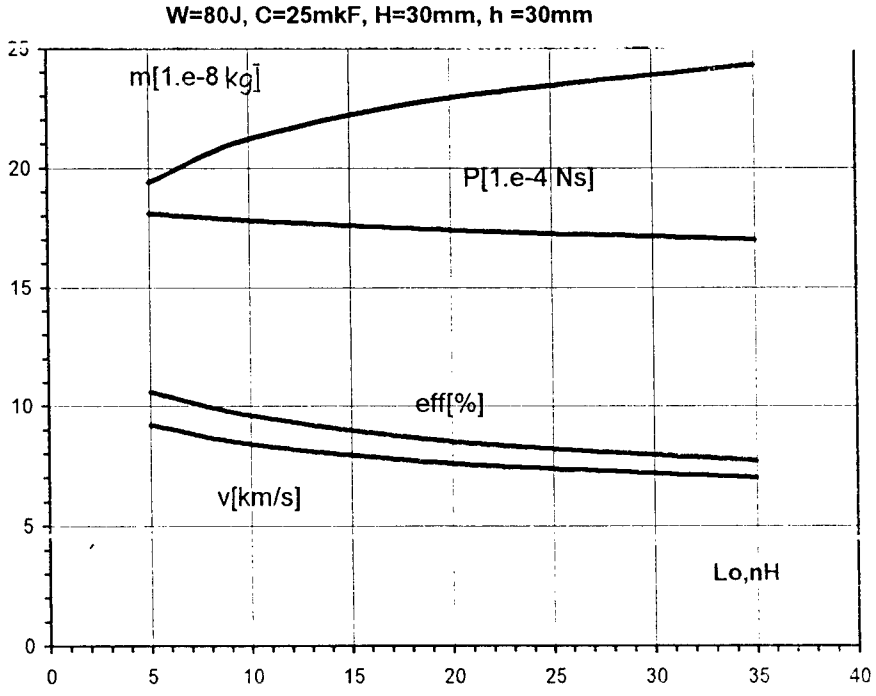

Fig.2.4. PPT integral parameters

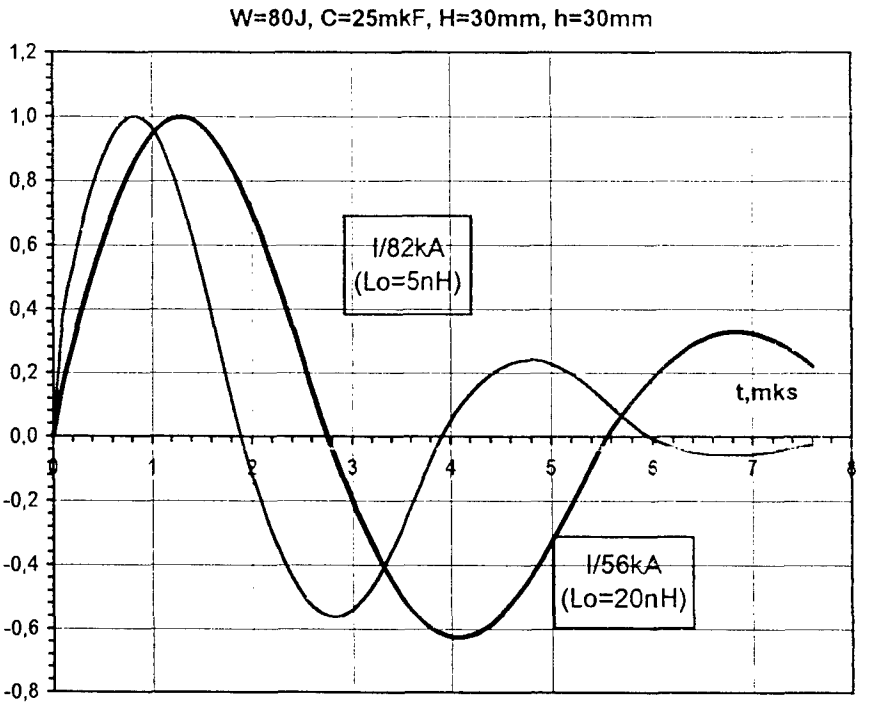

Fig.2.5. Discharge current

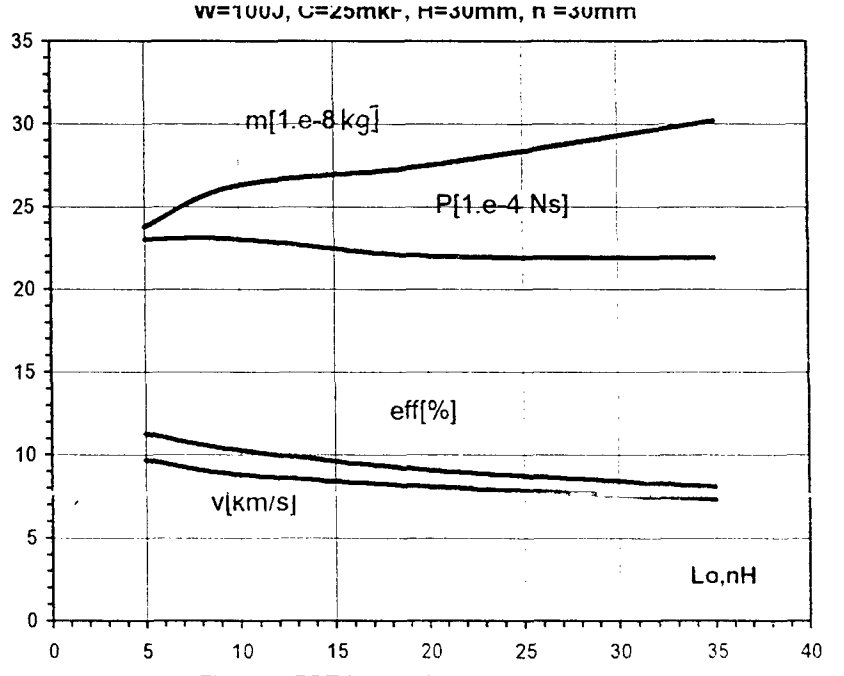

Fig.2.6. PPT integral parameters

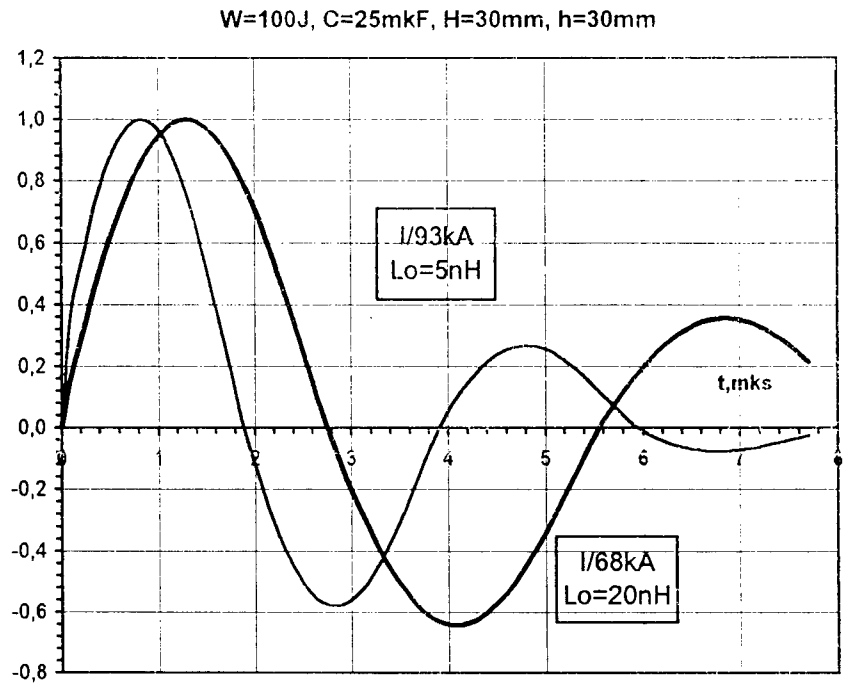

Fig.2.7. Discharge current

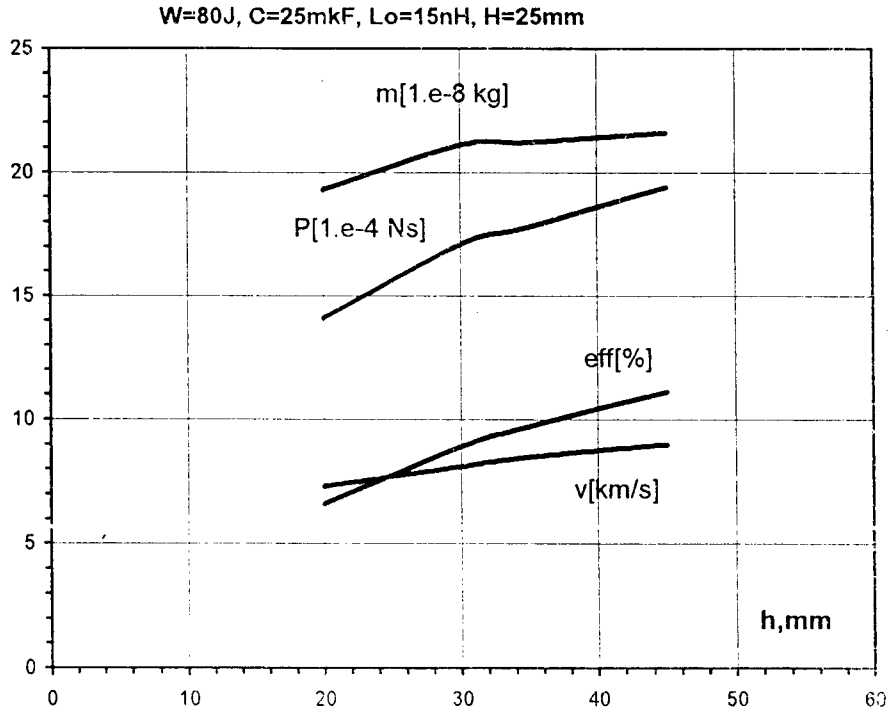

Fig.2.8. PPT integral parameters

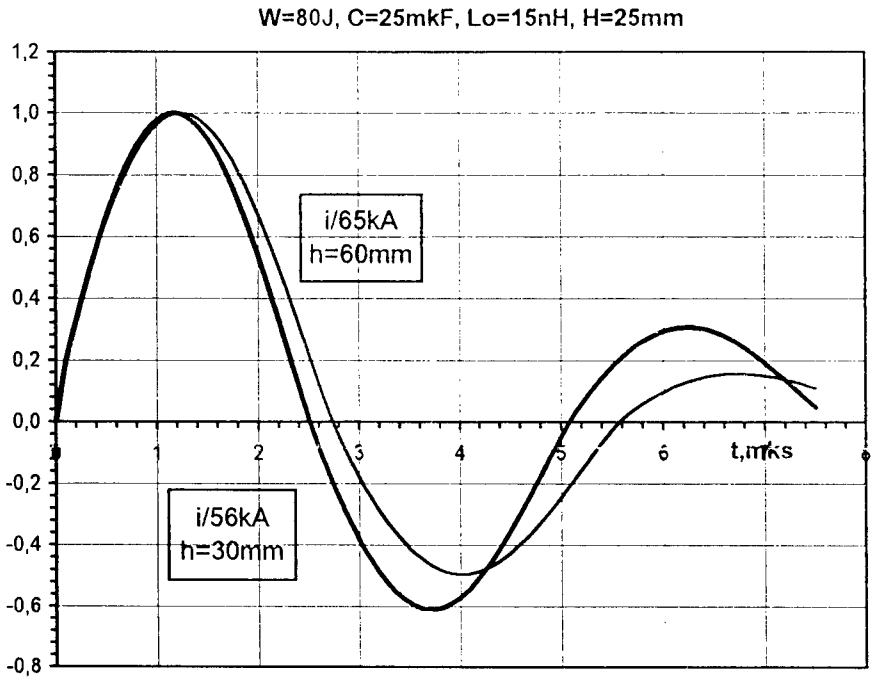

Fig.2.9. Discharge current

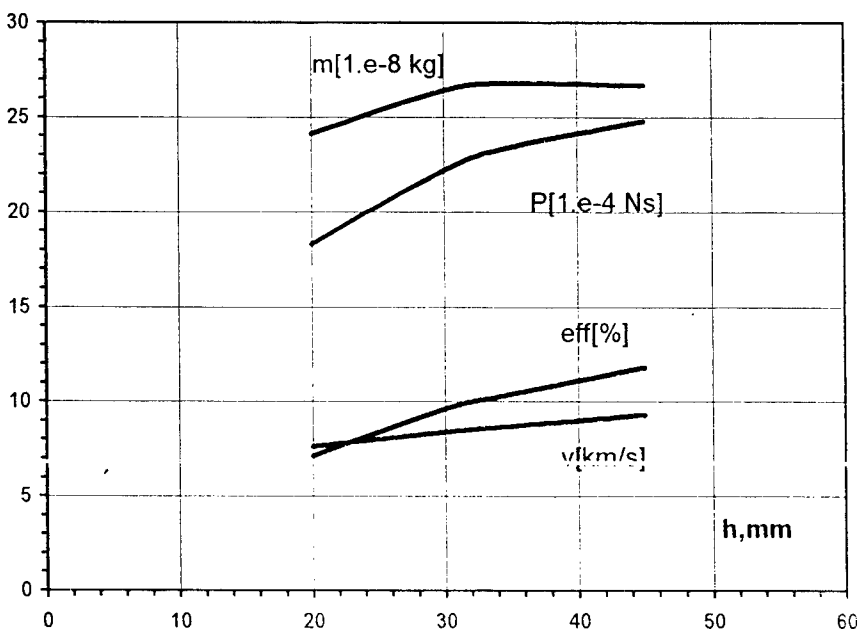

Fig.2.10. PPT integral parameters

is 9 km/s. Comparison of discharge current oscillograms given on Figs.2.9,11 shows increase of attenuation with the growth of linear inductivity.

Thus, transition to aperiodic discharge by lowering initial inductivity or increasing linear inductivity leads to growth of thrust efficiency. This result coincides with the conclusion made from electrodynamic model of PPT, presented in Chapter 2.1.

Calculated influence of storage system capacitance at initial inductivity of 15 nH on the PPT integral characteristics of the PPT are presented on Figs.2.3,12,14. Capacitor battery capacitance influence on the oscillogram form of the discharge current is presented on Fig.2.13. As it stems from the presented graphical materials, transition from oscillatory to aperiodic form of discharge at the expense of increasing capacitance practically does not influence the PPT specific parameters – thrust efficiency and effective outflow rate. It follows from the electrodynamic model, because capacitance is not used in the equations (2.3), (2.4). It is not surprising, because electromagnetic plasma acceleration in the presented PPT model is described in the frames of electrodynamic approximation.

On Fig.2.15 the calculated dependencies of the PPT integral parameters on the bars width – H, are presented (see Fig.1.2), which practically coincides with the discharge channel depth. Diminishing of the channel depth from 25 mm to 10 mm leads to the drop of mass outflow per impulse (from 0.22 mg to 0.14 mg), and decrease of the thrust impulse. At that electromagnetic mechanism share in plasma acceleration increases (see relationship P_i/P on the Figure). It is supported by the increase of mean mass plasma flow rate up to 11.5 km/s. If initial inductivity is 15 nH, thrust efficiency practically does not change and remains (11...12)%.

The PPT integral parameters dependencies on the discharge channel width –

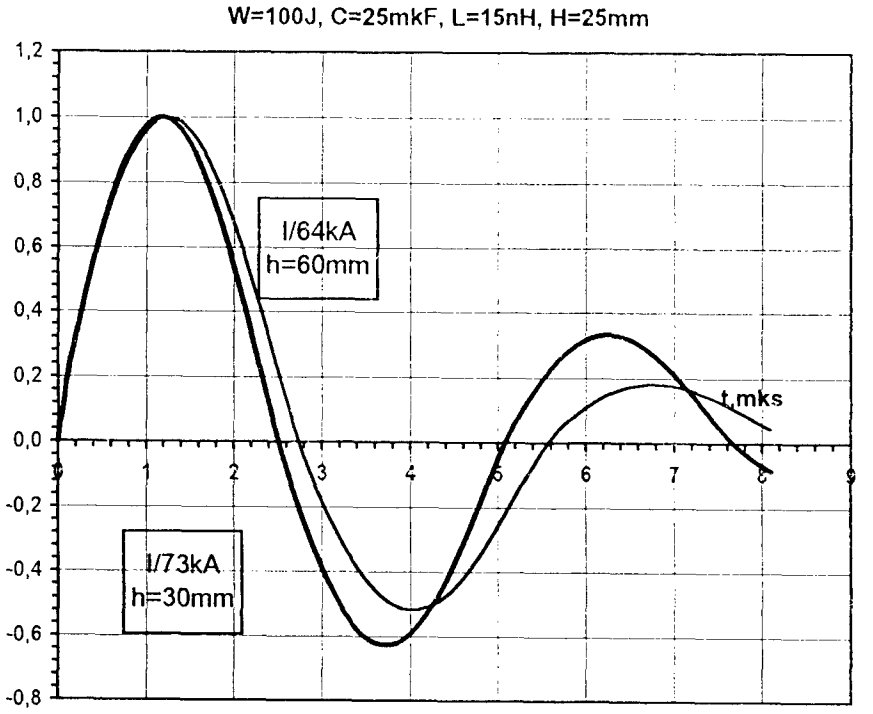

Fig.2.11. Discharge current

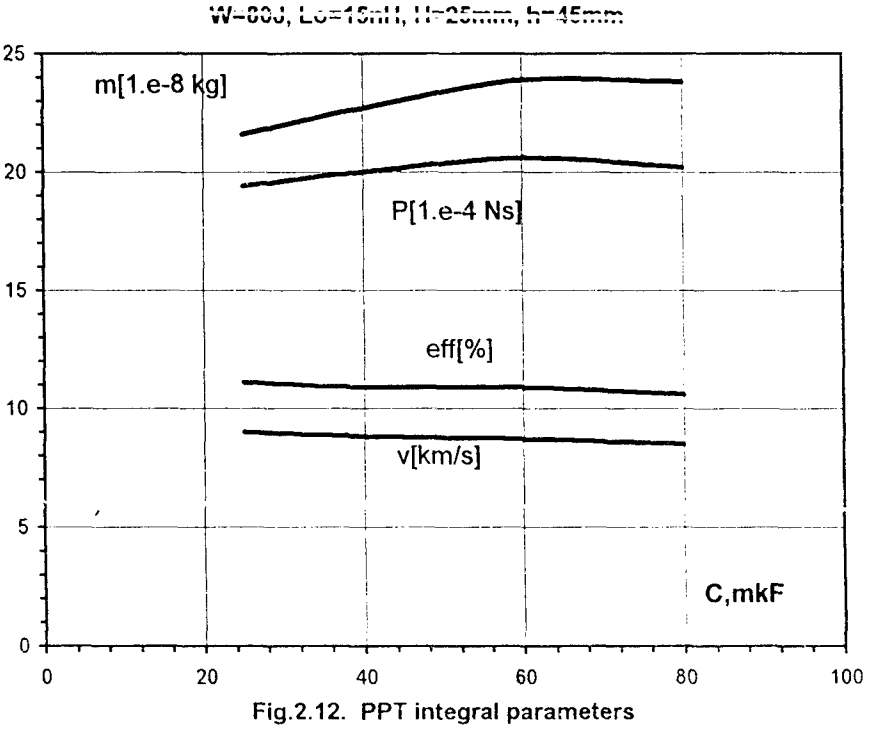

Fig.2.12. PPT integral parameters

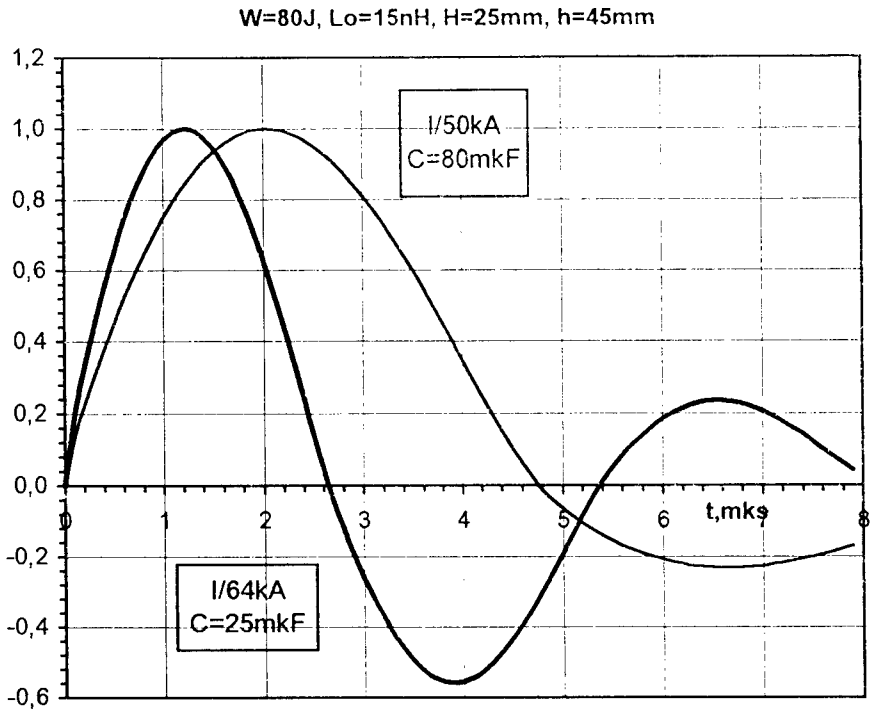

Fig.2.13. Discharge current

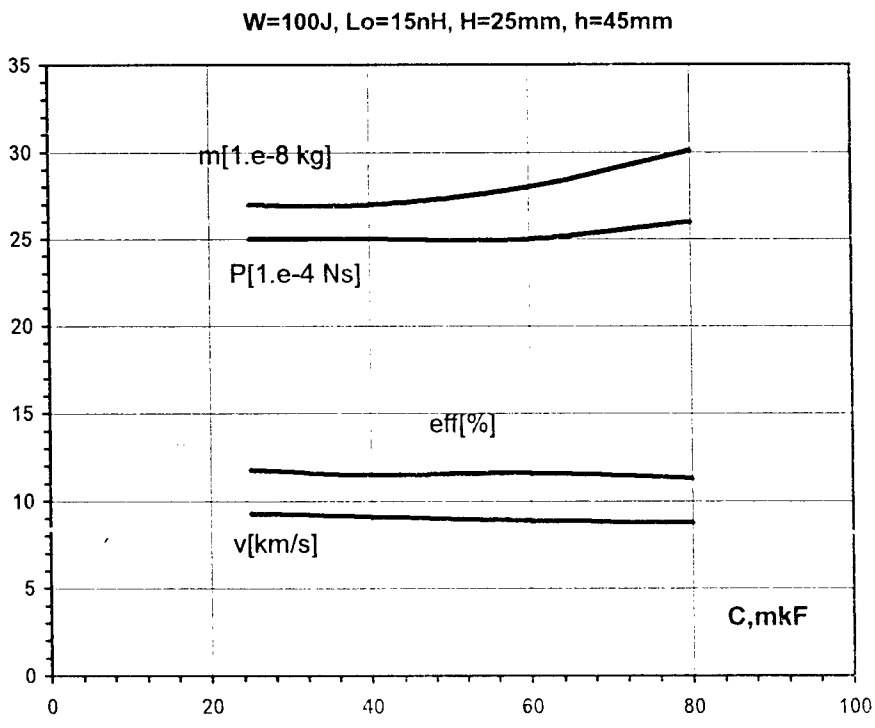

Fig.2.14. PPT integral parameters

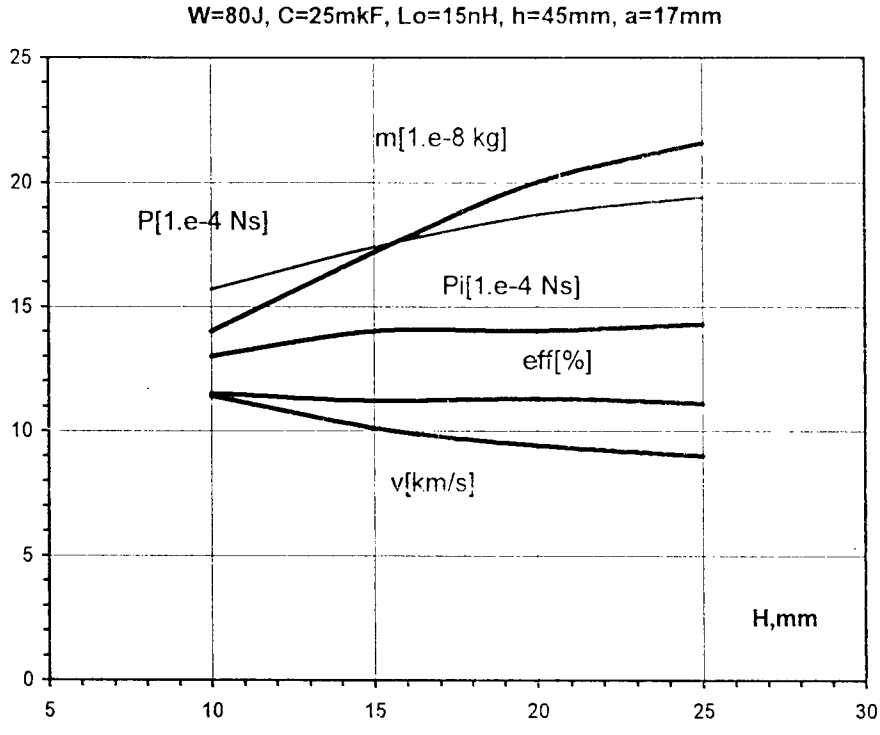

Fig.2.15. PPT integral parameters

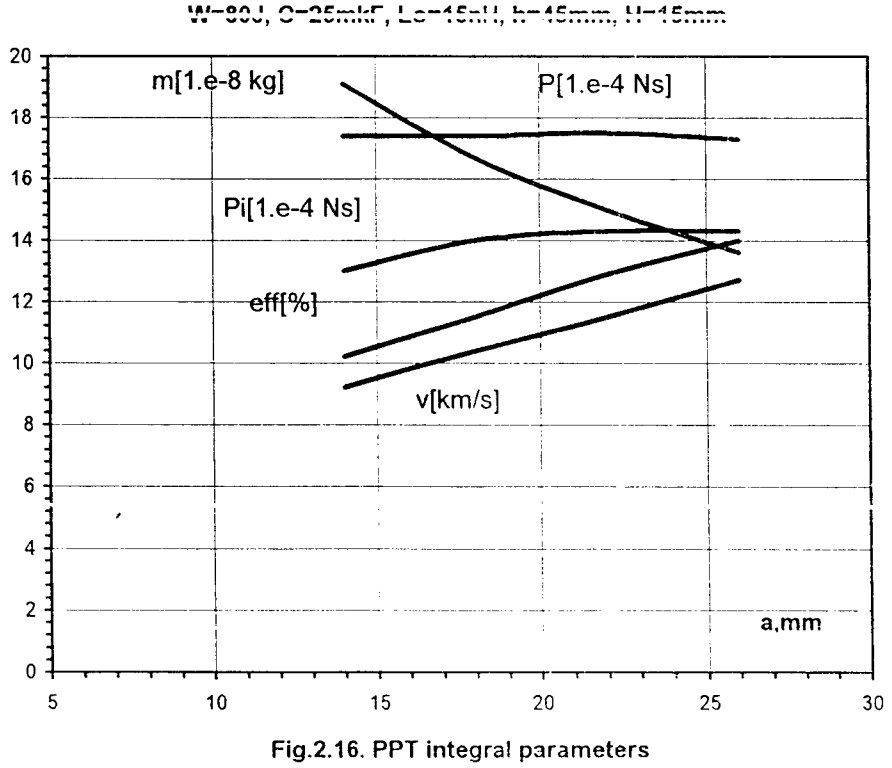

Fig.2.16. PPT integral parameters

a, are presented on Fig.2.16. Widening of the discharge channel leads to the decrease in mass outflow per impulse. Thrust impulse does not change, that is why thrust efficiency increases. Electromagnetic mechanism share in plasma acceleration increases a little. When the discharge channel is 26 mm wide calculated value of the thrust efficiency is about 14%, and mean mass outflow rate of plasma flow is about 13 km/s.

Thus, calculated analysis of the PPT showed the possibility of obtaining thrust efficiency of 12...14% when energy in the impulse is 80...100 J, and presented the ways of realization of these parameters. If it is true, only the experiment on a certain thruster model can show. Unfortunately not all calculated predictions can be put into practice. For example, it is impossible to widen considerably the discharge channel because carbon film deposits on the surfaces of the propellant bars, when energy density in the channel is lower than the critical one.

Figs.2.17...2.23 show oscillograms of the PPT discharge current with various L-C parameters of the forming line at constant stored energy of 80 J, and stable distance between electrodes of 45 mm. Inductivity of current supplies coming from capacitor bank to electrodes L_o is 10 nH in calculations. Resistance in the forming line stages is 1 mOhm. These values of inductivity and resistance are not crucially low for the laboratory model of the PPT, but are quite acceptable for the flying variant of the thruster for design reasons.

Figs.2.17...2.21 show comparative oscillograms of the PPT discharge current with one- and two-stage RLC-contours. It is clear from the pictures that the use of two-stage forming line allows transition from harmonious damping oscillogram with current pulsation in the range of each semi-period, when total storage capacitance is constant. Inductivity L_1 in the second stage of the forming line was chosen so

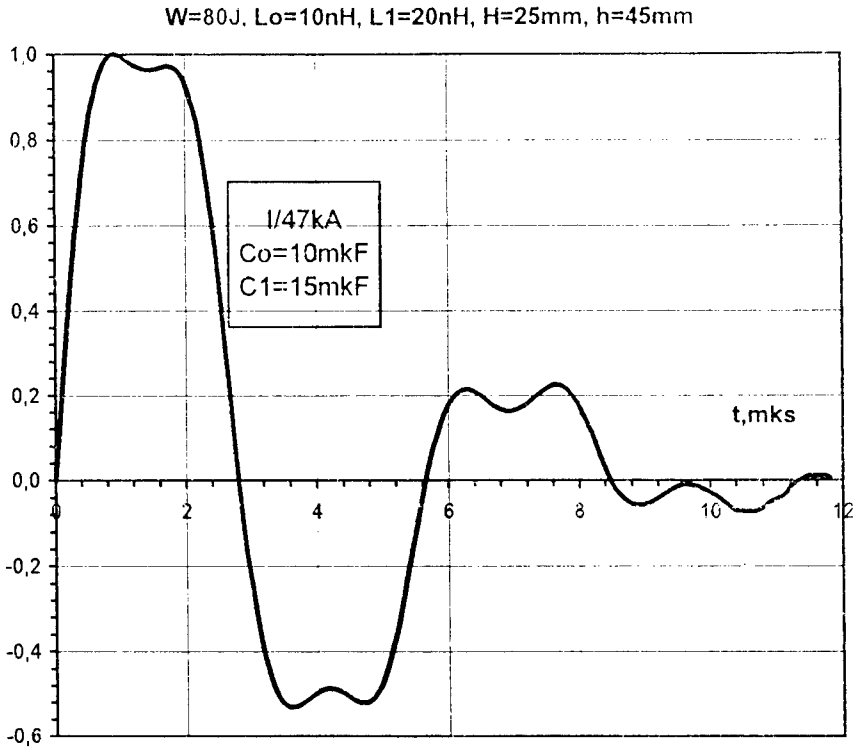

Fig.2.17. Discharge current

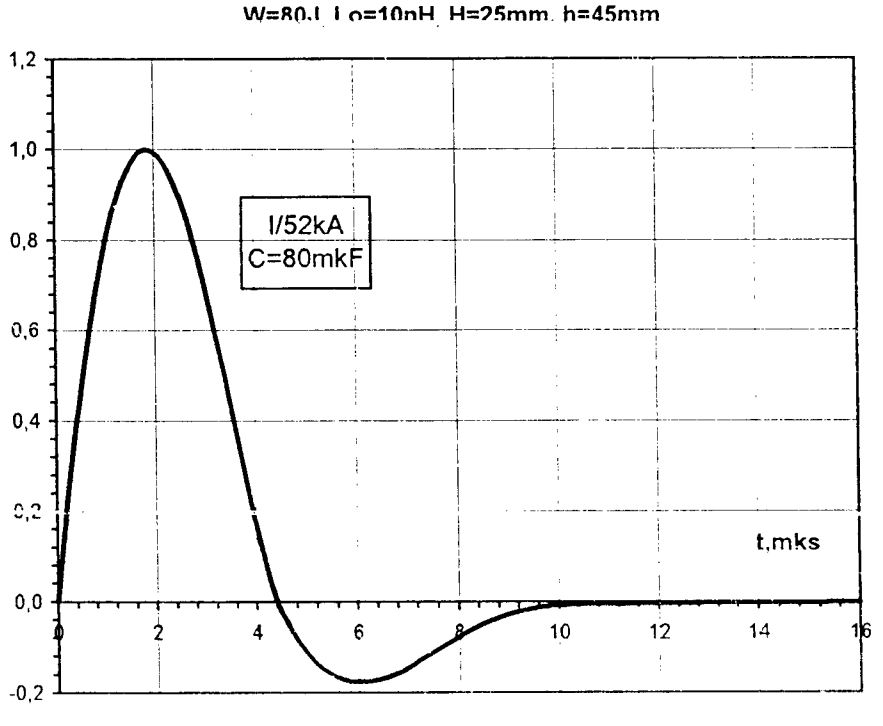

Fig.2.18. Discharge current

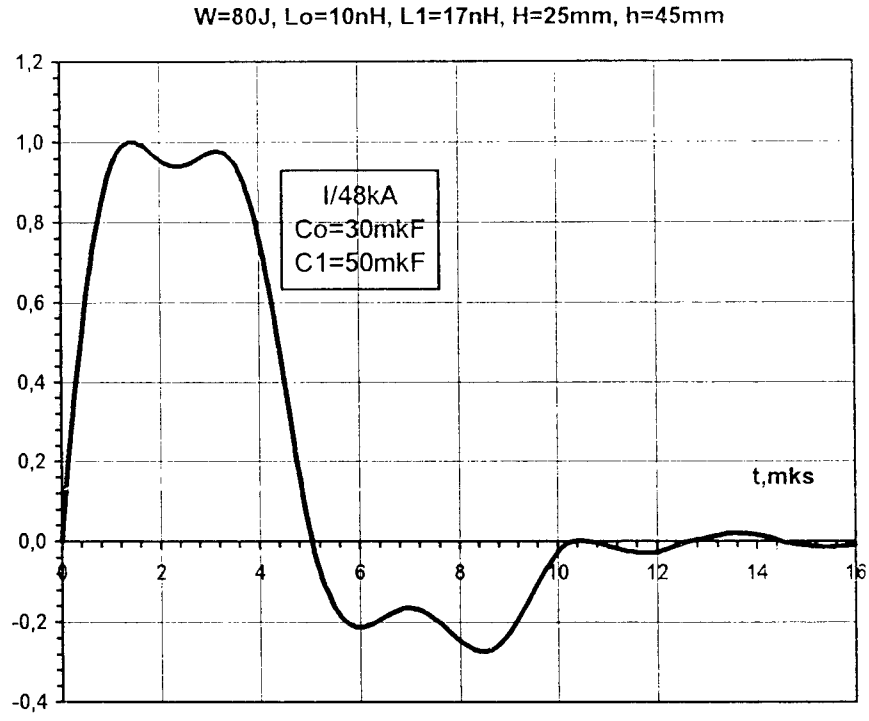

Fig.2.19. Discharge current

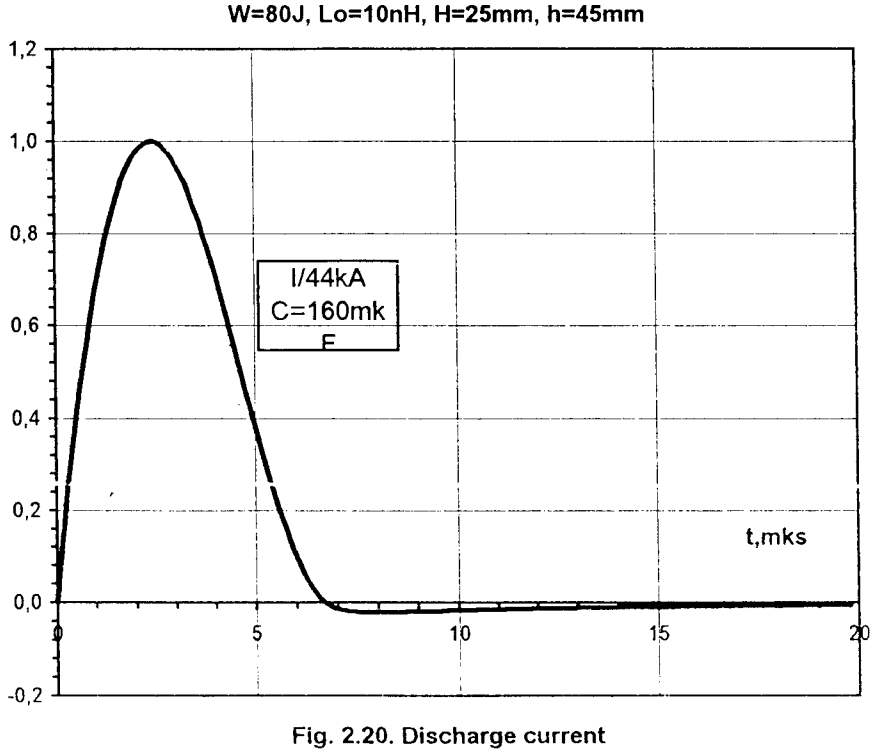

Fig. 2.20. Discharge current

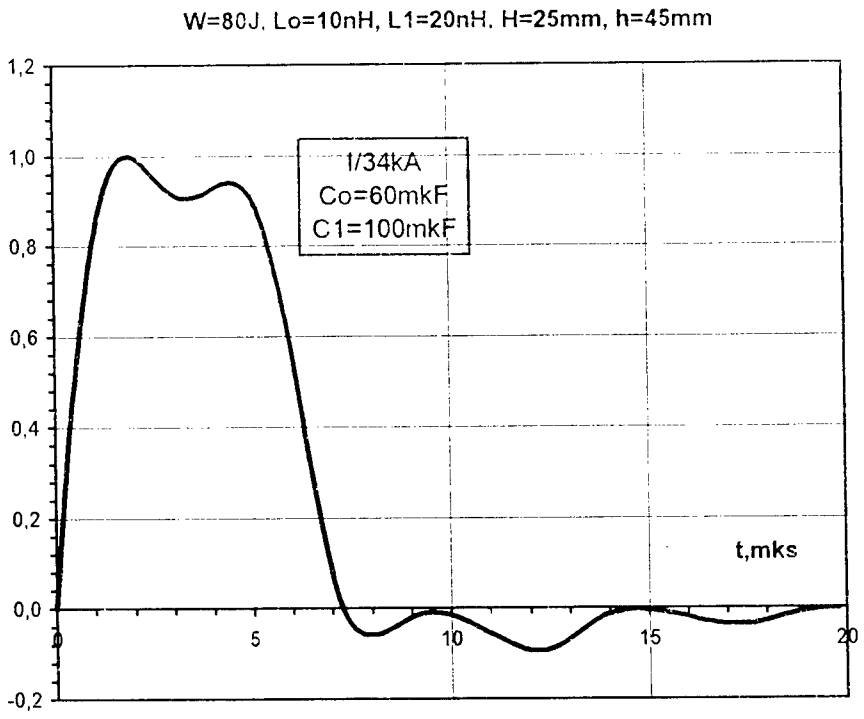

Fig.2.21. Discharge current

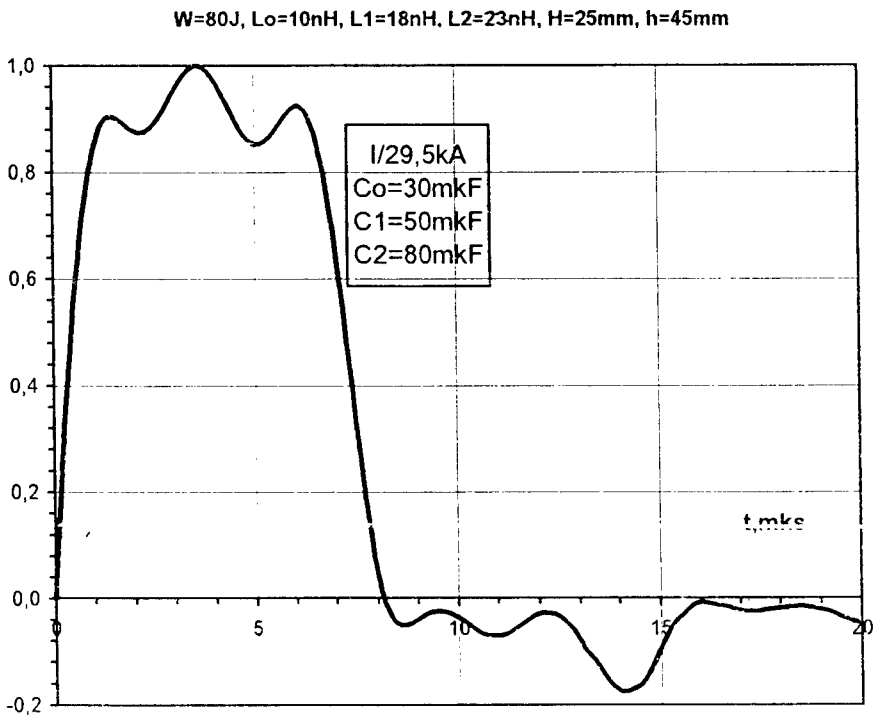

Fig.2.22. Discharge current

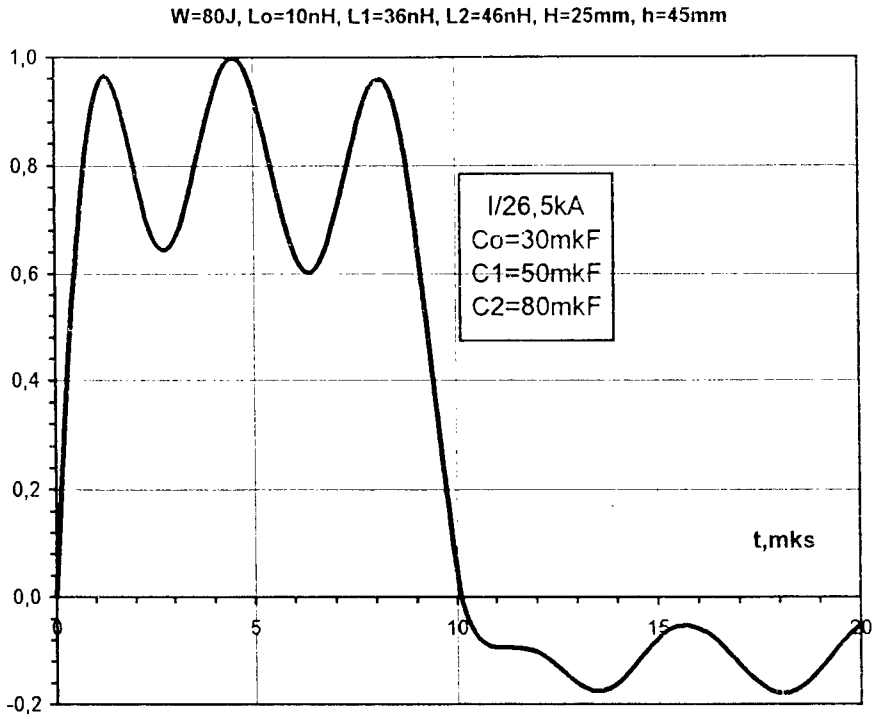

Fig.2.23. Discharge current

that to provide pulsation amplitude not more than 10% from the maximal value of the discharge current. The number of pulsations in each semi-period is equal to the number of stages of the forming line, which in this case is equal to 2. The analysis of the presented calculated oscillograms shows that the use of two-stage forming line does not allow the transition from periodical discharge to aperiodic one without increasing total capacitance; more than that – current amplitude in the second semi-period increases. Duration of the first semi-period increases a little at the expense of introducing inductivity L_1, but gradients of increase and decrease of the current practically do not change. Thus, according to the current oscillogram transition to the two-stage forming line leads to splitting of each semi-period into two, while the area under the current curve is preserved.

On Figs.2.20,23 the comparative oscillograms of the discharge current with one-, two- and three-stage RLC-contour are presented at total capacitance of 150 mcF in order to provide the discharge close to aperiodic one. It is evident that the number of pulsations on the first semi-period correspond exactly to the number of stages in the forming line. On Figs.2.21,22 inductivities in the second and third stages were chosen under the condition of obtaining 10% pulsation amplitudes. On Fig.2.23 inductivities in the second and the third stages were doubled comparing to the Fig.2.22. As it is seen it leads to the increase of pulsation duration and their amplitude while the area under the current curve was preserved, which is equal to the capacitor bank charge – $(C+C_1+C_2)U_0$.

Thus, for the chosen energetics and geometry of the PPT with the cross-sectional supply of the propellant, the parameters of the RLC-contour were defined in order to provide the discharge form close to aperiodic.

Some conclusions and recommendations

1. In order to obtain maximal PPT thrust efficiency initial (spurious) circuit inductivity must be considerably lower than the acceleration channel inductivity, which in the studied thruster is evaluated about (14...18) nH. For the presented PPT design diagram initial inductivity can be cut down to the value of (10...15) nH. At reasonable increase of height and width of the discharge channel and decrease of its depth the thrust efficiency grows. According to the evaluations, for the traditional PPT diagram (see Fig.1.2) with the cross-sectional supply of the propellant bars (Teflon) at energy in the impulse of 80...100 J the thrust efficiency can be expected of about 12...14%.

2. As the calculations showed, in the frames of the presented mathematical model, transition to the aperiodic discharge at the expense of increasing the capacitance does not influence the thrust efficiency, but it demands experimental tests.

It is unreasonable to use the forming line without increasing total capacitance for the PPT with periodic discharge (in order to transit to aperiodic discharge).

3. DEVELOPMENT AND STUDY OF PULSED PLASMA THRUSTER MODULE (MPPT-3)

3.1. Pulsed Plasma Thruster (MPPT-3) design

Pulsed plasma thruster (PPT) module MPPT-3 consists of: storage and supply system unit (SSS) of the working body (Teflon); discharge chamber unit; energy storage unit and discharge initiation unit (DIU). All the components of the thruster are placed in one body.

Fig.3.1. shows the design diagram of the MPPT-3 thruster and its basic elements.

Since the study model of the thruster failed to face the demands on minimal mass-size characteristics and on providing the required thermal mode at long-term frequency operation, while working on the design its authors stuck to the simplicity of the module, easiness of substitution and reconstruction of the PPT elements.

The basic load-bearing member of the structure is a round fiber glass laminate plate (1) to which all the elements (units) of the thruster are fixed. The plate is connected with the bottom plate of the PPT (2) by means of four hollow members (3) with the diameter of 10 mm. They form rigid construction of the "squirrel cage" type. Outside this construction non-load-bearing cylindrical enclosure (4) is placed between the load-bearing plate and the bottom. This enclosure is made of sheet duralumin 0.8 mm thick. The enclosure isolates the thruster elements from plasma influence injected by the thruster.

SSS of the working body is placed between the load-bearing plate and upper lead of the thruster module. It consists of the working body bars (5) and rotation spring (6) which moves the bars into the discharge channel area while the bars are

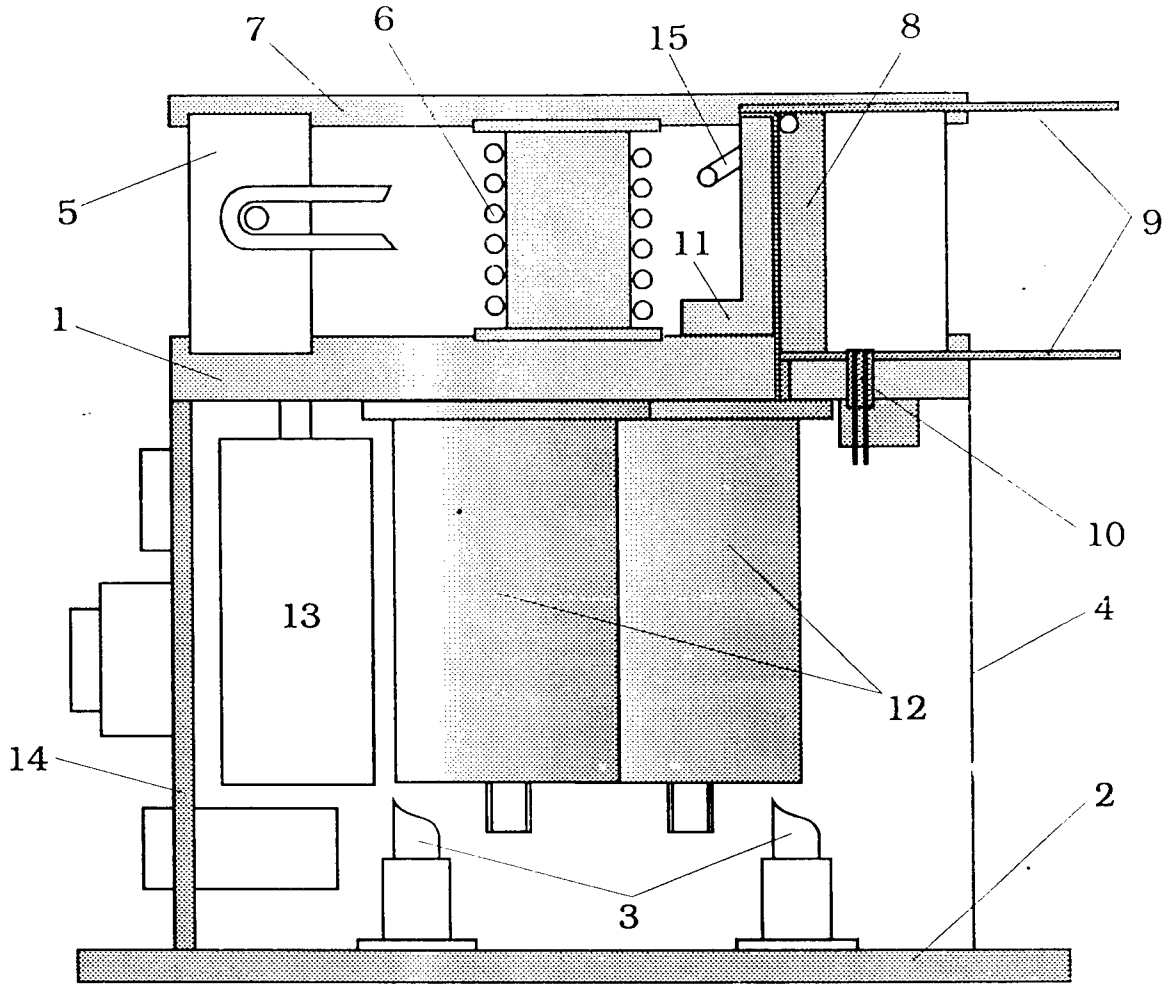

Constructive scheme of MIPD-3 thruster.

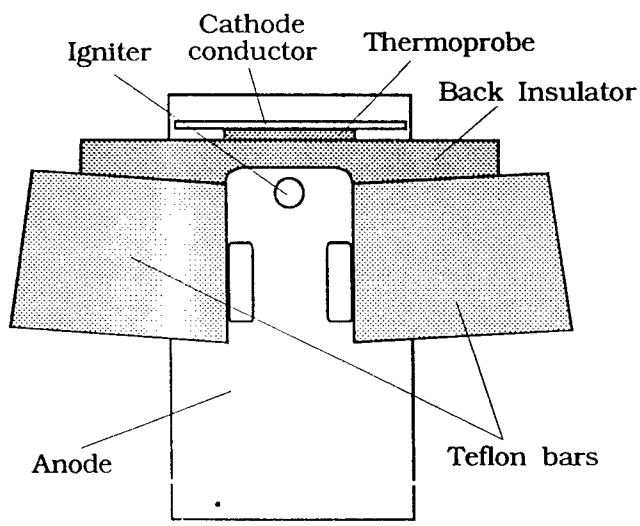

Horizontal cross-section
of discharge chamber.

Fig.3.1.

being worked out. The bars are made as two semi-rings with maximal outer radius of 128 mm and radial cross-section of 45x25 mm. Working body storage is expected for $5 \cdot 10^6$ PPT operations. Two circular grooves with the width of 1.5 mm and depth of 3 mm are made on the outer cylindrical surfaces of the bars to eliminate electrical self-breakdowns along the outer surface in the electrodes area.

The rotation spring is made of the steel wire with the diameter of 1.5 mm and is winded on the central grommet with the diameter of 30 mm, which connects the load-bearing plate with the thruster lead (7). The force from the spring to the bars is sent through the stops fixed in the non-operating back ends of the bars. During the operation the bars move in the azimuth direction to the stop on the anode along the circular slide guides.

Discharge chamber unit is formed by the working ends of the Teflon bars, back insulator (8) and thruster electrodes (9). The unit also includes the main discharge initiating igniter (10) put in the anode area. In the thruster model the initial width of the discharge channel (distance between the working ends of the Teflon bars) is equal to 20 mm, and its height (the distance between the electrodes) is 45 mm. Channel length formed by the bars working surfaces is 25 mm. The back ceramic insulator made of boron nitrite, has the working surface turned into the channel. This surface has the concave groove thus forming the precombustion chamber with the maximal depth of 3 mm. In order to eliminate the electrical self-breakdowns along the conducting metal-carbon layer which can form on the surface of the precombustion chamber in the process of PPT operation, the transverse slots with the width of 1 mm and depth of 1.5 mm are made. In order to provide the structural strength the thickness of the insulator back wall was not less than 4 mm taking into account the transverse slots. Precombustion chamber serves

to form the stable plasma cord in the initial part of the discharge channel. It prevents carbon layer from deposition on the bars working surface in the area of their contact with the ceramic insulator. While assembling PPT the back insulator is raised to the inner surfaces of bars with the help of the stop (11'), and this structure helps to take up gaps between insulator and bars, and the tightness of the discharge chamber is provided from the point of view of plasma passing through these gaps. The stop (11) is also a fastening element for the cathode. In order to eliminate electrical self-breakdowns along the surface of mating the end ceramic insulator and inner cylindrical surface of bars two rectangular steps are made on their contact surface.

The main discharge electrodes are made of copper with the width of 34 mm and thickness of 3 mm. The working body of the electrodes is flat. The length of the part of the electrodes bulging out of the working body bars is equal to 30 mm. It was chosen on the basis of the previous experiment so that it would be approximately equal to the length of the flux carry-over traces which form on the electrodes after long PPT operation. In the precombustion chamber area anode has a hole with the diameter of 4.8 mm for igniter injection. Anode has a steps against the bars ends. The length of the steps is 10 mm.

Energy storage unit consists of 5 pulsed capacitors (12) with parallel switching. Their total capacity is equal to 25 mcF designed for the maximal operational voltage of 2.8 kV. Thus maximal accumulated energy in the battery is about 100 J. Capacitors are placed according to honeycomb diagram which provides the densiest packing. That means that there is a chance to obtain minimal inductivity of the switch. But since the said thruster allowes to install three various types of capacitors (with the body diameters of 65, 50 and 40 mm), the structure of the hexahedral

current collector through which the capacitor's switch to the anode busbar is performed and the capacitor is fixed to the load-bearing plates is a little bit large for the capacitor with the diameter of 50 mm set in the presented model of PPT. Capacitors switch is performed through two flat copper busbars 0.6 mm thick (cathode busbar) and 1.0 mm (anode busbar). Teflon film 0.2 mm thick is used as insulator between current-bearing busbars, to which they fit snugly.

DIU (13) is designed to form short pulses with the voltage about 30 kV. DIU is compiled according to the three-electrode diagram, and there is a possibility to use it in the two-electrode variant. High-voltage pulses are supplied to the igniter electrodes in order to initiate the main discharge. DIU is fixed to the load-bearing plate (1) between the capacitors unit and the back plate of the thruster (14).

Igniter is introduced through the hole in the anode into the discharge channel very close to the back wall of the precombustion chamber. Igniter has a ceramic tube made of aluminium oxide which has a diameter of 4.5 mm with lengthwise holes with the diameter of 1 mm. In these holes igniting copper electrodes are placed. When the two-stage (three-electrode diagram) initiation diagram is used, the third DIU lead is connected with the hollow copper cylinder, which becomes the third ignition electrode. The working end of the igniter does not bulge out the anode surface. Plasmoid which ignites the main discharge, is formed as a result of high-voltage break-down along the carbon film deposited on the igniter operational surface from the main discharge. The choice of proportion of the discharge initiation and main discharge initiation allowed to provide dynamic stability of carbon film thickness on the igniter working end and to eliminate its erosion.

Electric connectors through which switch of the thruster module with the PPU, as well as output of the signals from the Rogovsky belt and temperature-

sensitive element are performed, are placed at the back plate of the thruster (14). The plate is fixed between the main load-bearing member and the module bottom, and is a supplementary reinforcing element of the structure.

Although the questions of heat extraction were not examined in detail while constructing the PPT, nevertheless the possibility of heat extraction from the capacitors bodies through fixing heatextracting metal plate on the threading places in the bottom part of the capacitors was studied. This plate is switched through the thin dielectric film to the bottom of the thruster unit so that good thermal conductivity contact and reliable electrical insulation is provided.

Experimental environment and diagnostic equipment

Experimental trial of the MPPT-3 thruster was held in the vacuum chamber with the volume of 2 m^3. Remaining gas pressure was not more than 0.01 Pa. Precombustion pumping off of the test-bench was performed with the mechanical two-piston pump VN-6. High evacuation was performed with the oil-diffusion pump VA-8-4. Main operational voltages to the thruster (2.5 kV for charging the main energy storage and 1.3 kV for charging initiating system capacitor), as well as impulses to start the thruster in the process of PPT laboratory trial were supplied from the test-bench power supply system.

The thruster operated both in the mode of separate impulses and contiguously with the impulses recurrence frequency of 0.5...2 Hz. At frequency operation of the thruster the number of impulses in the series was $(1...3) \cdot 10^3$.

In the process of experimental trial initial voltage on the capacitor battery and oscillograms of the thruster discharge current were registered, its average thrust at frequency mode was calculated periodically. After several series at operating age

about $(2...4) \cdot 10^3$ impulses weighting of working body bars was performed in order to determine working body consumption per impulse. Besides the control of temperature mode was determined at various cyclograms of work. Also measures of bars wear-out profiles during the whole experimental trial were taken.

Recording of the discharge current was made with the help of the digital oscillograph. The signal from the Rogovsky belt (№15 on Fig.3.1.) which embraced the cathode busbar in the cathode area, was supplied to the digital oscillograph input. Signal output from the belt was performed with the help of coaxial cable through the connector placed on the back plate of the propellant unit. In order to integrate the signal the RC-integrator was connected into the coaxial circuit outside the vacuum chamber. Sensitivity of the Rogovsky belt with the integrator was 17 kA/V.

Average PPT thrust was measured with the help of the thrustmeter with the direct effect. Design diagram of the thrustmeter is presented on Fig.3.2. The thrustmeter consists of the stationary frame (1) on which movable platform (3) is hung on three steel strings (2) with the diameter of 0.6 mm and 70 cm long. The studied thruster (4) is situated on the platform.

The thrust measures were held in the following way. The platform moves in the direction opposite to the plasma jet injection due to the thrust created by the thruster. The thrust at frequency mode is $P_t=I*f$ (where I – thruster draft impulse, f – frequency operation). At small angles of strings deviation as it is in the given thrustmeter, the platform shifts in horizontal direction (along the Z axis). Shift value is fixed by the change of the gap between the inductive sensor (D) and the plate made from the magnetically soft stuff, fixed rigidly on the platform. In order to damp the platform spurious oscillations which can arouse because of the

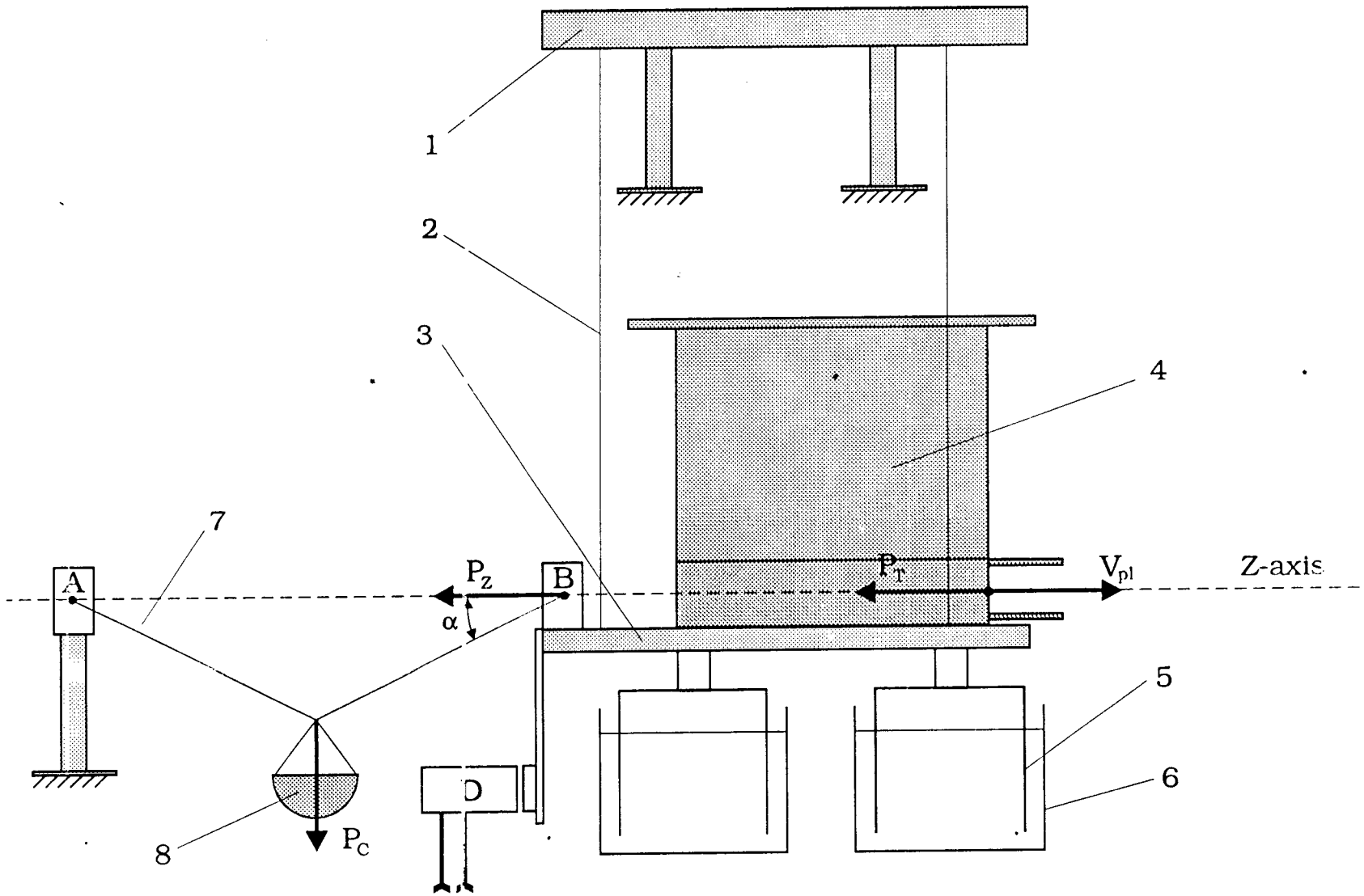

Fig.3.2. Scheme of thrustmeter and calibration system.

vibrations of vacuum chamber and pulsed operation of the thruster, and in order to quiet the thrustmeter platform after measures, two glasses (5) made from thin steel are fixed on the platform, and are placed into the glasses (6) of a larger diameter, which are filled with the vacuum oil.

Evaluations made according to the simplest mathematical simulation assuming that the said thrustmeter can be regarded as a simple pendulum, showed that at PPT operation frequency more or about 2 Hz the measured values exhibit an error of not more than 3%. This error is attributed to the pulsed (and not stationary) mode of thrust application.

Absolute value of the thrust is defined while the thrustmeter calibration. In order to do that a string (7) was tightened between the platform and stationary bracket, in the middle of which a cup (8) is fixed. At tuning the thrustmeter it is necessary that points A and B were on the axis Z, that is the axis of PPT thrust vector. Then at a certain angle α calibrating force P_c is equal to force P_z which while calibrating is applied to the platform along Z-axis and simulates thrust P_t. It is not difficult to calculate this angle – it is equal to 26.56°. Calibrating force P_c is created by putting into the cup (8) one or several weights (in the described experiments the weights with the mass of 0.33 g were used). Calibrating is made when the vacuum chamber is evacuated just before measuring PPT thrust and after measuring if necessary.

Total error of thrust measuring with the help of the described device is not more than 5%.

In order to estimate the working body consumption per impulse bars were weighted on the analytical balance before and after the series of several thousands impulses. Weighing accuracy is 1 mg, which at the working body consumption

during the series not less than 200 mg corresponds to the working body consumption measures per impulse not worse than 0.5%.

Effective velocity of plasmoid outflow and thruster efficiency were calculated on the data of thrust pulse and mass consumption per impulse.

Thruster temperature control condition was held with the help of thermal resistance placed in one of the most thermal stress areas of the thruster unit – on the cathode busbar near the back wall of the end ceramic insulator (see Fig.3.1.). Temperature-sensitive element resistance is 50±0.3 Ohm taking into account the resistance of commuting wires with environmental temperature of 20°C. Thermal resistance sensitivity is 0.18 Ohm/ °C. Temperature sensitive element resistance was made with the digital ohmmeter with accuracy 0.01 Ohm.

Temperature measures were taken while frequency mode operation of PPT with frequency of 0.5 and 1 Hz, and while non-operating thruster cooling in vacuum and when air was supplied into the vacuum chamber.

3.2. Experimental studies of MPPT-3

The main tasks of experimental studies of MPPT-3 were:

– tests of operation of the discharge channel with the height h=45 mm in the supplied energy range of 60...100 J;

– the studies of the influence of the width - a and depth - H of the MPPT-3 discharge channel on its integral parameters in order to increase thrust efficiency;

– studies of thermal mode of the thruster operation.

As the calculation studies of the PPT showed (the results are given in Part 2 of this report) thrust efficiency increases when initial inductivity of the discharge circuit decreases and linear inductivity and channel width increases. These

conclusions were the basis for the design principles and improvements of the MPPT-3 in the process of its experimental development.

MPPT-3 was designed with the discharge channel 45 mm high and with the rails width of 35 mm and at minimizing current-supply busbars inductivity from the capacitor battery to main discharge electrodes. The calculated estimations and experiments on the battery discharge on the conductor which imitates plasma cord in the precombustion chamber cave (see. Fig.1.3) show that initial inductivity of the thruster does not exceed 16 nH. For the arrangement of the PPT, which approaches the flying variant, such value of the initial inductivity can be regarded if not record, then quite satisfactory. Initial width of the step on the electrode which specifies the minimal width of the channel was chosen equal to 14 mm (in the process of the PPT operation working surfaces of the bars obtain a complex profile, and real width of the channel increases) (see Fig.1.5). The designed channel depth (the bars size along the electrodes) was made 25 mm.

Fig.3.3 presents traditional oscillogram of the discharge current of the MPPT-3 for the stored energy of 80 J. Below, on Fig.3.4 the discharge current of MPPT-1 at the same energy is presented. Duration of the discharge current first semi-period of the thrusters does not differ much, because their total inductivity (initial inductivity plus discharge channel inductivity) practically did not change, but proportion of its components in favour of the discharge channel inductivity changed. Its mean value (in the process of the discharge the channel inductivity depends on the current distribution along the channel) in MPPT-3 modification is estimated on the level of 20...25 nH, that is one and a half times higher than initial inductivity. In the MPPT-1 modification initial inductivity even slightly exceeded the discharge channel inductivity; which prevented reaching relatively high values of

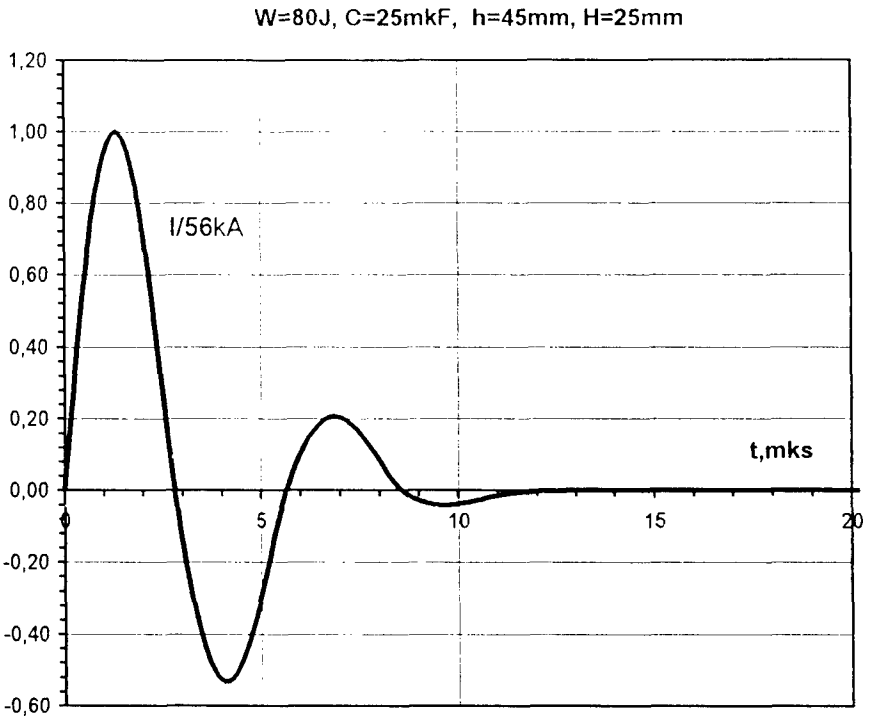

Fig.3.3. MPPT-3 discharge current.

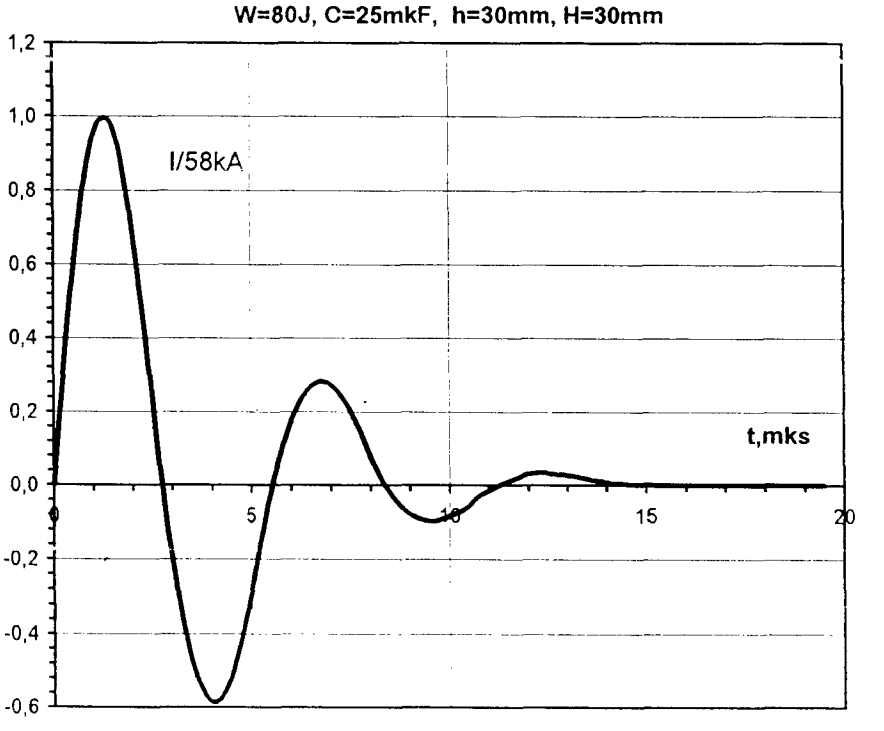

Fig.3.4. MPPT-1 discharge current.

the thrust efficiency. Thus, first experiments with MPPT-3 showed its potential possibilities in improvement integral characteristics obtained with MPPT-1 (see Fig.1.4).

The designers have always taken care of providing specified heat mode of the thruster, because its reliability strongly depends on it. It is especially important that during the PPT operation the capacitors temperature did not exceed a certain permissible value. When the capacitors are overheat their resource can be substantially reduced comparing to their normative. In order to prevent overheating for each specific thruster it is necessary to specify the duration of continuous operation with the specified frequency, when temperature of the capacitors does not exceed the permissible value.

The development of the MPPT-3 did not face the task of study of its heat diagram in accordance with the requirements to the flying model. That is why in the discharge circuit heat resistors between the discharge channel and capacitance battery were not installed. Heat release from the current carrying elements on the PPT body through thin-film dielectric was not provided. It was supposed during the thruster operation that the releasing heat energy from its current-carrying elements will be carried through energy supply circuits. For the capacitors with specific mass of 0.05 kg/J which were used in the process of life-time tests of the MPPT-1, there was no overheating problem at long hours operation with frequency of 0.5 Hz; capacitor battery worked as heat accumulator. In the MPPT-3 the capacitors with specific mass of 0.02 kg/J were used. It allowed to decrease the thruster module mass considerably, but the problem of thorough control of the heat mode of the capacitors appeared. Maximal permissible temperature for the central outlet of the capacitors was 70°C, when the body temperature was 55°C.

In order to control the capacitors temperature during experimental development of the MPPT-3 resistance-type thermal sensor was used. The sensor was stuck to the current carrying busbar near the discharge channel. It helped to control the temperature of central outlets of the capacitors. It was found that at impulses frequency mode of 0.5 Hz and stored energy of 80 J the thruster can operate non-stop without exceeding the temperature permissible for the capacitors. If frequency increases to 1 Hz, permissible non-stop operation time shortens by 15 minutes.

From Fig.1.5 it is clear that total operation not less than $2 \cdot 10^5$ impulses is necessary for full running in of the discharge channel in order to obtain its final profile. But the same curve shows that after approximately $8 \cdot 10^4$ impulses profile stabilization finishes for 90% and then the process is very slow. As at this stage of experimental study of the MPPT-3 the task on improvement of its thrust efficiency was put, it was decided to make partial stabilization of the channel at the designed width of the step a=14 mm, in order to devote more experimental time to improvement of the thrust efficiency. The experiments showed that dynamics of stabilization of the MPPT-3 discharge channel goes exactly as with MPPT-1, and there are no surprises. It was also found that in energy range of 60...100 J carbon film does not deposit on the working surfaces of the bars. It means that energy density in the discharge channel is enough for the thruster normal operation.

The second stage of the experimental studies of the MPPT-3 was the studies of the discharge channel width – **a** on the integral characteristics of the thruster. As in the process of running-in the discharge channel width changes in height and depth, in further the value **a** will be the width of the electrode step (or minimal distance between the bars). The studies of the channel width (the step width)

influence were held at capacitor battery energy of 80 J.

As it follows from the calculations results (see Fig.2.16) when the channel widens in the vast range thrust impulse is practically constant, and thrust efficiency increases at the expense of the decrease of mass outflow per impulse. Fig.3.5 shows calculation and experimental dependencies (curves with experimental points) of the integral parameters from the channel (step) width. Comparison of the calculation and experimental results shows its good qualitative and quantitative agreement in the range of the channel width change of 14...20 mm. Insignificant decrease in the thrust impulse in the experiment is a bit disappointing because it did not allow to reach the calculated value of the thrust efficiency – 12%. In the experiment when the channel was 20 mm wide, thrust efficiency was a little more than 10%. The further widening of the channel seems unreasonable. There are two reasons for this. First, when the channel widens from 14 to 20 mm working surface of the Teflon bars changed from glossy into dull-white. It speaks of the approach to the energy critical density in the discharge channel, and in case of exceeding this value carbon film can deposit on the Teflon. Second, when the channel widens experimental value of the thrust efficiency diverges more and more from the calculated one, becoming stable. The said reasons do not permit to increase further efficiency at the expense of widening the channel.

Fig.3.6 shows the calculated and experimental dependencies of MPPT-3 integral parameters on capacitor battery energy with the channel 20 mm wide. Good agreement of calculations and experiments can be observed at energy more than 60 J. This energy should be regarded as lower boundary of the effective thruster operation. Reason for this limit can be energy critical density in the discharge channel. At energy of 100 J the thrust efficiency of more than 11% can

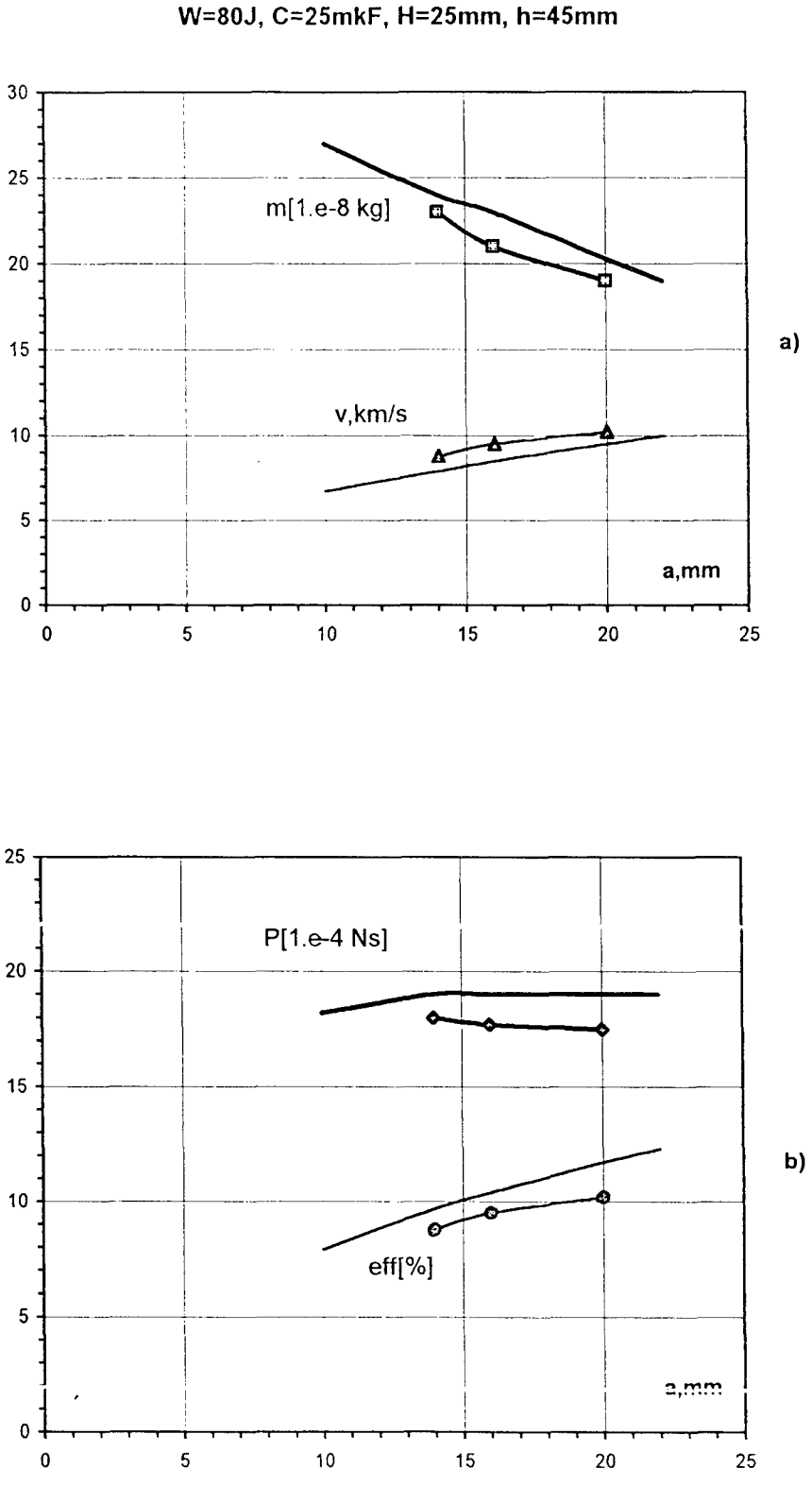

Fig.3.5. MPPT-3 integral parameters: calculation and experiment

C=25mkF, H=25mm, h=45mm, a=20mm

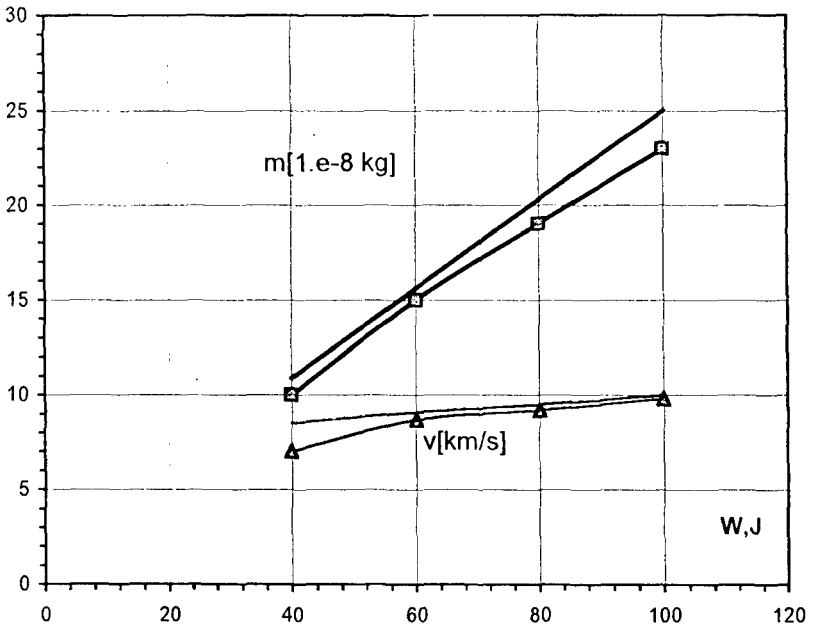

a)

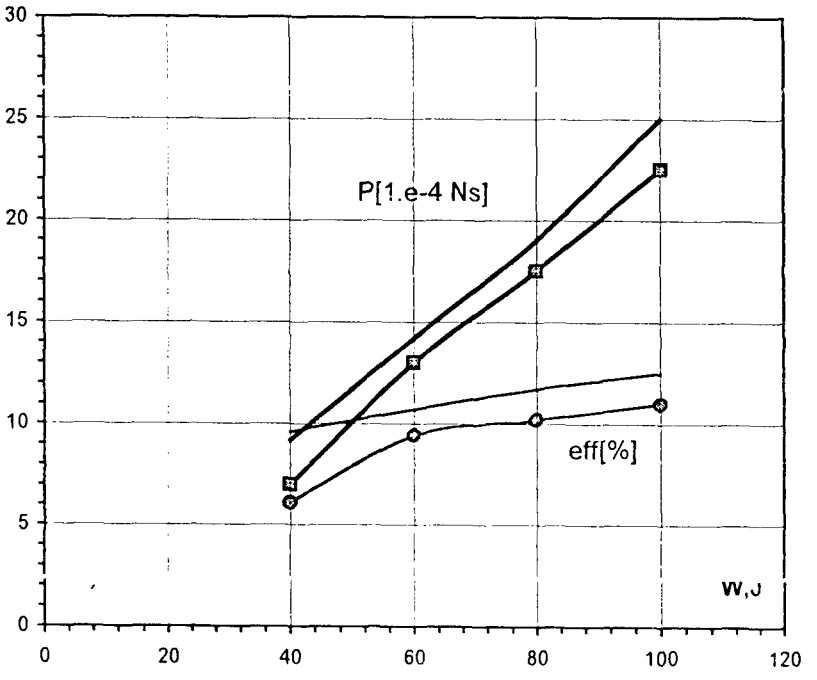

b)

Fig.3.6. MPPT-3 integral parameters: calculation and experiment

be achieved.

As calculations showed (see Fig.2.15) when the channel depth - H decreases thrust efficiency increases poorly, and the main result is in more effective use of the mass in discharge. Mass outflow decreases. When energy critical density limits the channel widening, energy density increase can be reasonable at the expense of the channel depth. It can give an additional push to thrust efficiency growth at the increased (comparing to the design) width of the channel. Unfortunately, calculation method presented in Part 2 does not take into account influence of energy density distribution in the discharge channel upon the thruster integral parameters. In order to answer this question the experiment was held with twice decreased (in comparison to the designed) channel depth of MPPT-3 (MPPT-3S). Decrease of the channel depth from 25 to 12 mm allowed to reach thrust efficiency value of 12% at energy of 80 J. But in this case thrust impulse was sacrificed – its value lowered to 1.45 mNs. Fig.3.7 presents integral parameters of the MPPT-3S (with the short channel) depending on the stored energy. Experimental results were obtained for the energies of 80 and 100 J. At energy of 100 J thrust efficiency was about 13%.

In conclusion on the results of experimental studies of MPPT-3 the stability of thrust characteristics and good repetition of the discharge current oscillogram for each thruster operation mode should be noted. Absence of carbon traces on the bars working surfaces in the studied range of energies of 60...100 J specifies energy limits for the confirmed thruster working capacity. Examination of working surfaces of the main discharge electrodes, igniter and end ceramic insulator did not show

C=25mkF, h=45mm, a=20mm, H=12mm

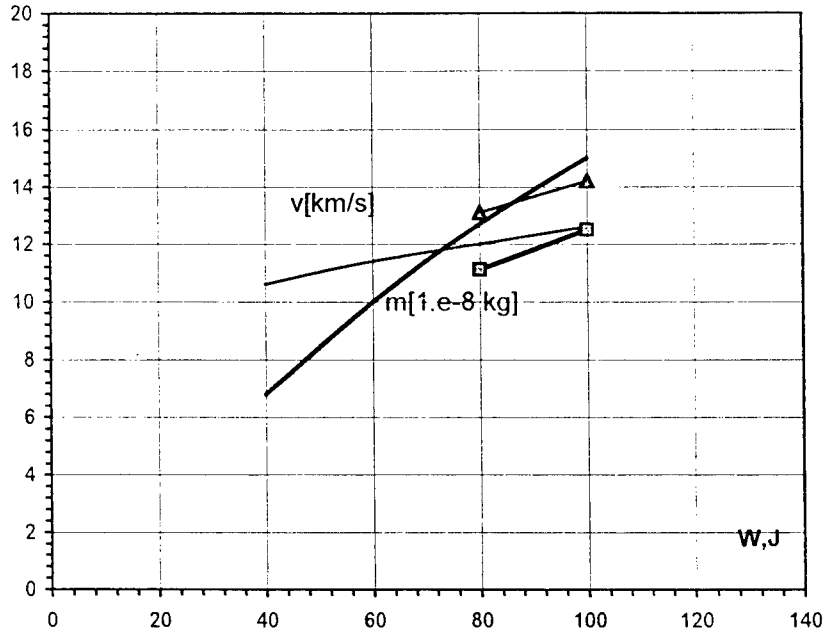

a)

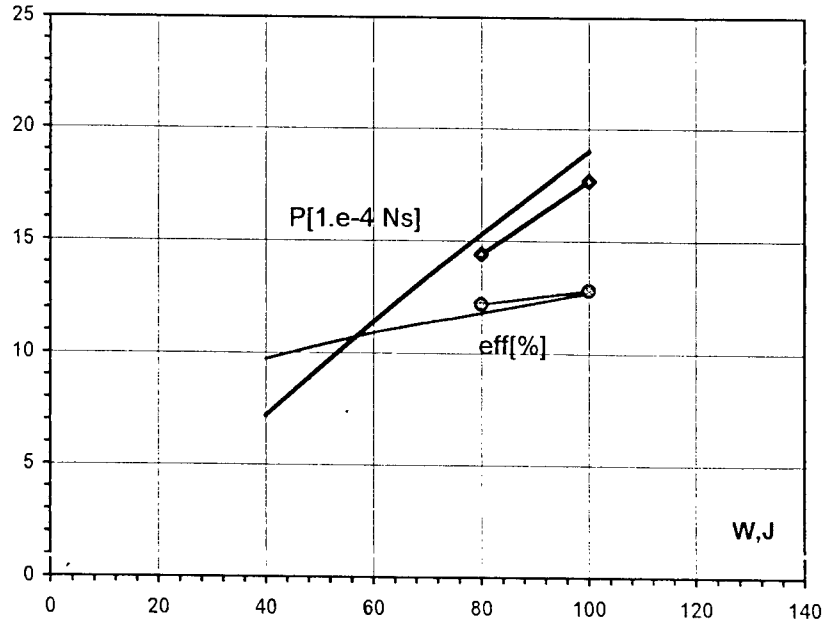

b)

Fig.3.7. MPPT-3 integral parameters: calculation and experiment.

traces of visible erosion of the main stuff of the said surfaces, protected by the carbon film[10].

3.3. Power processing unit (PPU) of the PPT

PPU is made as a separate unit and is designed for transformation of voltage and discharge stabilisation by the constant level of power of high-voltage power capacitors (Fig.3.8).

Input voltage of the PPU of 27^{+7}_{-4} V is transformated at +2.5 kV and +1.2 kV and goes into the accumulating capacitor which periodically is discharged through the discharger with frequency of 1 Hz. It also goes into the Discharge Initiation Unit (DIU) inlet. Capacitor discharge is automatic when voltage level of 2.5 kV ± 50 V is reached, and block switch is performed through the control panel or by a telemetering signal.

Accumulating capacitor (capacitors unit) with its nominal capacitance of 25 mcF charged up to 2.5 kV, provides necessary discharge power. At that inlet consumed current from the network is at the level of 3 A (at U_{inl}= 27 V). At that efficiency is not less than 0.8.

PPU supply unit is a voltage transformer of the inlet network of +27 V stabilized by the range-pulsed modulation, with the galvanic isolation between inlet and outlet.

Constructive diagram of the supply unit is presented on Fig.3.9. where F1 – inlet LC-filter, CS – current sensor, PA – power amplifier, HR – high-voltage rectifier, RCA – reverse connection amplifier, PDM – pulse-duration modulator, CG – cadence generator, IG – ignition generator.

The device operates in the following way:

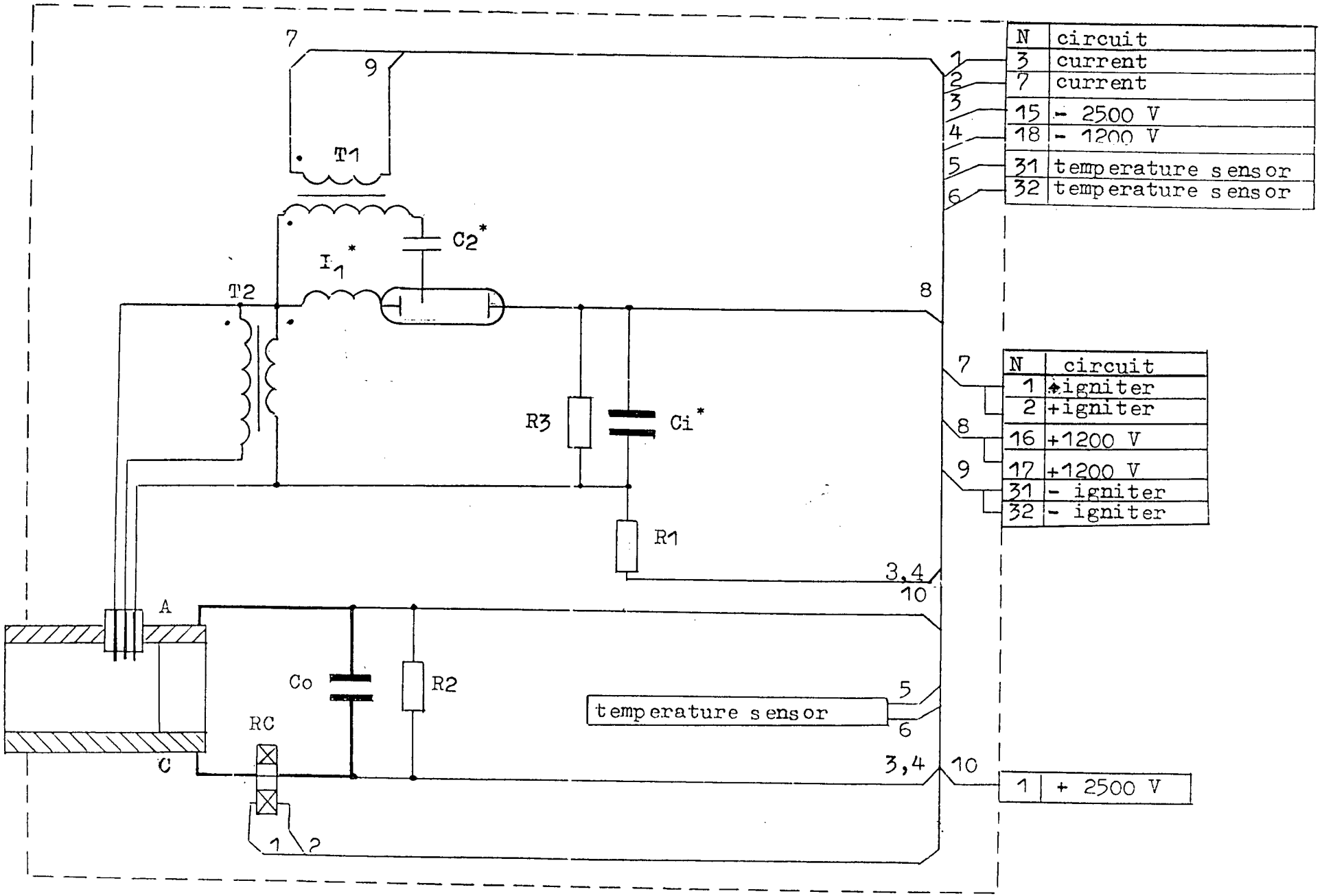

N	circuit
3	current
7	current
15	- 2500 V
18	- 1200 V
31	temperature sensor
32	temperature sensor

N	circuit
1	-igniter
2	+igniter
16	+1200 V
17	+1200 V
31	- igniter
32	- igniter

1	+ 2500 V

Fig. 3.8

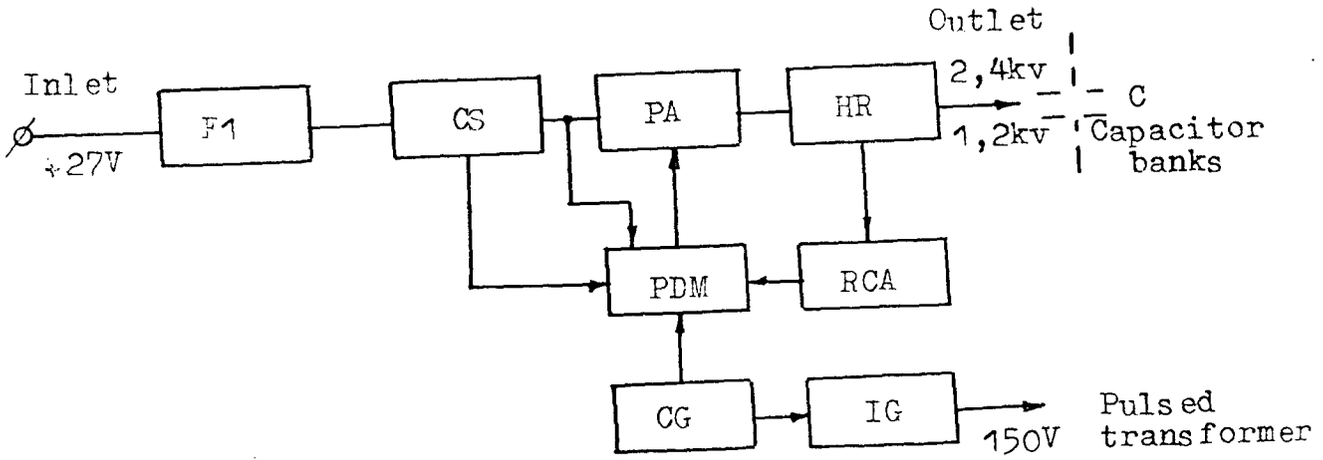

Fig. 3.9

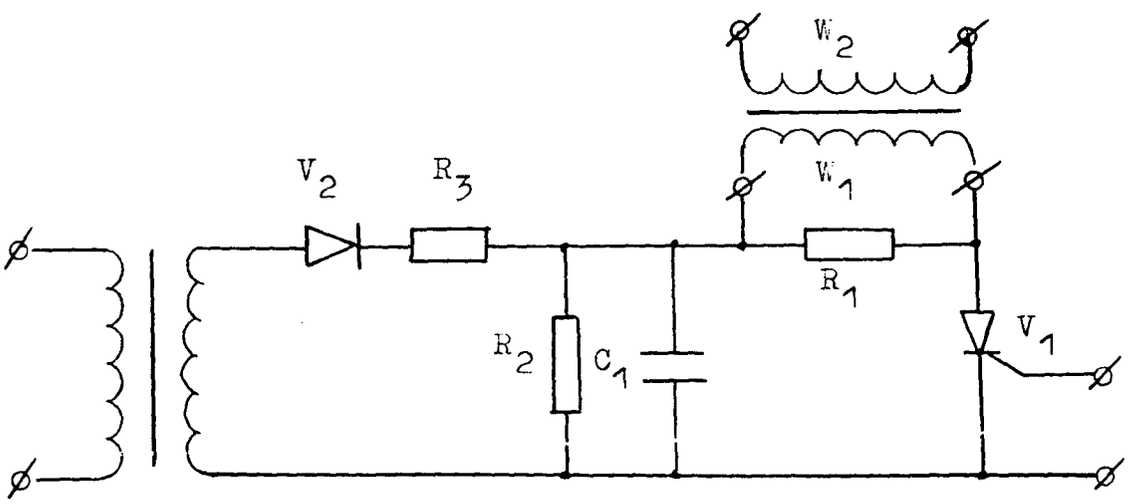

Fig. 3.10

Inlet supply line voltage goes to the integrating inlet filter F1 which is necessary to smooth the consumed pulsing current and to decrease high-frequency components of radio interference's. From the filter the outlet voltage goes into the current sensor (CS) from which current signal is picked off for limitation the equipment of the charge current of the capacitance accumulator. The signal goes into the inlet of operational amplifier of pulse duration modulator (PDM).

From the outlet of the current sensor voltage is supplied to the power amplifier (PA) which is necessary to transform low voltage into high outlet voltage. PA comprises transformer for providing galvanic isolation between the inlet and outlet.

Transformation frequency is specified by the specifying generator which is a part of PDM and is equal to 70–80 kHz.

Constructive-power primary windings are divided into two coils and connected in a parallel way. Outlet windings are divided into two coils each of which is winded in three sections.

From the high-voltage rectifier (HVR) outlet which was compiled with the power microcircuits, the voltage goes to the capacitance accumulator.

Reverse connection signal (in order to stabilize the outlet voltage) is picked off from additional low-voltage winding of the power transformer, is rectified, filtered and supplied to the operational amplifier inlet of the reverse connection. From the operational amplifier outlet one signal goes to the (PDM), and the second one goes to the cadence generator (CG) inlet.

CG forms the signals :

– of the PDM blocking;

– duration of the pause of the blocked PDM (during the time of the discharge

of the capacitance accumulator);

– signal of switching on of the ignition generator (IG).

When the inlet voltage is supplied, the signal from the CS limits the duration of the PDM impulse. This provides "soft" charge of the capacitance accumulator and thus limits pulsed currents of the power elements of the circuit and the inlet.

During the charging C duration of the PDM impulse increases from 1 mcs to 10–12 mcs. When at C accumulating voltage of 2.5 kV is reached, the reverse connection signal is formed according to the voltage values, then the signal of switching off PDM and the signal of control of the ignition generator are formed. The transformer is switches off, ignition generator forms powerful current impulse which through the isolation and cable network is supplied to the discharge initiation unit (DIU) inlet.

After picking the tiristor control signal off (~ 100 mcs) PDM blocking signal is switched off, generator starts and "soft" charging of the capacitance accumulator begins. All the processes are repeated.

General features of the PPU:

efficiency ≥ 80% U_{outl1} = 2.5 kV

I_{inl} = 3 A U_{outl2} = 1.2 kV

U_{inl} = 23÷34 V C_{outl} = 20 mcF.

Specific characteristics:

gravimetric characteristics Q ≥ 120 W/kg

volumetric characteristics V ≤ 80 W/dm^3

In its construction the PPU unit is made in the body with thin walls. It was milled from the D16AT alloy. It has four ears to fix it on the device. The body is the heat-remover for the power elements of the circuit. Electric circuits were

compiled in the forms of separate plates fixed on the stands in the body. Power circuits are connected between each other by the copper busbar. High-voltage rectifiers are placed on the insulator spacer. Power transformers are placed on the base of the body through heat-conducting insulator spacer (from beryllium oxide). Control plates are made by the printed method on the foiled fiber glass. When the unit was arranged the following things were provided: maximal area of filling the body, minimal lengths of the wires of inter-unit and inter-plates compilation. On the side wall of the body there are plug isolators for the cables which connect PPU and PPT and the board of the device. PPU body is closed with the lead.

Discharge initiation unit (DIU)

Discharge initiation unit (DIU) is designed for obtaining powerful high-voltage spark, necessary for "ignition" of the main discharge in the thruster discharge channel.

Discharge initiation unit consists of two stages. Ignition unit of the first stage, the diagram of which is presented on Fig.3.10 operates in the following way: enabling signal from the cadence generator outlet enables tiristor V1. Capacitor C1 which was preliminary charged through additional winding of the power transformer and limiting resistor R3, is discharged through the primary winding W1 of the pulsed transformer and tiristor V1. Capacitor C1 voltage is ~ 150 B. Discharge current is ~ 50 A. Resistor R3 is necessary to limit charge current and current of blocking tiristor V1. After C1 is discharged, tiristor V1 is blocked and capacitor C1 is smoothly charged. Then the process is repeated.

Ignition unit of the second stage, presented of Fig.3.10 operates in the following way: when powerful impulse passes through the primary winding of the

outlet transformer of the primary stage, powerful impulse necessary for starting metal-ceramic discharger RT-53 is formed. C_i – capacitor of ignition discharge contour. When the discharger is enabled, it discharges through the primary winding of the outlet pulsed transformer T2. In the secondary winding of transformer T2 powerful high-voltage impulse is aroused, which is supplied to two initiating electrodes between which high-voltage breakdown occurs. At that the formed plasma shorts the third initiating electrode (in this circuit it is the cathode) and all the remaining energy of the capacitor C_i is discharged directly without passing through the transformer T2. At that initiating spark energy is considerably increased.

In order to increase the operation time of the discharge initiation unit elements in the process of manufacturing MPPT-3 inductivity of primary windings of pulsed transformers T1 and T2 was increased, also the dividing capacity C2 is introduced.

Inductivity L1 was chosen at tuning so that the whole gap between anode and cathode was broken by the controlling impulse. It leads to the more reliable operation of the discharger.

Structurally the discharge initiation unit (DIU) is made in the following way. The body from fiber glass serves as the body, on which unit elements are fixed by the mounted wiring of thick copper belts. These units are filled with special heat-conducting compound. The circuits of control and supply are connected with the first stage of the cable unit through two isolations. High-voltage outlets are made with the special high-voltage wire.

The appearance of PPT model jointly with PPU and DIU which is situated into body of thruster are shown on Fig.3.11.

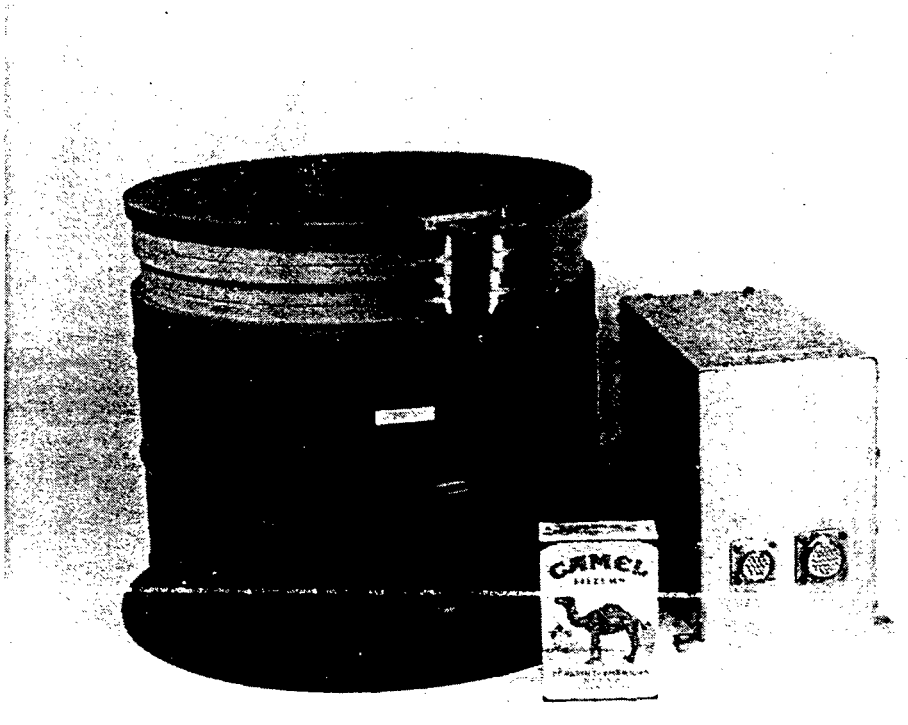

Fig.3.11. The appearance of PPT model.

CONCLUSION

Results of developing the PPT model and studies of its operation process, presented in the report, support the idea expressed in the Introduction that the task of raising the thrust efficiency is far from ordinary. Speaking about it one should bear in mind that solution of this problem is made more complicated by the fact that high thrust efficiency is important not just as it is, but in combination with rather high thrust impulse. That is why simple solution connected with the reduction of the propellant consumption in the impulse is acceptable only till a certain limit, which apparently has been already achieved. Nevertheless there are certain reserves of increasing efficiency. The results of processed data of magnet probes measurements presented in this report support this idea. One can see that in the second semi-period of the current curve when the accumulator discharges, current shell does not move. It means that in the second semi-period electromagnetic mechanism of plasma acceleration practically does not "work". In its turn, it means that irrational energy consumption supplied into the discharge takes place. Now the problem is to find the possibility of affecting the process in the discharge channel in order to make current shell move or to decrease considerably the share of energy supplied into the second semi-period. The first attempts in this direction have already been made, as it follows from the Report. As a result, thrust efficiency of the PPT model has been increased to 13% while energy supply was 100 J.

In the near future measurements of plasma parameters in the thruster channel and in the outflow are planned to held by electrical probes, as well as by non-contact diagnostical means (spectrometry and laser interferometry). Complex use of independent methods of diagnostics allows to obtain true picture of PPT plasma processes and will help to solve the problem of raising thrust efficiency of erosion thruster up to 15–20%.

REFERENCES

1. R.Vondra, K.Thomassen, A.Solbes Analysis of Solid Teflon Pulsed Plasma Thruster./J. Spacecraft. Vol.7. №12. 1970.
2. A.Solbes, R.Vondra Performance Study of a Solid Fuel Pulsed Electric Microthruster./J. Spacecraft. Vol.10. №6. 1973.
3. Avdushin S.I. et al. Using of Plasma Accelerators for Searching of Physical Processes in Space.//Plasma Accelerators and Ion Injectors./Morozov A.I. – M.: Nauka, 1984. pp.232–240. (in Russian)
4. Pulsed Plasma Accelerators./Alexandrov V.A. et al. – Kharkov: KhAI, 1983. (in Russian)
5. Palumbo D.J. and Guman W.J. Effect of Electrode Geometry and Propellant on Pulsed Ablative Thruster Performance./AIAA Paper. №75–409, March 1975.
6. Guman W.J. and Nathanson D.M. Pulsed Plasma Microthruster Propulsion System for Synchronous Orbit Satellite./J. Spacecraft and Rockets, Vol.7. №4. 1970. p.409.
7. A.Rudikov, N.Antropov, G.Popov. Pulsed Plasma Thruster of Erosion Type for a Geostationary Artificial Earth Satellite. IAF-93-S.5.487./44th CONGRESS OF THE INTERNATIONAL ASTRONAUTICAL FEDERATION – October 16-22, 1993. Graz, Austria.
8. Electric Thrusters for Spacecrafts./Grishin S.D., Leskov L.V. – M.: Mashinostroenie, 1989. (in Russian)
9. Vondra R. A Flight Qualified Pulsed Electric Thruster for Satellite Control./AIAA 10th Electric Propulsion Conference, 1973.

10. N.Antropov, V.Gundobin, G.Popov, A.Rudikov, S.Shibanov. Preliminary Results on Service Life Development of PPT Scale Model./24th International Electric Propulsion Conference./Summaries of the Abstracts of the Papers. Moscow, Russia. September 19-23. 1995. pp.172–174.
11. Plasma Accelerators./Grishin S.D. et al. – M.: Mashinostroenie, 1983. (in Russian)
12. Minko L.Ya. Generation and Investigation of Pulsed Plasma Flows. – Minsk: Nauka i Technika, 1970. (in Russian)
13. L.Gomilka, G.Popov, A.Rudikov. Mathematical Simulation for PPT Operation./24th International Electric Propulsion Conference./Summaries of the Abstracts of the Papers. Moscow, Russia. September 19-23. 1995. pp.187–189.
14. Chernousko F.L., Banichuck V.P. Variational Problems of Mechanics and Control. – M.: Nauka, 1973. (in Russian)
15. Fedorenko R.P. Approximated Solution of Problems of Optimal Control. – M.: Nauka, 1978. (in Russian)
16. Shneerson G.A. Fields and Transition Processes in the Equipment of Superstrong Currents. – L.: Energoizdat, 1981. (in Russian)

APPENDIX

Below the results of one-dimensional calculation of linear density of the current $j_y(x)$ in the acceleration channel on measured values of the cross-sectional component of the induction of the magnetic field $B_{z\ exp}(x)$ are shown. On the plots the calculated curves $j_y(x)$ (solid lines) and corresponding to them curves $B_z(x)$ (dotted lines) are presented. Experimentally measured values of $B_{z\ exp}(x)$ are marked with crosses. Calculated moment of time T, measured full discharge current J, calculated inductivity of the discharge channel L and relative root-mean-square deviation S of the calculated values of magnetic field induction $B_z(x)$ from experimentally measured ones $B_{z\ exp}(x)$ are also presented on the plots.

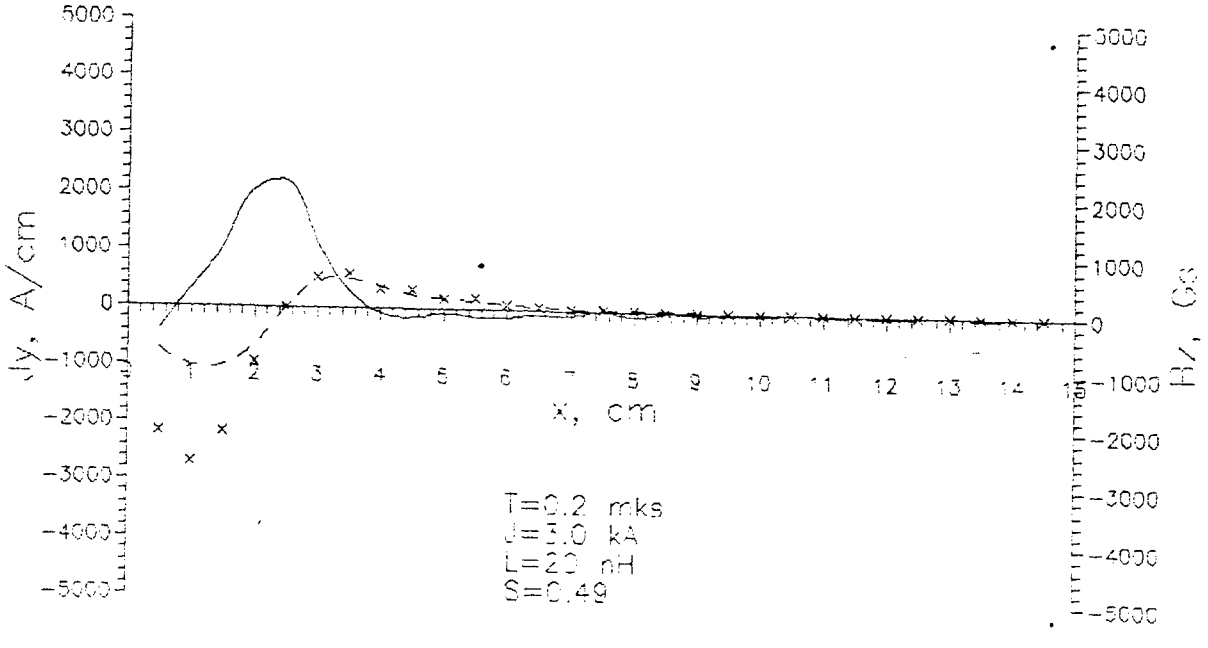

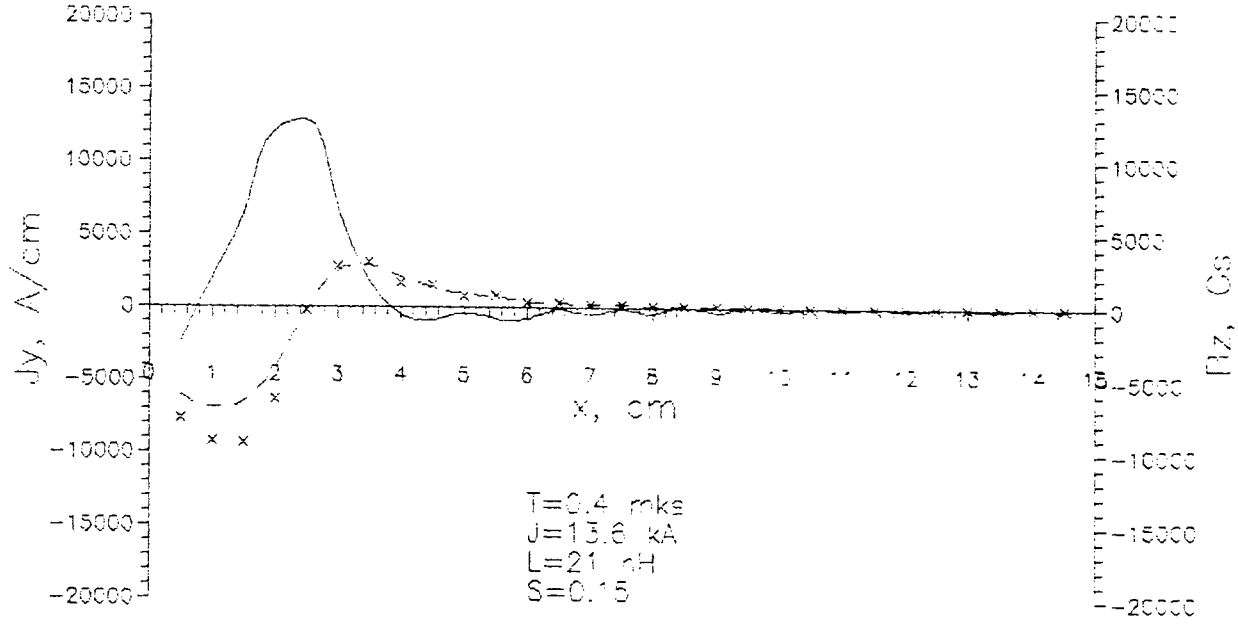
Jy, A/cm
Bz, Gs
x, cm
T=0.4 mks
J=13.6 kA
L=21 nH
S=0.15

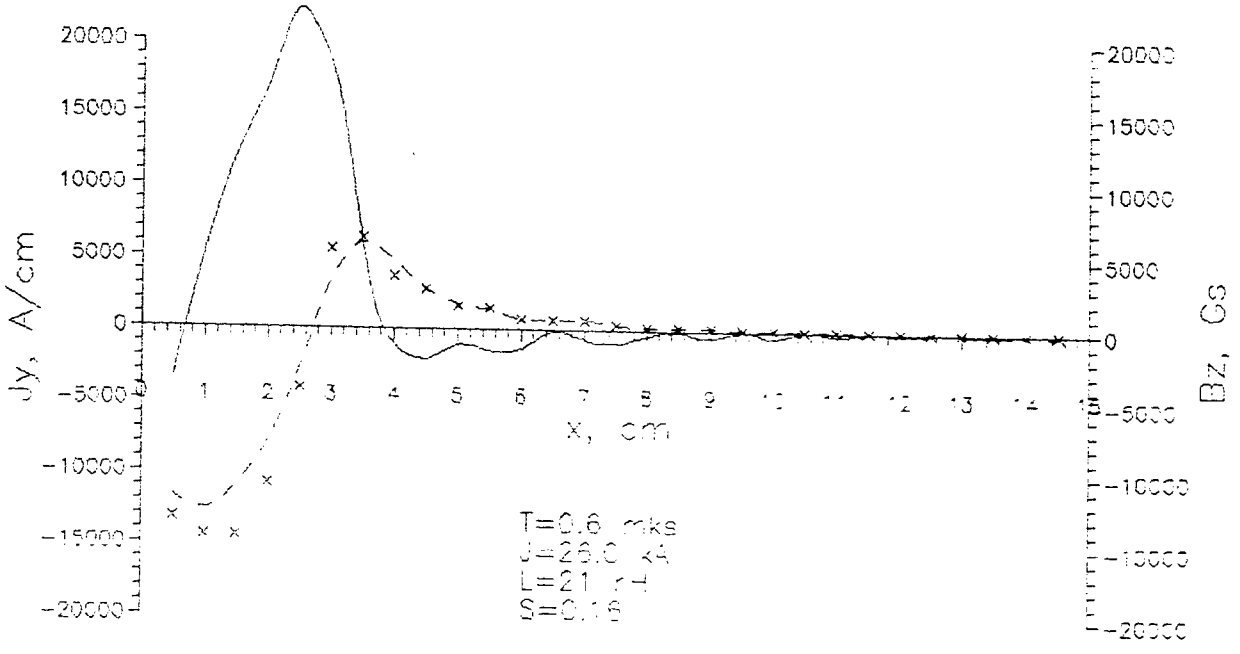
Jy, A/cm
Bz, Gs
x, cm
T=0.6 mks

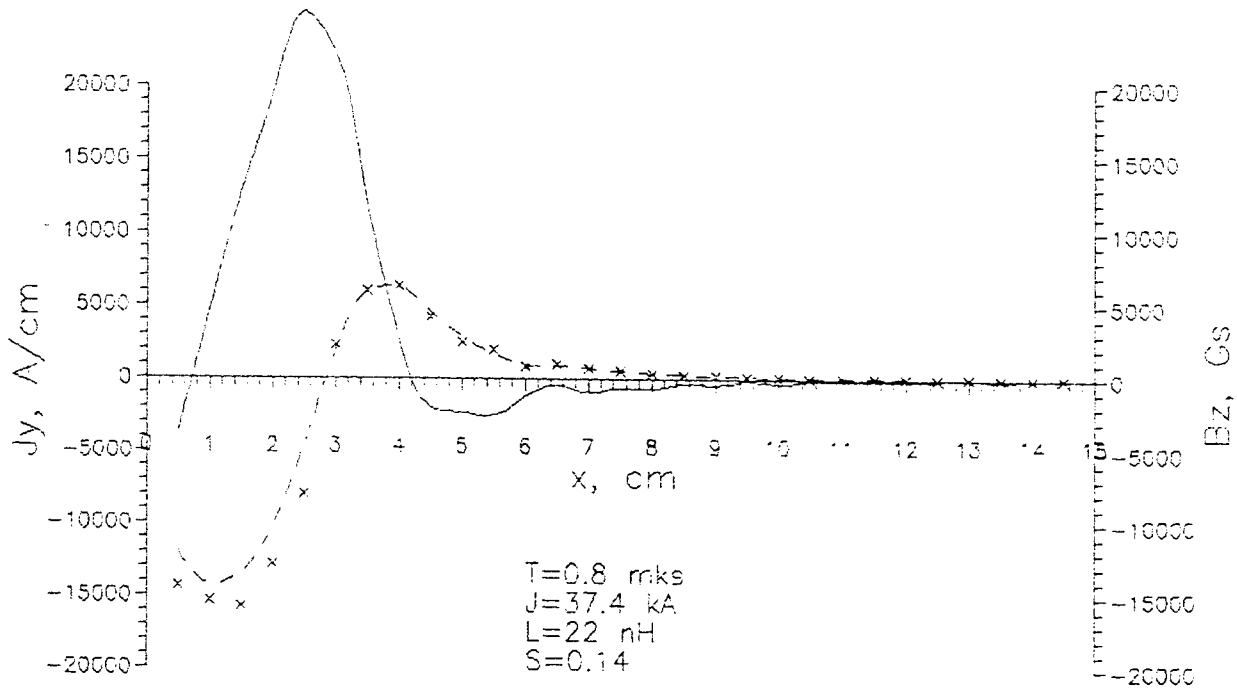
Jy, A/cm
Bz, Gs
x, cm
T=0.8 mks
J=37.4 kA
L=22 nH
S=0.14

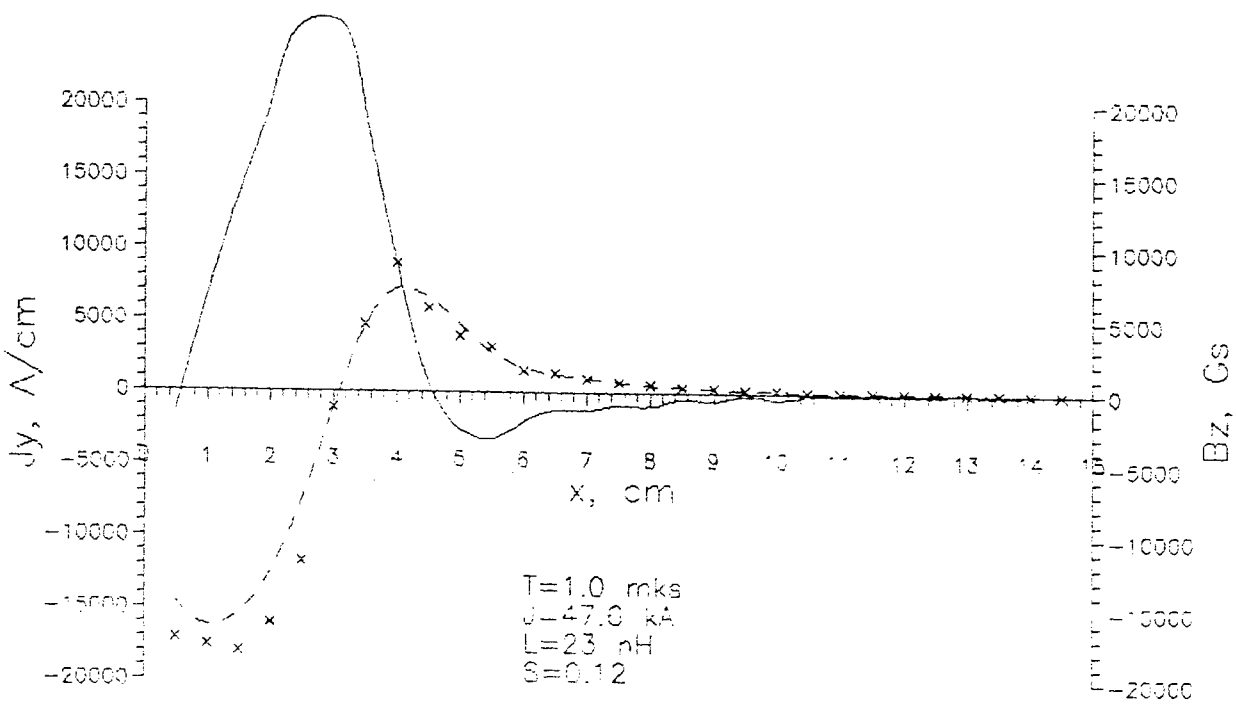
Jy, A/cm
Bz, Gs
x, cm
T=1.0 mks
J=47.0 kA
L=23 nH
S=0.12

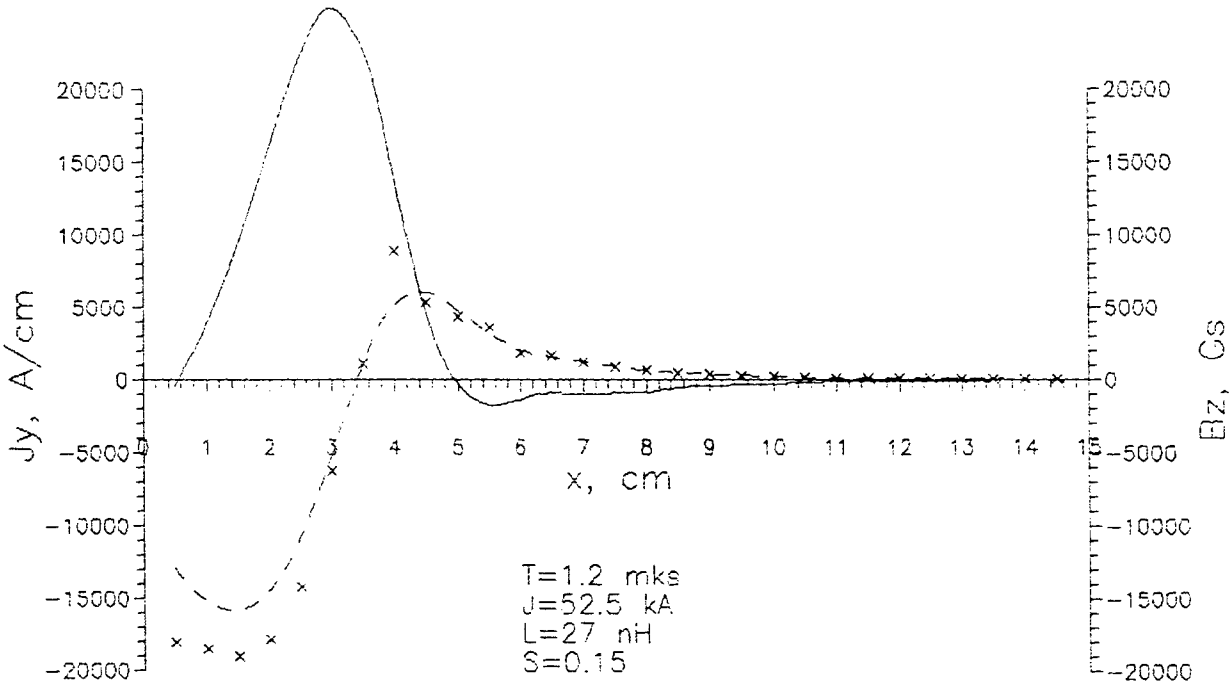
Jy, A/cm
Bz, Gs
x, cm
T=1.2 mks
J=52.5 kA
L=27 nH
S=0.15

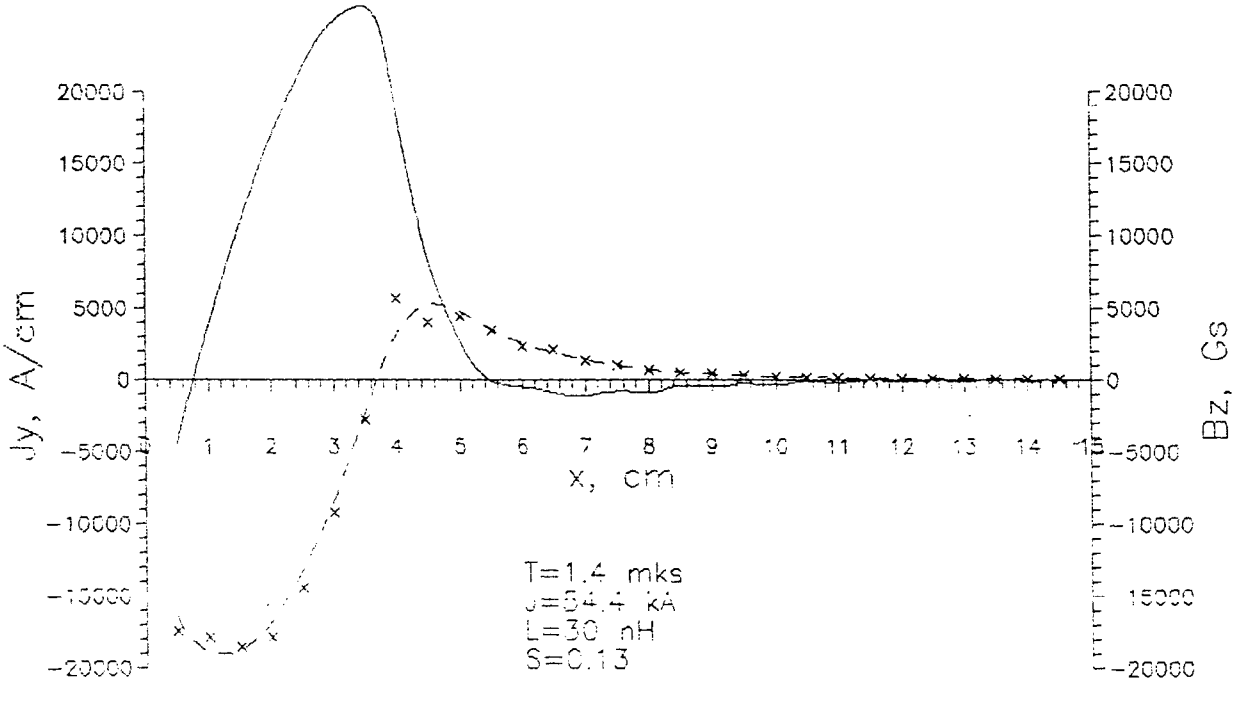
Jy, A/cm
Bz, Gs
x, cm
T=1.4 mks
J=54.4 kA
L=30 nH
S=0.13

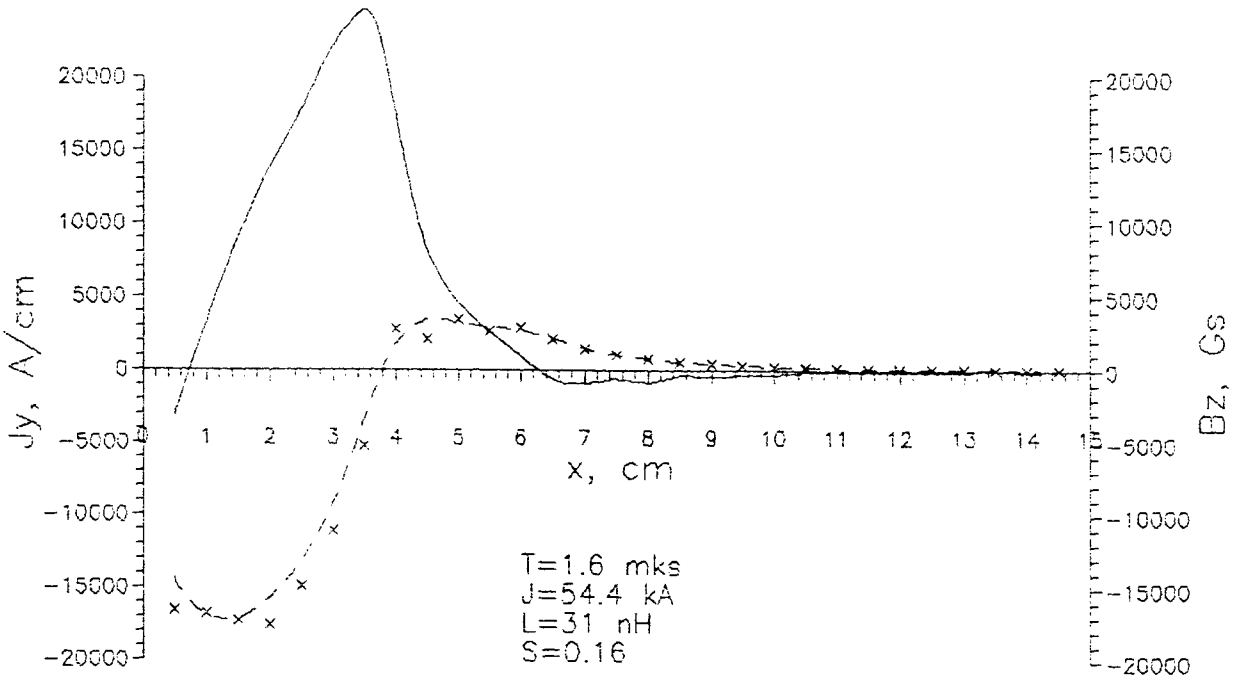
Jy, A/cm
Bz, Gs
x, cm
T=1.6 mks
J=54.4 kA
L=31 nH
S=0.16

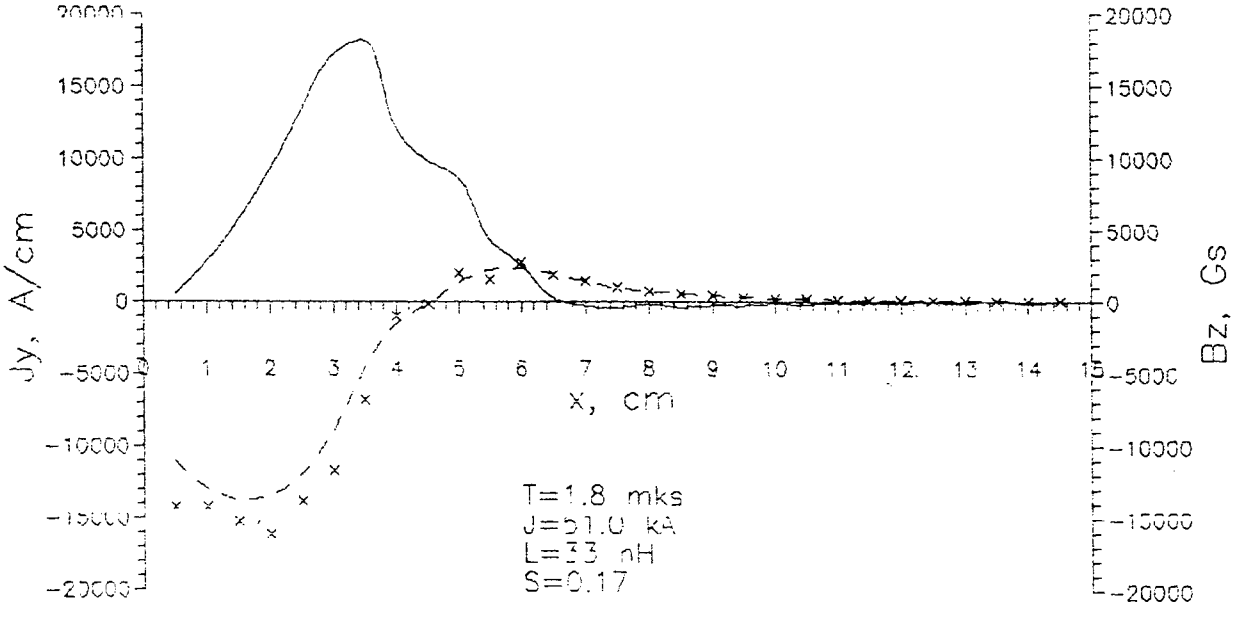
Jy, A/cm
Bz, Gs
x, cm
T=1.8 mks
J=51.0 kA
L=33 nH
S=0.17

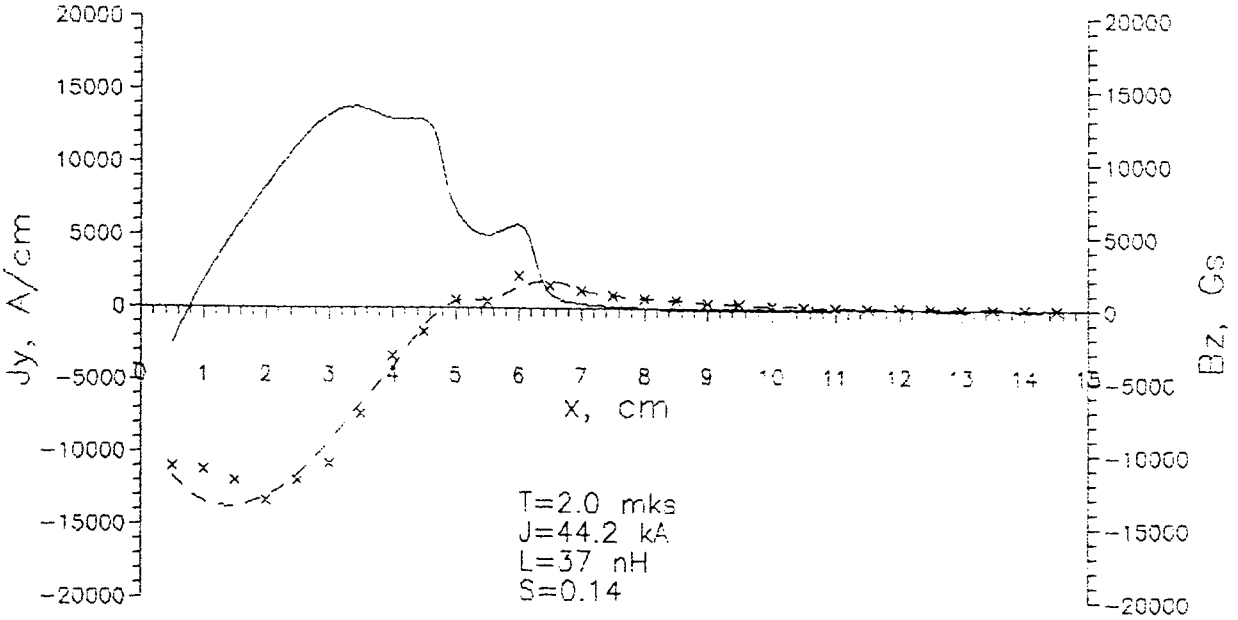
Jy, A/cm
Bz, Gs
X, cm
T=2.0 mks
J=44.2 kA
L=37 nH
S=0.14

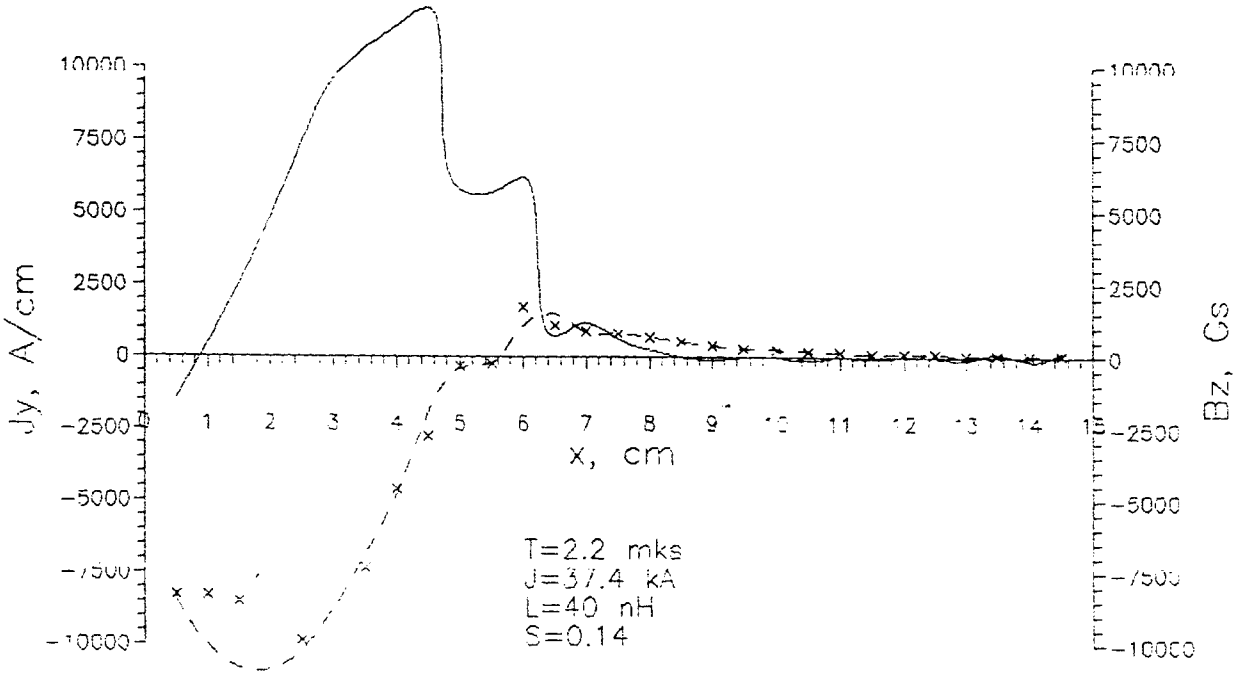
Jy, A/cm
Bz, Gs
X, cm
T=2.2 mks
J=37.4 kA
L=40 nH
S=0.14

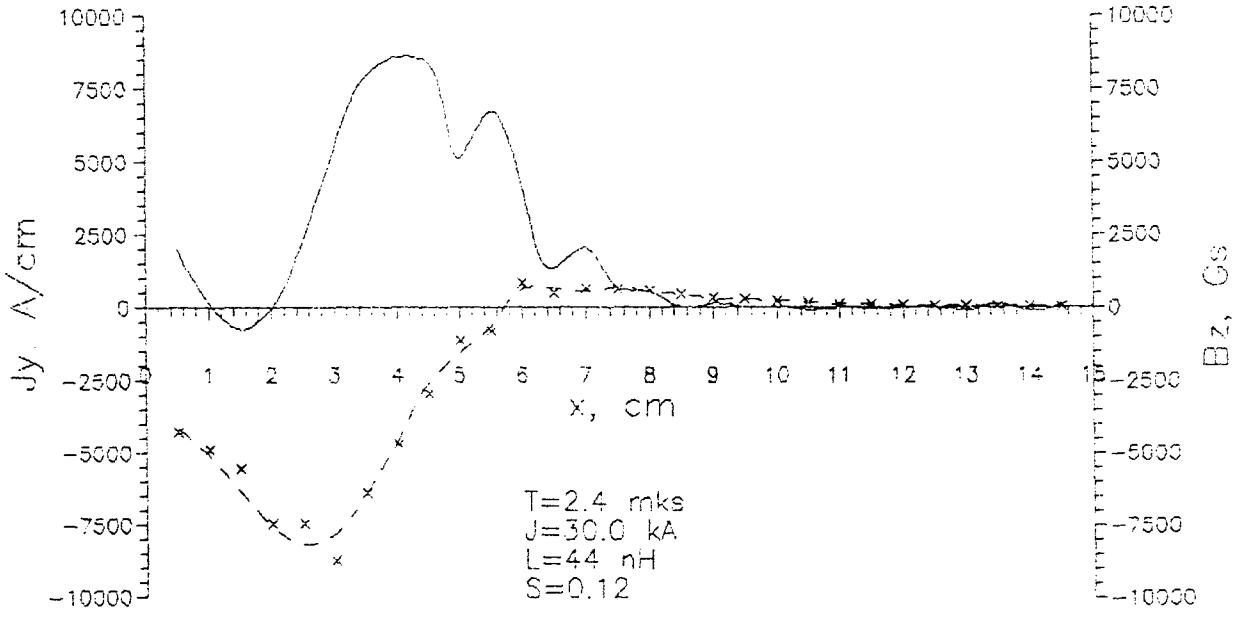
Jy, A/cm
Bz, Gs
x, cm
T=2.4 mks
J=30.0 kA
L=44 nH
S=0.12

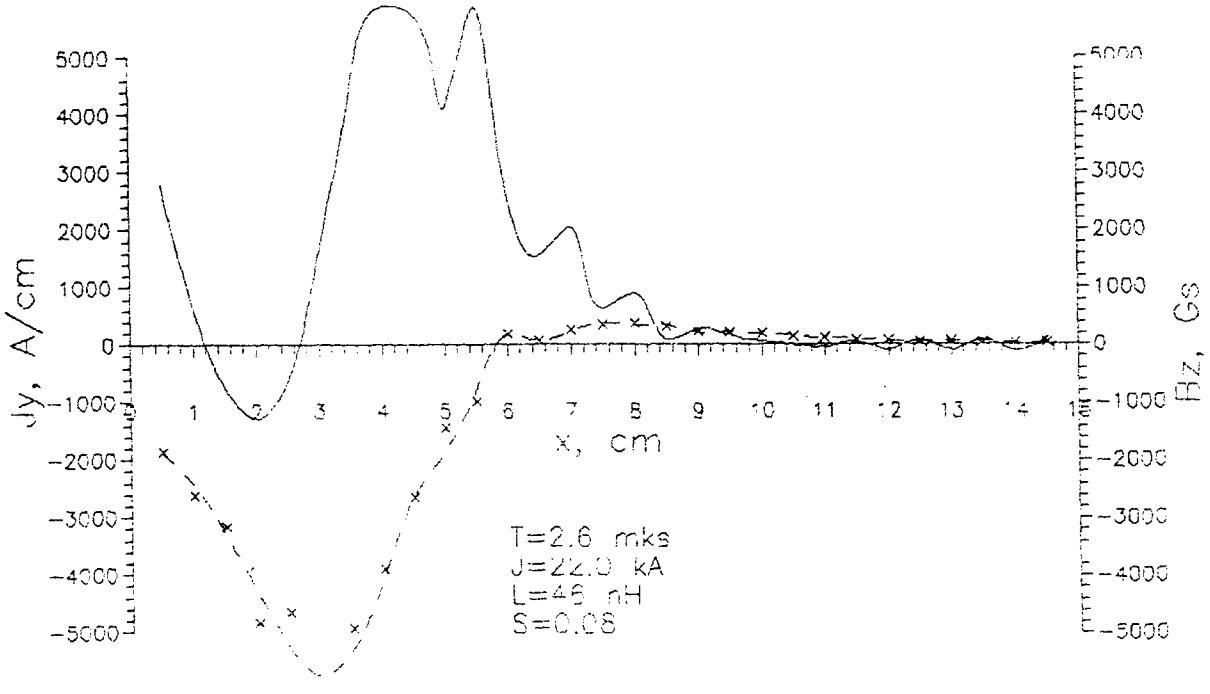
Jy, A/cm
Bz, Gs
x, cm
T=2.6 mks
J=22.0 kA
L=46 nH
S=0.08

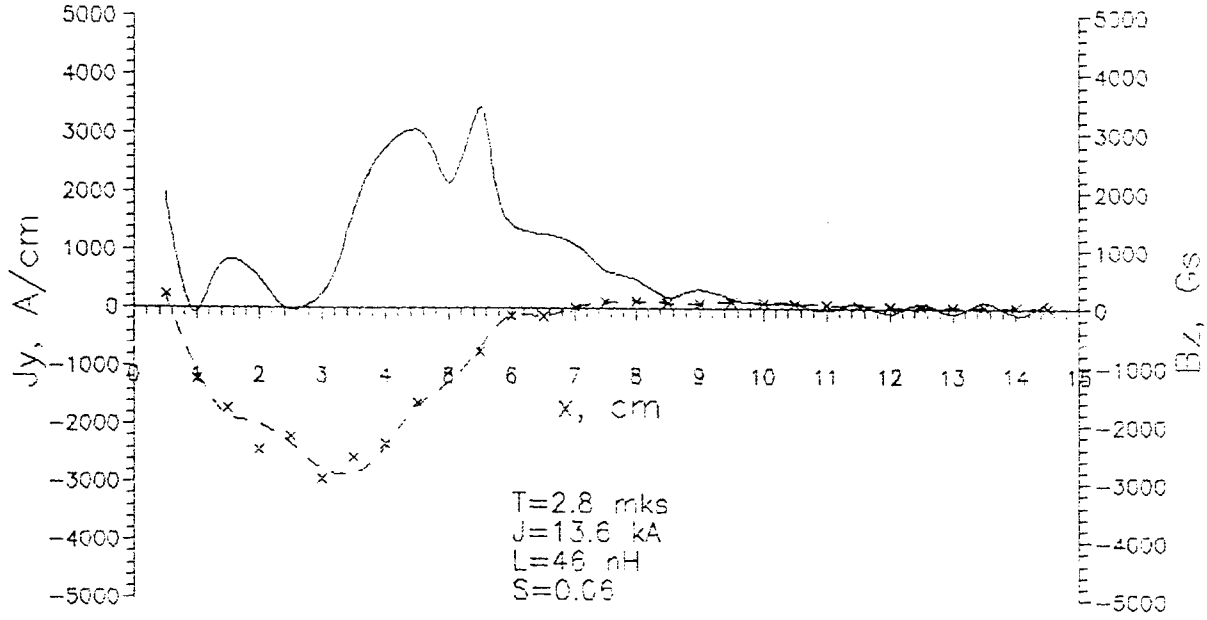
Jy, A/cm
Bz, Gs
x, cm
T=2.8 mks
J=13.6 kA
L=46 nH
S=0.06

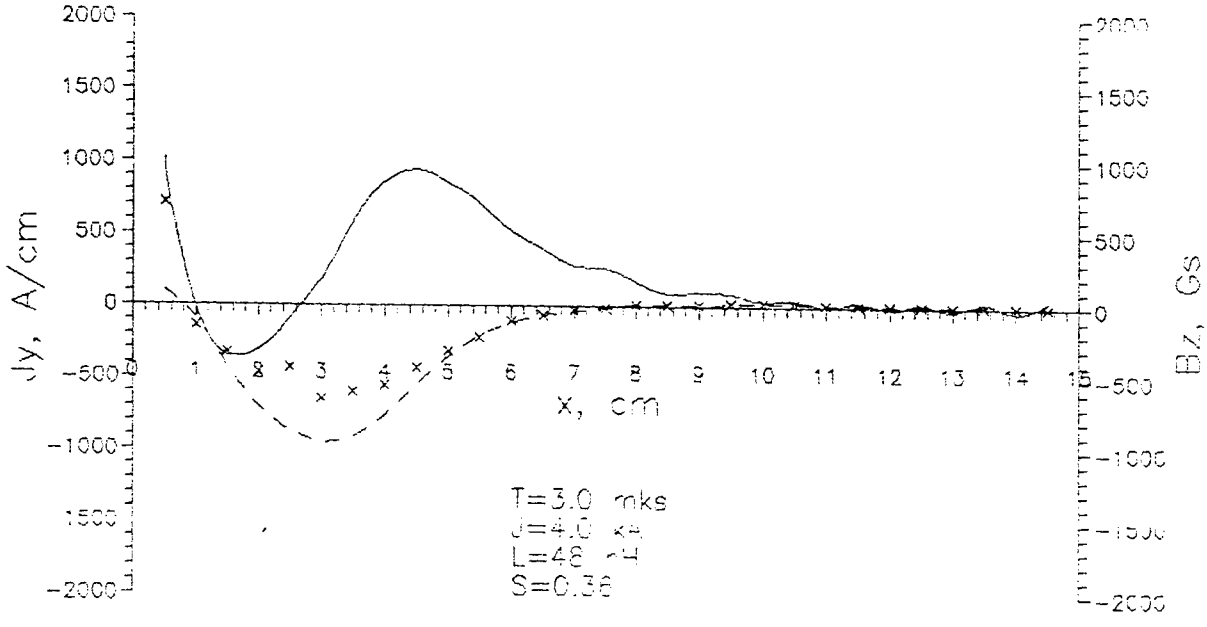
Jy, A/cm
Bz, Gs
x, cm
T=3.0 mks
J=4.0 kA
L=46 nH
S=0.36

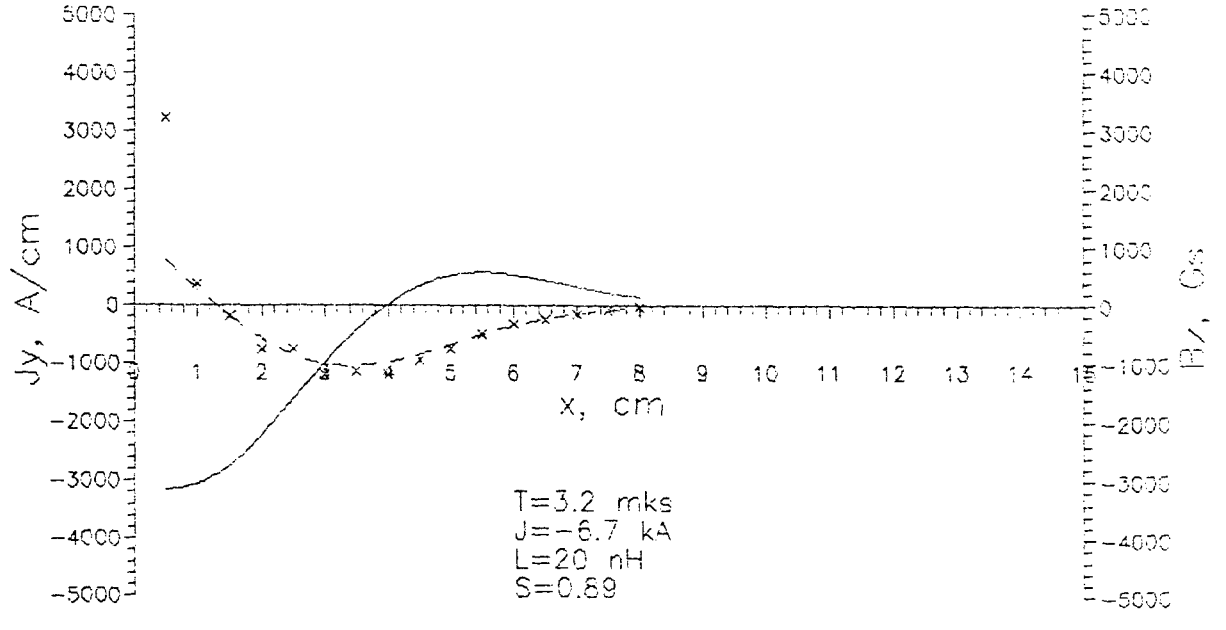
Jy, A/cm
Bz, Gs
x, cm
T=3.2 mks
J=-6.7 kA
L=20 nH
S=0.89

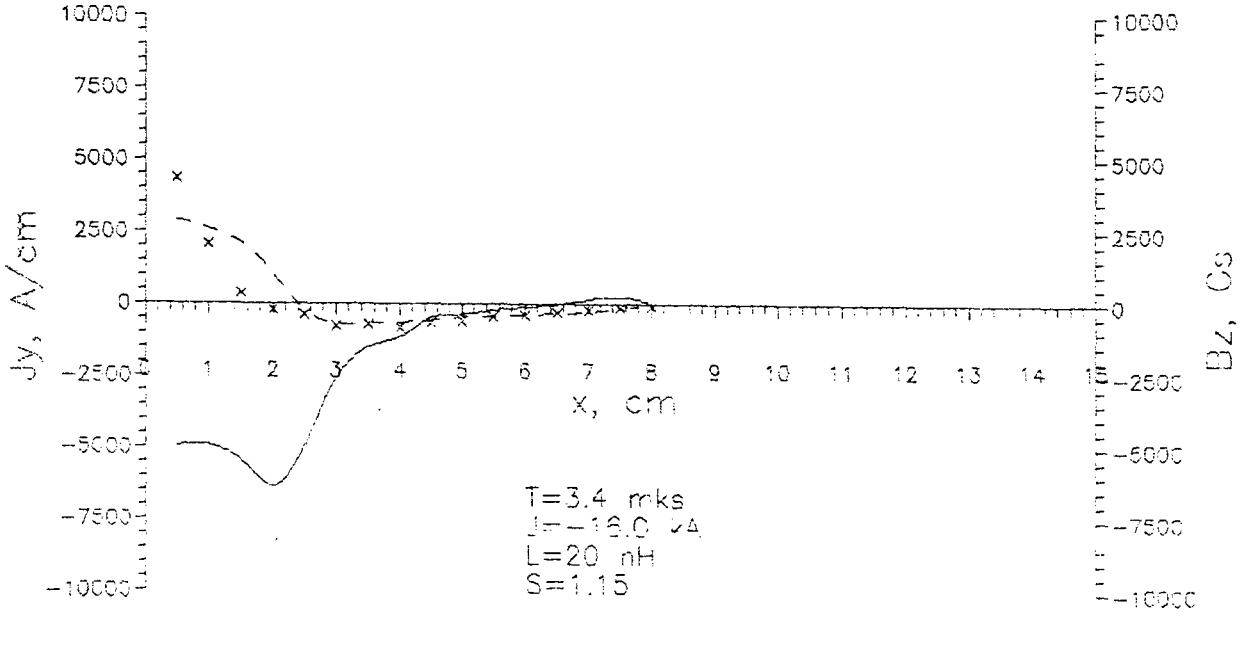
Jy, A/cm
Bz, Gs
x, cm
T=3.4 mks
L=20 nH
S=1.15

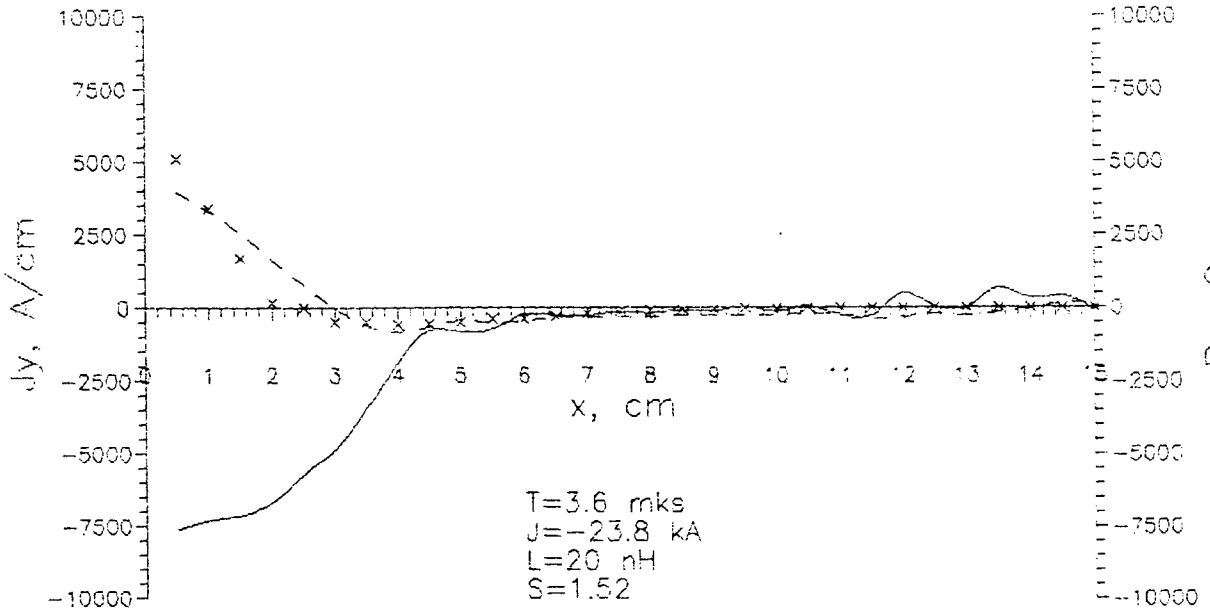
jy, A/cm
Bz, Gs
x, cm
T=3.6 mks
J=-23.8 kA
L=20 nH
S=1.52

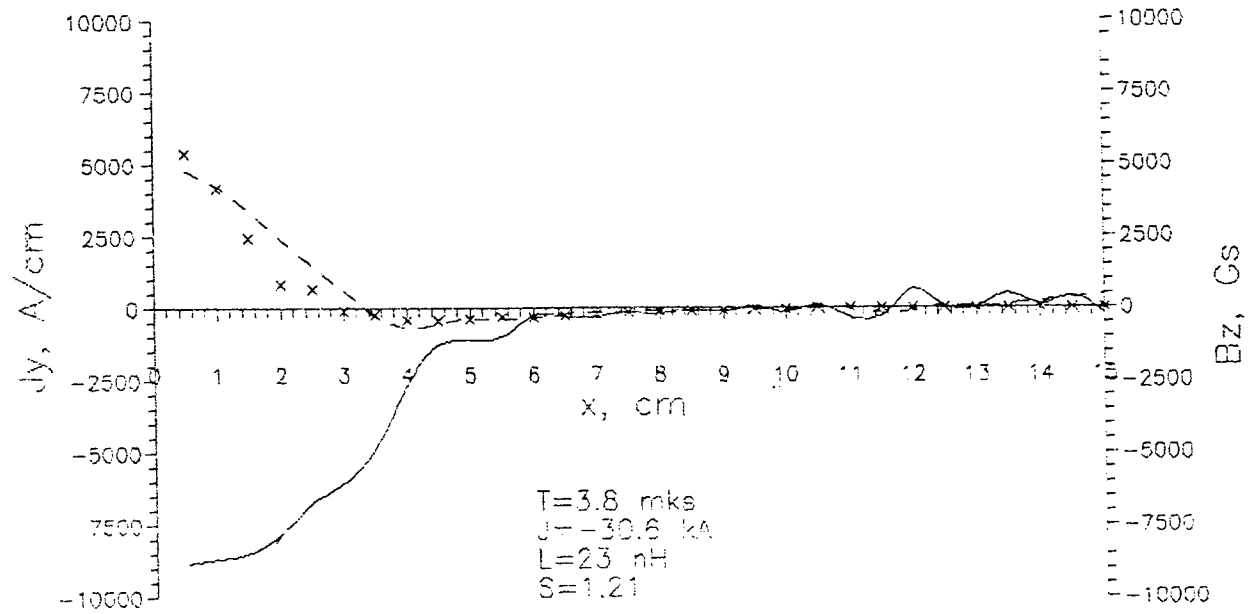
jy, A/cm
Bz, Gs
x, cm
T=3.8 mks
J=-30.6 kA
L=23 nH
S=1.21

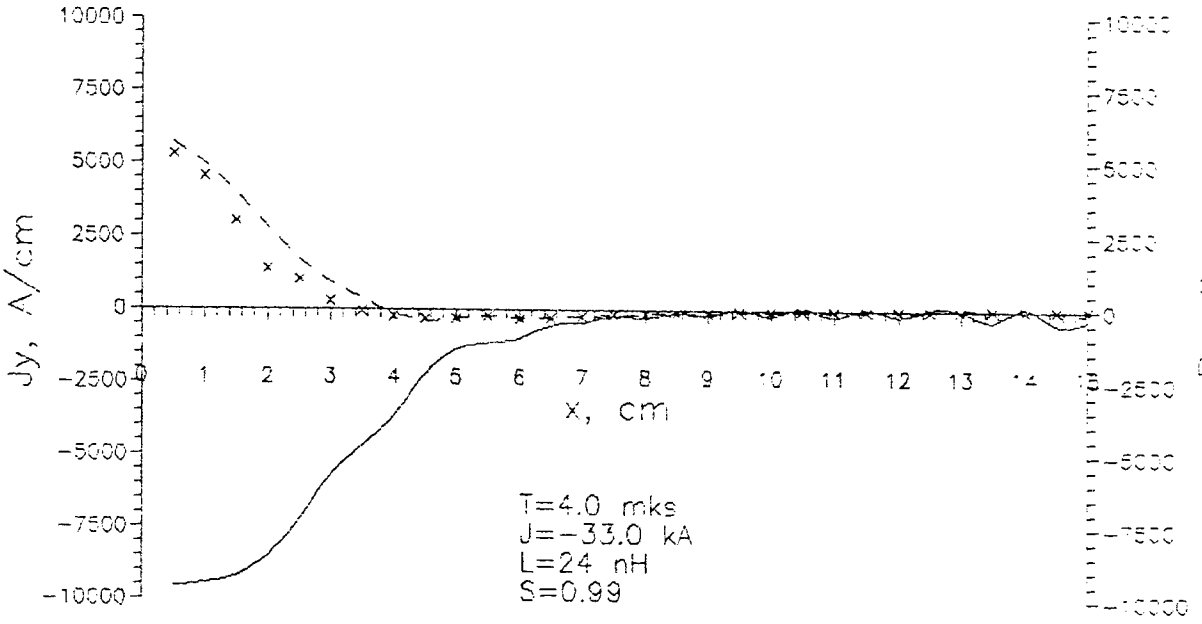
10000
7500
5000
2500
0
-2500
-5000
-7500
-10000
Jy, A/cm
Bz, Gs
1 2 3 4 5 6 7 8 9 10 11 12 13
x, cm
T=4.0 mks
J=-33.0 kA
L=24 nH
S=0.99

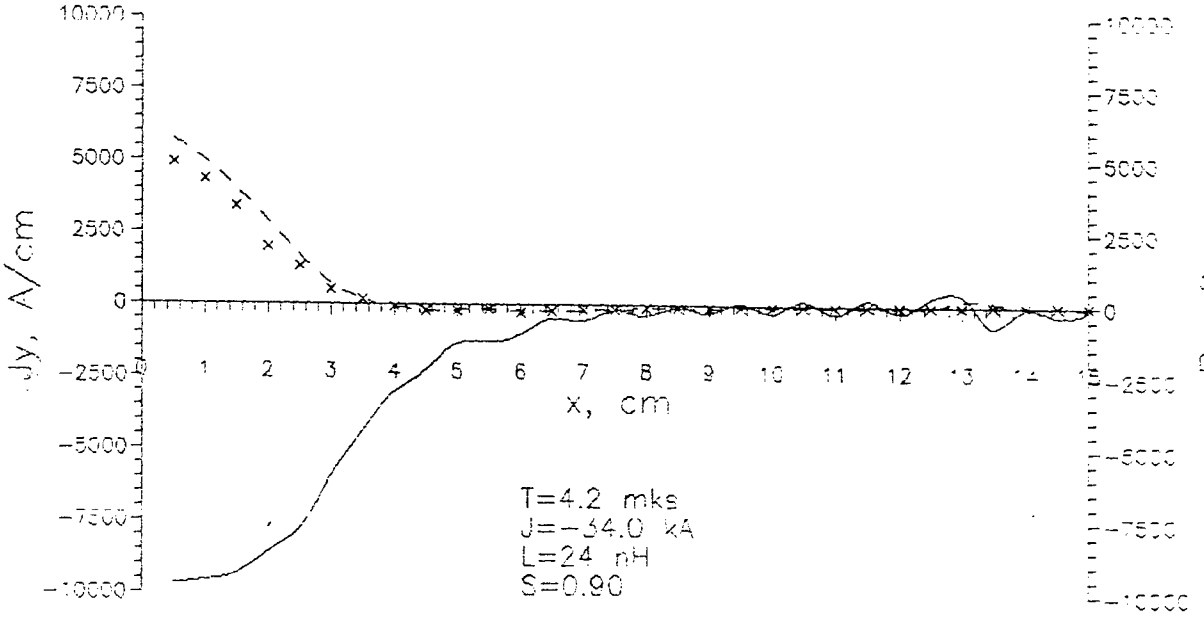
10000
7500
5000
2500
0
-2500
-5000
-7500
-10000
Jy, A/cm
Bz, Gs
1 2 3 4 5 6 7 8 9 10 11 12 13
x, cm
T=4.2 mks
J=-34.0 kA
L=24 nH
S=0.90

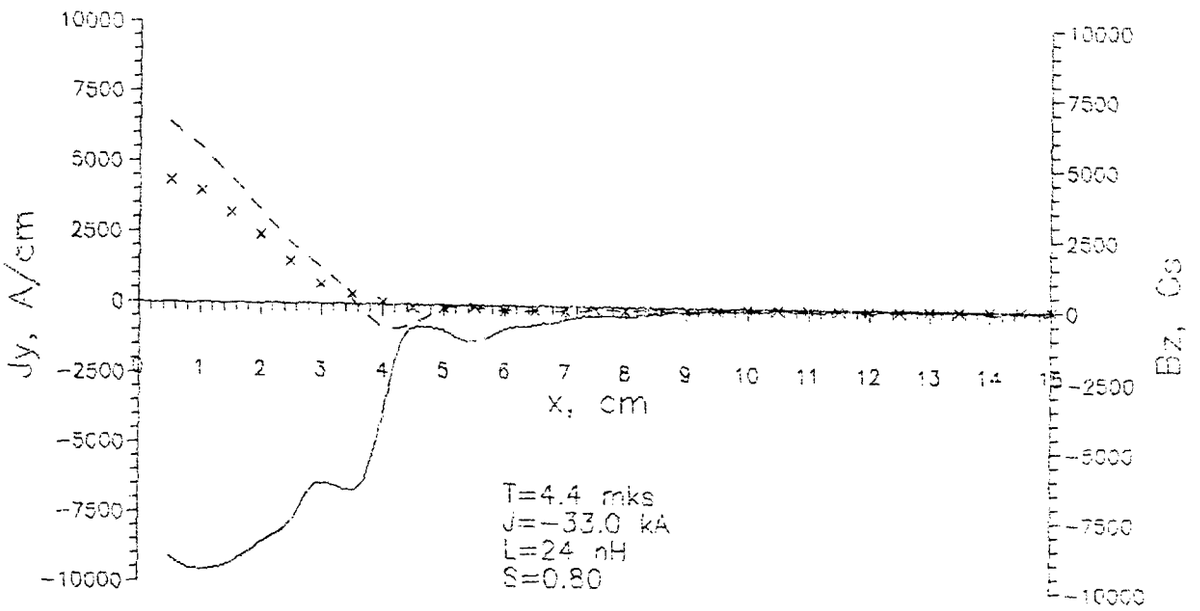
10000
7500
5000
2500
0
-2500
-5000
-7500
-10000
Jy, A/cm
1 2 3 4 5 6 7 8 9 10 11 12 13 14
X, cm
Bz, Gs
T=4.4 mks
J=-33.0 kA
L=24 nH
S=0.80

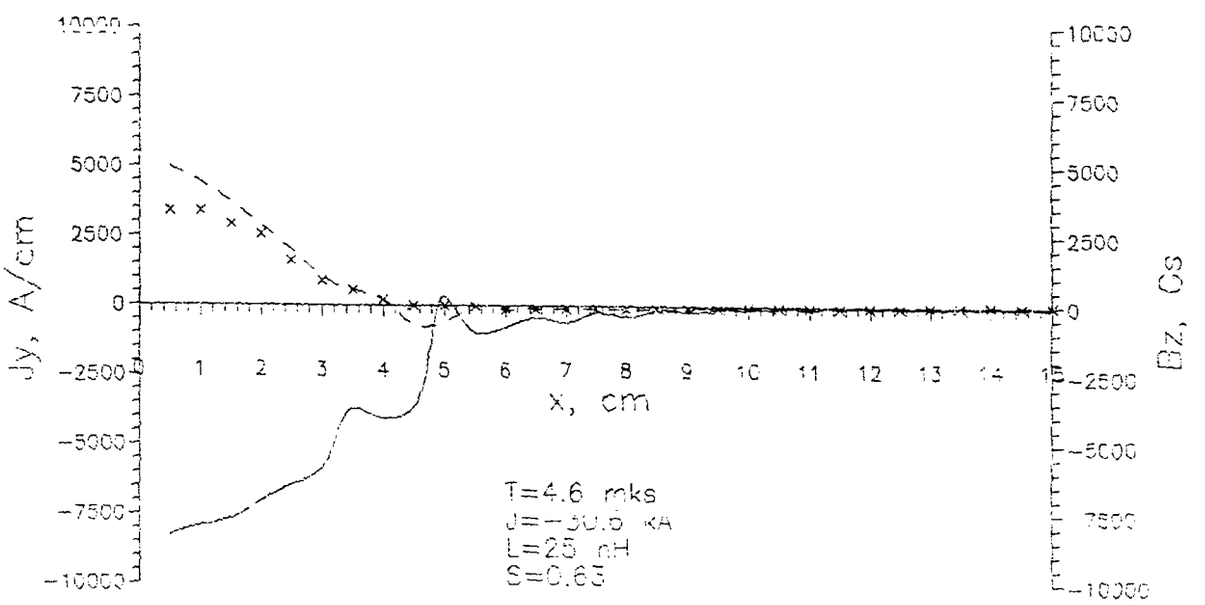
10000
7500
5000
2500
0
-2500
-5000
-7500
-10000
Jy, A/cm
1 2 3 4 5 6 7 8 9 10 11 12 13 14
X, cm
Bz, Gs
T=4.6 mks
L=25 nH
S=0.63

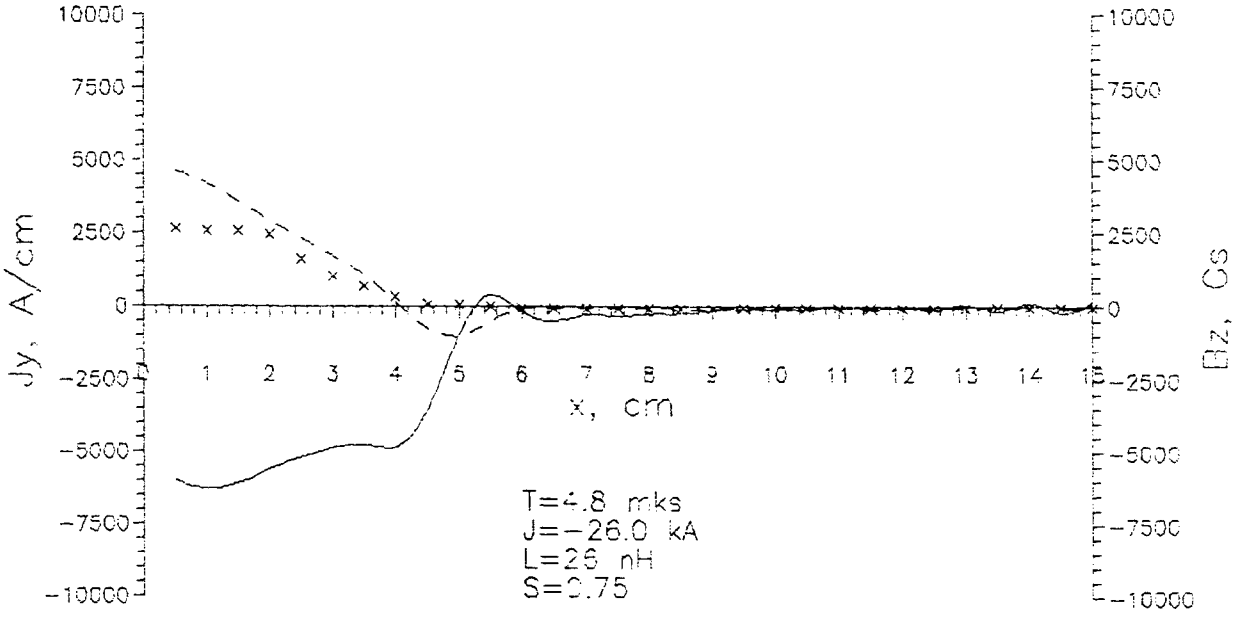
10000
7500
5000
2500
0
-2500
-5000
-7500
-10000
Jy, A/cm
Bz, Gs
1 2 3 4 5 6 7 8 9 10 11 12 13 14
x, cm
T=4.8 mks
J=-26.0 kA
L=26 nH
S=0.75

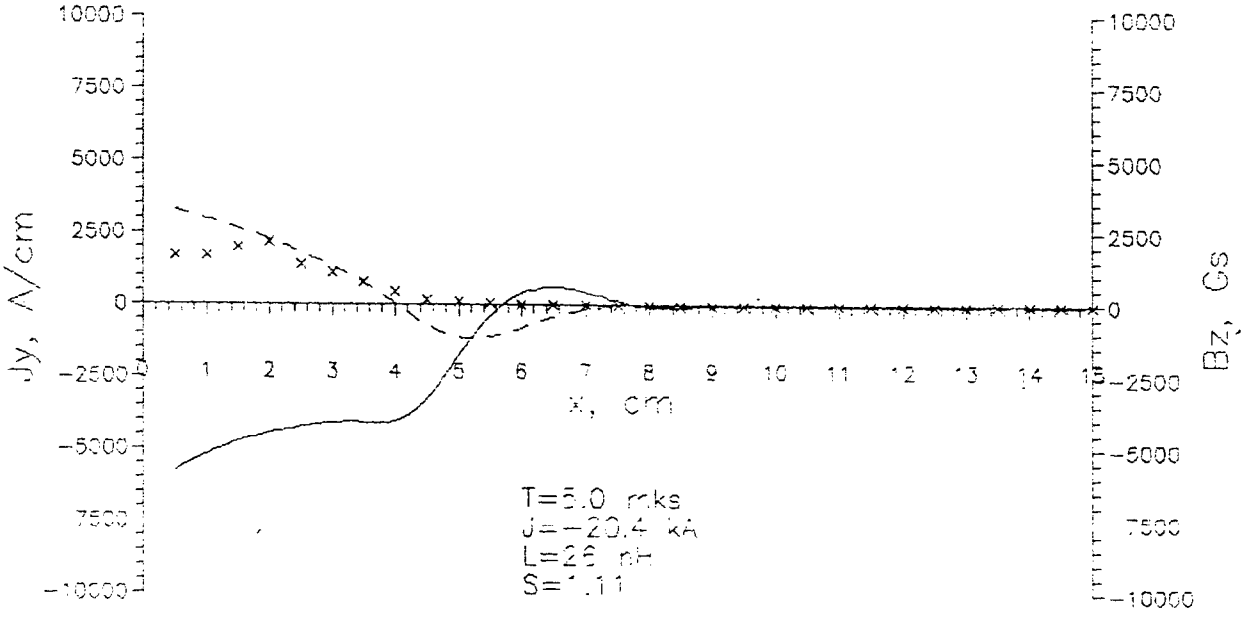
10000
7500
5000
2500
0
-2500
-5000
-7500
-10000
Jy, A/cm
Bz, Gs
1 2 3 4 5 6 7 8 9 10 11 12 13 14
x, cm
T=5.0 mks
J=-20.4 kA
L=26 nH
S=1.11